การปรับปรุงพฤติกรรมการเกิดผลึกของพอลิแล็กไทด์โดยใช้ไคตินวิสเกอร์ดัดแปรเป็นสารก่อผลึก

นางสาวณิชาภัทร ภัสสรประสิทธิ์

วิทยานิพนธ์นี้เป็นส่วนหนึ่งของการศึกษาตามหลักสูตรปริญญาวิทยาศาสตรมหาบัณฑิต
สาขาวิชาวิทยาศาสตร์พอลิเมอร์ประยุกต์และเทคโนโลยีสิ่งทอ ภาควิชาวัสดุศาสตร์
คณะวิทยาศาสตร์ จุฬาลงกรณ์มหาวิทยาลัย
ปีการศึกษา 2560

IMPROVEMENT OF CRYSTALLIZATION BEHAVIOR OF POLYLACTIDE USING MODIFIED CHITIN WHISKER AS NUCLEATING AGENT

Miss Nichaphat Passornraprasit

A Thesis Submitted in Partial Fulfillment of the Requirements
for the Degree of Master of Science Program in Applied Polymer Science and Textile Technology
Department of Materials Science
Faculty of Science
Chulalongkorn University
Academic Year 2017

Thesis Title	IMPROVEMENT OF CRYSTALLIZATION BEHAVIOR OF POLYLACTIDE USING MODIFIED CHITIN WHISKER AS NUCLEATING AGENT
By	Miss Nichaphat Passornraprasit
Field of Study	Applied Polymer Science and Textile Technology
Thesis Advisor	Assistant Professor Wanpen Tachaboonyakiat, Ph.D.

Accepted by the Faculty of Science, Chulalongkorn University in Partial Fulfillment of the Requirements for the Master's Degree

.....Dean of the Faculty of Science

(Professor Polkit Sangvanich, Ph.D.)

THESIS COMMITTEE

.....Chairman

(Associate Professor Duangdao Aht-Ong, Ph.D.)

.....Thesis Advisor

(Assistant Professor Wanpen Tachaboonyakiat, Ph.D.)

.....Examiner

(Assistant Professor Anyaporn Boonmahitthisud, Ph.D.)

.....External Examiner

(Assistant Professor Amornrat Lertworasirikul, Ph.D.)

ณิชาภัทร ภัสสรประสิทธิ์ : การปรับปรุงพฤติกรรมการเกิดผลึกของพอลิแล็กไทด์โดยใช้ไคตินวิสเกอร์ดัดแปรเป็นสารก่อผลึก (IMPROVEMENT OF CRYSTALLIZATION BEHAVIOR OF POLYLACTIDE USING MODIFIED CHITIN WHISKER AS NUCLEATING AGENT) อ. ที่ปรึกษาวิทยานิพนธ์หลัก: ผศ. ดร. วันเพ็ญ เตชะบุญเกียรติ, 99 หน้า.

งานวิจัยนี้ต้องการปรับปรุงพฤติกรรมการเกิดผลึกของพอลิแล็กไทด์ด้วยไคตินวิสเกอร์ซึ่งสกัดแยกจากเกล็ดไคตินผ่านการไฮโดรไลซิสด้วยกรด แต่เนื่องจากไคตินวิสเกอร์มีแนวโน้มที่จะเกาะกลุ่มกัน ผู้วิจัยจึงปรับปรุงการกระจายตัวของไคตินวิสเกอร์ผ่านวิธีการดัดแปรทางเคมีด้วยกระบวนการกราฟพอลิแล็กทิกแอซิดน้ำหนักโมเลกุลต่ำลงบนพื้นผิวของไคตินวิสเกอร์โดยใช้สารคู่ควบ จากนั้นจึงนำไคตินวิสเกอร์และไคตินวิสเกอร์ดัดแปรมาผสมขึ้นรูปกับเม็ดพอลิแล็กไทด์ด้วยกระบวนการอัดรีดเป็นวัสดุเชิงประกอบระดับนาโนแบบแผ่น โดยมีองค์ประกอบของไคตินวิสเกอร์และไคตินวิสเกอร์ดัดแปร 0.1, 0.2 และ 0.3 ส่วนโดยน้ำหนักของเรซินร้อยส่วน โดยจากการศึกษาพฤติกรรมการเกิดผลึกพบว่าทั้งไคตินวิสเกอร์และไคตินวิสเกอร์ดัดแปรสามารถเป็นสารก่อผลึกสำหรับพอลิแล็กไทด์ได้ แต่ไคตินวิสเกอร์ดัดแปรสามารถทำหน้าที่เป็นสารก่อผลึกที่ดีกว่าไคตินวิสเกอร์เมื่อศึกษาด้วยเทคนิค DSC ควบคู่ไปกับ POM ที่พบว่าไคตินวิสเกอร์ดัดแปรสามารถเพิ่มอุณหภูมิการเกิดผลึกและปริมาณผลึก รวมทั้งยังลดอุณหภูมิการเกิดผลึกเย็นของพอลิแล็กไทด์ได้ นอกจากนี้ยังพบการเกิดสเฟียรูไลต์ได้เร็วและสมบูรณ์กว่า โดยประสิทธิภาพการเป็นสารก่อผลึกนี้สอดคล้องกับการกระจายตัวของไคตินวิสเกอร์และไคตินวิสเกอร์ดัดแปรในเมทริกซ์ของพอลิแล็กไทด์ซึ่งพบว่าไคตินวิสเกอร์ดัดแปรมีการเกาะกลุ่มกันน้อยกว่า โดยเฉพาะที่ปริมาณของไคตินวิสเกอร์ดัดแปร 0.1 ส่วนโดยน้ำหนักของเรซินร้อยส่วนทำให้เกิดการกระจายตัวในเนื้อพอลิแล็กไทด์ดีที่สุดและขนาดของวิสเกอร์มีขนาดเล็ก ซึ่งโดยรวมแล้วนั้นการเติมไคตินวิสเกอร์ดัดแปรเพียงเล็กน้อยก็ก่อให้เกิดประสิทธิภาพสูงสุดสำหรับการก่อผลึกในพอลิแล็กไทด์

ภาควิชา วัสดุศาสตร์ ลายมือชื่อนิสิต .....

สาขาวิชา วิทยาศาสตร์พอลิเมอร์ประยุกต์และเทคโนโลยีสิ่งทอ ลายมือชื่อ อ.ที่ปรึกษาหลัก .....

ปีการศึกษา 2560

5971968423 : MAJOR APPLIED POLYMER SCIENCE AND TEXTILE TECHNOLOGY
KEYWORDS: POLYLACTIDE / CHITIN WHISKER / CRYSTALLIZATION / NUCLEATING AGENT / NANOCOMPOSITE

NICHAPHAT PASSORNRAPRASIT: IMPROVEMENT OF CRYSTALLIZATION BEHAVIOR OF POLYLACTIDE USING MODIFIED CHITIN WHISKER AS NUCLEATING AGENT. ADVISOR: ASST. PROF. WANPEN TACHABOONYAKIAT, Ph.D., 99 pp.

This work focuses on the enhancement of crystallization behavior of polylactide (PLA). The small crystalline of polymer was used to induce nuclei for crystallization. The small crystalline of chitin whisker (CW) was prepared by acid hydrolysis. In order to enhance the compatibility between CW and PLA matrix, CW was grafted with acid terminated poly(D,L-lactic acid) (PDLLA) by coupling reaction to obtain PLA-g-CW. Then, the CW and PLA-g-CW were used as nucleating agents by compounding with PLA pellets at various contents from 0.1-0.3 phr by cast film extrusion. The SEM images of nanocomposites showed more agglomeration of whiskers with the increasing of CW or PLA-g-CW contents. Nevertheless, PLA/PLA-g-CW exhibited smaller size of agglomerated particles and better dispersion comparing to PLA/CW at same compositions due to the compatibility between CW and PLA was increased by grafting with PDLLA. The SEM images related to the DSC and POM results which indicated that the PLA-g-CW nanocomposite showed more effective nucleating agent of PLA than CW because of their well-dispersion. The introduction of PLA-g-CW at 0.1 phr significantly decreased the Tcc and increase Tc of nanocomposite. Moreover, PLA/PLA-g-CW0.1 also exhibited the highest degree of crystallinity comparing with the others. Therefore, PLA-g-CW at 0.1 phr was the most effective nucleating agent which enhanced the crystallization rate and degree of crystallinity of PLA.

Department:	Materials Science	Student's Signature	.....
Field of Study:	Applied Polymer Science and Textile Technology	Advisor's Signature	.....
Academic Year:	2017		

ACKNOWLEDGEMENTS

I would like to take this opportunity to extend my deepest gratitude for the following people who have kindly support during my study.

Foremost, I would like to gratefully express the sincere appreciation to my advisor, Assist. Prof. Wanpen Tachaboonyakiat, who give an extensive knowledge, dedicate to support on conducting research, and provide invaluable guidance and direction throughout this research. In particular, I am pleased to express my profound gratitude to the thesis committee, Assoc. Prof. Duangdao Aht-ong, Assist. Prof. Anyaporn Boonmahitthisud and Assist. Prof. Amornrat Lertworasirikul for generously offering their valuable time and comments on reviewing this research. I would like to offer my heartfelt thanks to Prof. Suwabun Chirachanchai and his students from the Petroleum and Petrochemical College (PPC), Chulalongkorn University, for all of your time and facilitating on some parts of my work there.

I am eternally grateful to my beloved family, Mr. Somkid Passornraprasit, Mrs. Jongrak Passornraprasit, Miss Kotchamon Passornraprasit, Miss Jindawan Pongchaiyaphum, Miss Janpen Pongchaiyaphum and Miss Kanjana Sanit for the best endless encouragement, inspiring and tireless helping. I would like to say a big thanks to everyone who assisted with my work such great friends and seniors, especially, Mr. Warrayut Kanabenja, Mr. Aphiwat Pongwisuthiruchte, Mr. Wesarach Samoechip, Miss Papatsorn Rattanapet, Miss Sirinya Sotthiudom, Miss Jasmine Pongkasem, Miss Sawitree Sinthu and Mr. Narongkorn Trisan for friendship, cooperation and giving their time, suggestion, constant encouragement and helping in lab. Their help has made my work more enjoyable. I would also like to thank profusely to the all the members of staff in Department of Materials Science, Faculty of Sciences, Chulalongkorn University for all support, scholarship, facility and allowing me to work on a good place.

Last but not the least, I sincerely appreciate to PTT public company limited, Thailand for financial support throughout this research.

The completion of this study could not have been possible without them. Thank you again for all supports through the successful research.

CONTENTS

Page

Page

Page

List of figures

List of tables

CHAPTER 1
INTRODUCTION

1.1 Background and Significance of Problem

For a very long decade, the widely used plastic which usually made from petroleum-based resources have been playing an important role in many utilizations of commodity plastic such as polypropylene (PP), polyethylene (PE), poly(ethylene terephthalate) (PET), polystyrene (PS) and poly(vinyl chloride) (PVC)[1, 2], which commonly used in daily life, as well as engineering plastic for the specific purposes. While the world keeps moving forward, we are entering the era of insufficient resources including the declining of oil and natural gas resources that will bring about the issues of inadequate well-provided carbon sources which often used to produce synthetic polymers [3, 4]. There is not only the lack of feedstock problems, but the synthetic polymer also affects to ecosystem comprising a number of plastic waste pollution on land and ocean due to their long-lifetime characteristics which make them take a very long period of time to decompose [3, 4]. Moreover, a large carbon footprint and the greenhouse gas emission during product life cycle cause the climate variability and global warming [3, 4]. The previous state problems drive people to pay more attention in the product made from biopolymer which is the effectively alternative routes to overcome that problems [2, 5].

Polylactide (PLA) is one of biopolymer produced from renewable resources and can be degraded in nature, which can alleviate the energy crisis and ecological issues. Additionally, PLA has processability and high mechanical properties that make its widely used in various application [6-9]. Nevertheless, the main drawbacks related to crystallization behavior of PLA have adversely affected the production cost and overall properties of manufactured products in terms of thermal, optical, barrier properties as well as mechanical properties, and chemical resistance [6-9]. At crystallization state from the melt, PLA has very low crystallization rate [10-15]. Therefore, it is difficult to obtain a material with high degree of crystallinity in a short time. Moreover, PLA naturally generates only few nuclei and each of nucleus greatly set apart from each

other [12], leading to the large crystalline in a consequence of inherent brittle characteristics [10, 14-17]. In order to reduce process cycle time, production cost and gain productivity, nucleating agents are frequently use in the manufacturing of PLA products to decrease the nucleation induction period and increase the number of nuclei during crystallization. Thereby, the obtained PLA products would contain high degree of crystallinity together with small crystalline. However, the utilization of nucleating agents mainly focused on inorganic materials such as talc, calcium carbonate, carbon-based materials [13, 15, 17-23] because of high crystallization efficiency. But the inorganic materials would be still existed after polymer degradation. Therefore, novel biodegradable polymeric nucleating agent for PLA was proposed in this research. Chitin is the second most plentiful polysaccharide, which mostly founded in the structure of marine invertebrate such as lobster, crab, shrimp [24-28] . Thailand is one of the top seafood industry nations in the world [29, 30] and produce a tremendous amount of worthless seafood wastes that is the biomass feedstock for chitin preparing.

With an idea of using small crystallized material to induce the crystallization of PLA, chitin, a semi-crystalline polymer, was hydrolyzed with an acid in the suitable condition, thus, the amorphous region of chitin was hydrolyzed. The nanosized chitin whisker (CW) in needle-like shape with highly crystallinity was obtained. Therefore, the small crystallized CW would expect to induce the crystallization of PLA. In this work, CW was used as nucleating agent in PLA due to its crystallinity, plenty availability and low cost. Furthermore, the biodegradability of chitin within the composite leads the overall material be able to be degraded. However, chitin was incompatible with PLA because of its hydrophilicity and the nanosized effect which lead to some agglomeration [31, 32]. Hence, CW was modified by grafting with low molecular weight (MW) poly(D, L-lactic acid) (PDLLA) with carboxylic end groups using *N*-(3-dimethylaminopropyl)-*N*'-ethyl carbodiimide hydrochloride (EDC.HCl) as coupling agent. The obtained PDLLA grafted chitin whisker (PLA-g-CW) was determined for its structure by Fourier Transform Infrared Spectroscopy (FTIR) and solid state ^{13}C nuclear magnetic resonance spectroscopy (^{13}C NMR), crystallinity by X-ray diffractometer (XRD),

morphology and aspect ratios by Transmission Electron Microscope (TEM). The PLA-g-CW was also used as nucleating agent by mixing with PLA pellets and then fabricated into film by melt casting process (extrusion process). The dispersion of CW or PLA-g-CW in PLA matrix were observed under Scanning Electron Microscope (SEM). The degree of crystallinity of PLA and the thermal properties including melting and cold-crystallization temperature were determined by Differential Scanning Calorimetry (DSC). The isothermal crystallization behaviors including crystallization rate, nuclei densities, spherulite growth rate of PLA with and without nucleating agents were investigated by Polarized light Optical Microscope (POM).

1.2 Research objectives

1. To improve the crystallinity of PLA by the addition of nucleating agents.
2. To develop the dispersion of CW and the compatibility between CW and PLA matrix by means of grafting acid terminated low MW PDLLA (PDLLA-COOH) onto CW by coupling reaction

1.3 Research scopes

1. CW was prepared by acid hydrolysis reaction following the procedure that described by Paillet and Dufresne [33], then grafted with PDLLA through coupling reaction.
2. CW or PLA-g-CW was used as nucleating agents by compounding with PLA and casting into film using extrusion process.
3. The dispersion of CW in PLA matrix was observed using SEM.
4. The degree of crystallinity and the transition temperature including crystallization, melting and cold crystallization temperature of PLA films were investigated using DSC.
5. The isothermal crystallization behaviors including crystallization rate, nuclei densities, spherulite growth rate of PLA with and without nucleating agents were investigated by POM.

CHAPTER 2
THEORY AND LITERATURE REVIEWS

2.1 Polylactide (PLA)

2.1.1. Basic knowledge of PLA

Polylactide (PLA) is a thermoplastic aliphatic polyester, composed of monomer unit of lactic acid which is shown in Figure 2.1. It is promising biopolymer which compete to oil-based polymer. It is usually applied in food industry for food-contact packaging with good gas barrier properties. PLA is processability, it is easy to fabricate by compression molding, extrusion, injection, etc. into many products. Moreover, PLA is environmentally friendly since it is biodegradable polymer derived from sustainable and renewable resources of the lactic acid which is the by-product of fermentation. The other applications include diapers, disposable garments and menstrual hygiene products [6, 8, 9]. Furthermore, PLA also used in medical fields such as screw, pins and scaffold for cell-implantation with its suitable mechanical properties that can transfer loading in the body.

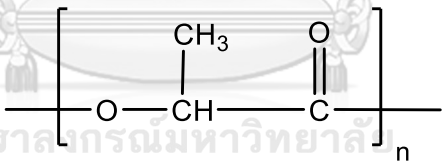

Figure 2.1 Chemical structure of PLA.

There are two main steps for PLA manufacturing process comprising the production of lactic acid and the process for converting lactic acid to PLA. Lactic acid or 2-hydroxy propionic acid, classified as an alpha-hydroxy acid, was isolated from sour milk by German Swedish chemist named Carl Wilhelm Scheele in 1780 [34]. In some bacteria and animal cells, lactic acid is founded as the by-product from glucose metabolism during anaerobic respiration. For the industrial manufacturing, it is produced by two ways; the chemical synthesis and the microbial fermentation of starch-rich agricultural product such as sugarcane and corn [35]. The manufacturing process of lactic acid is presented in Figure 2.2.

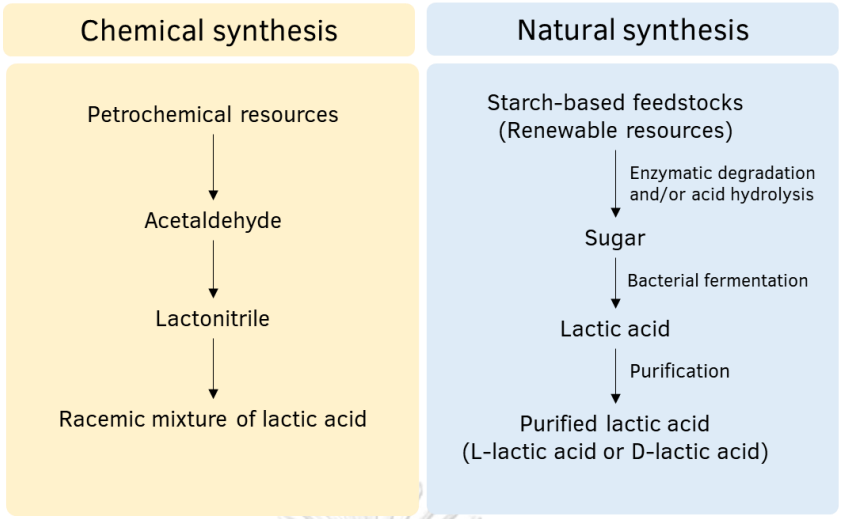

Figure 2.2 Manufacturing process of lactic acid by chemical and natural synthesis.

Naturally, lactic acid is one of the simplest chiral molecules which exist as pair of stereoisomers and optically active. Its stereoisomers are enantiomers (optical isomers) which two molecules are mirror images to each other but cannot superimposable. L-lactic acid mostly generated from both mammals and bacteria system while D-lactic acid only produced from bacterial fermentative [34]. The difference of these two isomers is the direction of plane-polarized light rotation. The plane -polarized light of L form rotates in dextrorotatory direction (clockwise). On the contrary, the D form rotates in levorotatory direction (counter-clockwise) [36]. Lactic acid which produced through chemical process presented as racemic form (a mixture of equal parts of both enantiomers) [35]. The optical active forms of lactic acid are illustrated in Figure 2.3.

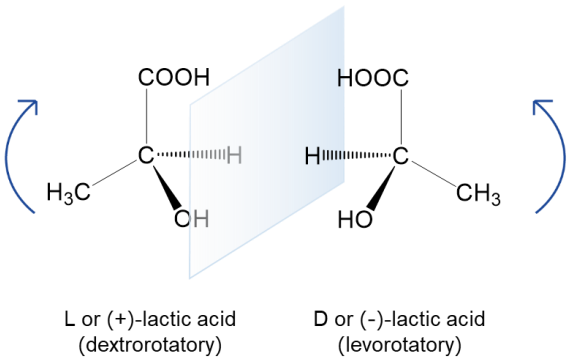

Figure 2.3 Two lactic acid enantiomers involving L- and D-lactic acid.

The cyclic dimer of lactic acid is normally known as lactide (3,6-dimethyl-1,4-dioxane-2,5-dione) [37]. It is obtained by the dehydration and cyclisation of two lactic acid molecules and also synthesized by depolymerization of low molecular weight (MW) PLA. The resulted lactides contain a mixture of three difference stereoisomeric forms including L-lactide, D-lactide and meso-lactide. Each is separated and purified by its boiling point. In addition, L-lactide and D-lactide can form a racemic stereoisomer so-called rac-lactide. L-lactide and D-lactide are optically active isomers but meso-lactide and rac-lactide are not. Figure 2.4 is represented the diastereomeric structures of lactide.

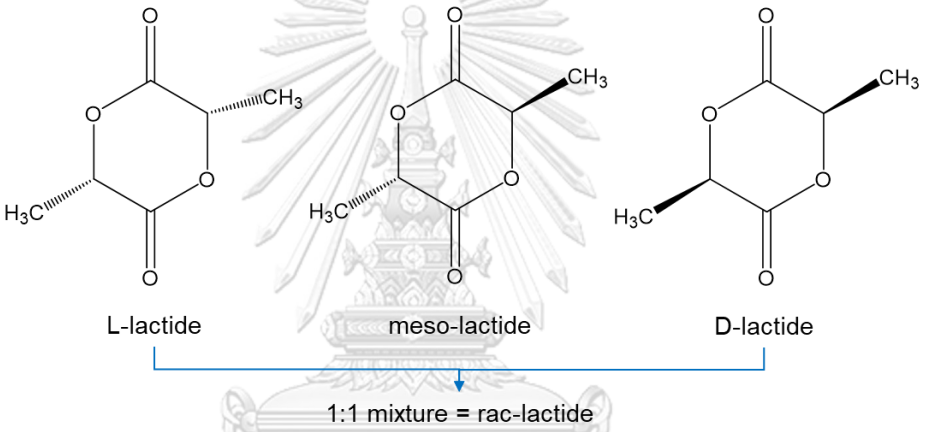

Figure 2.4 Lactide stereoisomers

Nowadays, high MW PLA is synthesized by three main difference methods compose of polycondensation, azeotropic dehydration polycondensation from lactic acids and ring opening polymerization (ROP) from lactides [8, 34, 38, 39]. Figure 2.5 depicts the production methods of high MW PLA.

Considering polycondensation, PLA can be processed by both solution and melt polymerization. In this route, the reaction take place directly by self-condensation of hydroxyl and carboxyl groups and yield low MW (approximately 2000-10,000) and brittle polymer because of some contaminations such as cyclization products from back-biting, impurities and the presence of water. The properties of low MW PLA are not suitable for many utilizations. So, the synthesis of high MW PLA is required. The synthesis of high MW PLA can be done by the addition of chain coupling agents such

as isocyanates, acid chlorides, anhydrides, epoxides, and so on to increase its chain length as well as MW.

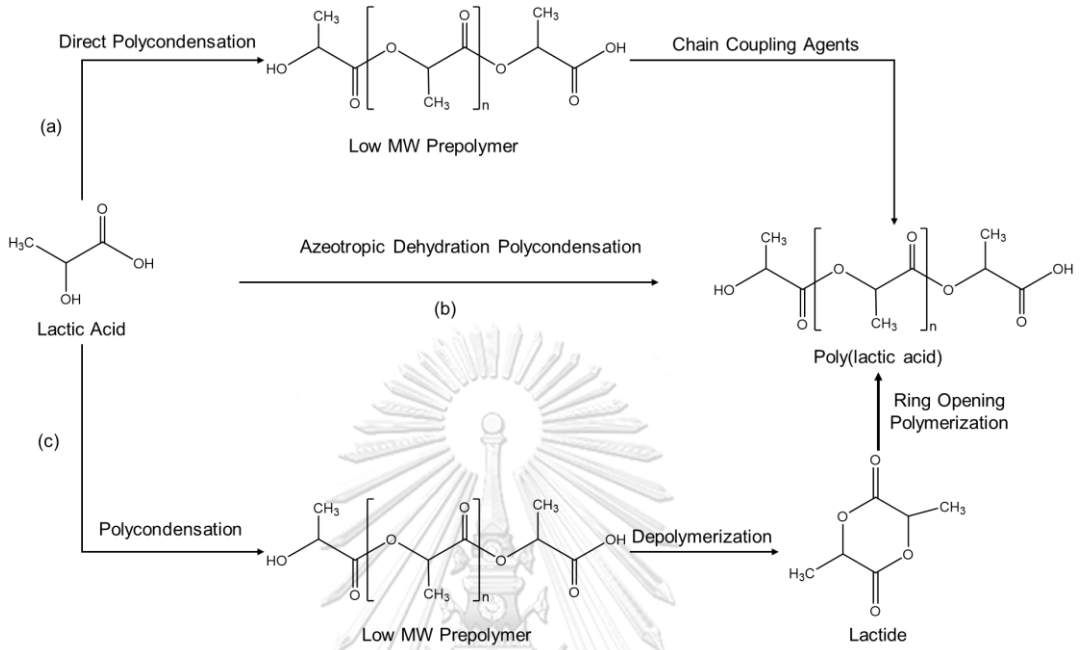

Figure 2.5 PLA synthesis routes involving polycondensation (a), azeotropic dehydration polycondensation (b) and ring opening polymerization (ROP) (c).

The coupling reaction is the least expensive process. But the final product may contain with some part of coupling agent molecules or contaminate with some impurities of unreacted oligomer, coupling agents or residual metal catalyst which still be the drawback of this process[8, 38, 39].

The second method is azeotropic condensation polymerization which demonstrated by Mitsui Toatsu Chemicals in 1994 [7, 8, 16, 34, 36-39]. It is a direct method to prepare high MW PLA without the use of chain extenders and correlated drawbacks. Briefly, PLA was polymerized by condensation polymerization together with azeotropically dehydrated the small molecules of water by-products at boiling point by reflux under pressure reduction to remove water from the reaction. Metals, metal oxides and some metals salts are used as catalyst. The obtained PLA has high MW more than 100,000 [8, 34, 37-39].

Alternative way to produce high MW PLA is ring opening polymerization (ROP). The ROP was first developed by Carothers in 1932 which cannot yield the high MW

PLA because of impure lactide monomer until Dupont improved the lactide purification techniques in 1954. Therefore, the high MW PLA can be polymerized through either cationic ROP and anionic ROP of lactide ring monomer [8, 34, 37-39].

2.1.2. The crystallinity and crystal structure of PLA.

Polymer chain must be orderly arranged in order to form the crystalline, influenced from two important factors. The first one, polymer chains have to possess the preferred stable conformation. The second factor is closed-pack ability. For example, homopolymer with linear isotactic stereoregularity arranges its molecule in closed-pack pattern by intermolecular attraction.

As described above, lactide exists three isomers (L-lactide, D-lactide and meso-lactide), hence, pure L-lactide or D-lactide are polymerized into crystallizable isotactic poly(L-lactide) or PLLA and poly(D-lactide) or PDLA, respectively. Whilst, the combination of both with equimolar amount gives rise to amorphous poly(D,L-lactide) or PDLLA due to atactic configuration. ROP of meso-lactide results in poly(meso-lactide) in syndiotactic configuration ((*S*)- and (*R*)- stereocenter positions) which arranges alternately along the chain or heterotactic configuration ((*S*)- and (*R*)- stereocenter positions which have doubly alternate arrangement) [9, 37, 40]. The different tacticity of linear PLA chain is shown in Figure 2.6.

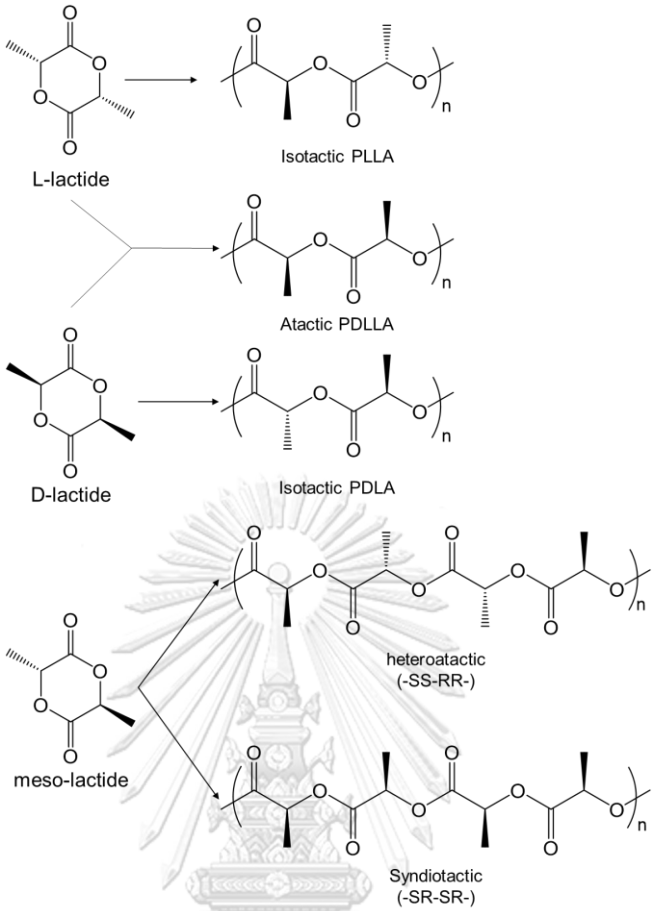

Figure 2.6 Configuration of PLA chain.

In addition, PLLA is polymorphism, the existence of many forms or crystalline structure in a solid material with the same chemical structure. PLLA prefers various manners of ordered chain or packing, and the different forms need nearly equal energy [8, 11]. PLLA crystallizes in three different crystalline forms including α-, β- and γ-form depending on the preparation conditions. The α -form is occurred under normal condition such as melt or solution crystallization [8, 11, 41]. PLLA with α -form has T_m 185 °C and more stable than β -form PLLA, which melted at 175 °C [8, 42] The β -form of PLLA generally grow at high-draw ratio with high-drawing temperature. At this condition, α -form is stretched into β -form (α -to- β transition) [8, 42, 43]. The γ-form of PLLA is prepared under epitaxial crystallization on hexamethylbenzene surface by Cartier, L. et al. [44]. The α -form of PLLA which has a limiting disordered modification is defined as the α'-form.

2.1.3. The crystallization behavior and thermal properties of PLA

Mainly, the crystallization behavior of PLA and its properties are significantly influenced by stereochemistry and thermal history [16]. Generally, the commercial PLLA typically contained 0.5-5 mol% D-lactic acid monomers, depending on the purity of monomer and synthesis techniques [41]. Van de Velde and Kiekens [45] demonstrated that PLLA had melting temperature at 170-200 °C. PLA with the ratio of PLLA higher than 90% tended to crystallize. Auras et al. reported that the melting and glass-transition temperature of PLA decreased with increasing of PDLA contents [7].

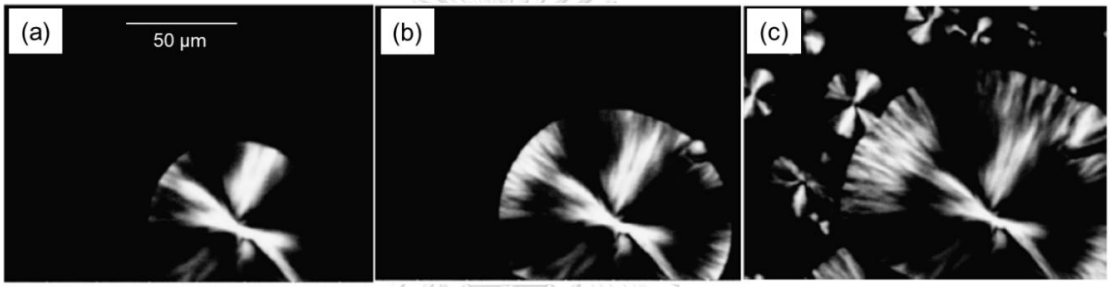

Figure 2.7 Optical microscope images of PLLA spherulites under difference cooling temperature (a) 130 °C (b) 120 °C (c) 110 °C at 5 °C/min.

(Di Lorenzo, M.L. Crystallization behavior of poly(l-lactic acid). European Polymer Journal 41(3) (2005): 569-575.) [10]

Many articles reviewed that PLA normally exhibited very slow crystallization rate and low degree of crystallinity [10, 12-15, 41]. The crystallization rate of PLA was high at crystallization temperature below 120 °C due to the high rate of spherulite growth and to the quite high nucleation density in this temperature range, described by Di Lorenzo, M.L. [10]. Figure 2.7 present the effect of nucleation rate on PLLA spherulites indicated that the smaller spherulites formed at lower crystallization temperature [10].

Nanthananon P. et al. [12] reported on the crystallinity behavior of PLA. It was found that PLA formed rather few number of nuclei and far apart from each other in a consequence of large spherulites without meet to form the grain boundary in 10h. In addition, the polarized light optical microscope (POM) image appeared in various

sizes of spherulite as a result of asynchronous crystallization, indicating that the nucleation process did not occurred at the same time, as shown in Figure 2.8

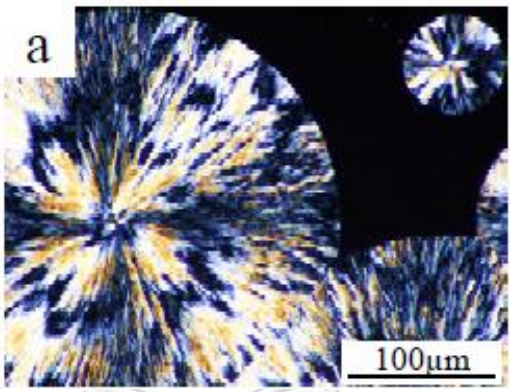

Figure 2.8 Asynchronous crystallization of PLA.

(Nanthananon, P., Seadan, M., Pivsa-Art, S., and Suttiruengwong, S. Enhanced crystallization of poly (lactic acid) through reactive aliphatic bisamide. IOP Conference Series: Materials Science and Engineering 87(1) (2015): 012067.) [12]

2.2 Crystallization of polymer

The properties of polymeric materials depend on its molecular characteristic which related to MW, chain orientation, morphology. Crystallinity is the one factor determined polymeric product properties. There are several techniques such as molecular architecture, copolymer, blending, adding with the varieties of additives, consequently negatively or positively effect to their crystallinity and hereby modified its properties. Furthermore, the fabrication conditions in terms of temperature profile, heating rate and cooling rate also influence to polymer properties. This section focused on the basic of polymer crystallization and the using of nucleating agent to improve the degree of crystallinity.

2.2.1. Basic scales of crystal structure

It is well-known that polymer is never 100% crystalline polymer due to its macromolecular structure with very long-chain, making it cannot fully arrange in order. Thus, crystallizable polymer consisted of crystalline parts (ordered arrangement) and

amorphous parts (disordered arrangement) and termed as semi-crystalline [46-48]. There are three basic scales of crystal morphology including unit cell, lamellae and spherulite that illustrated in Figure 2.9.

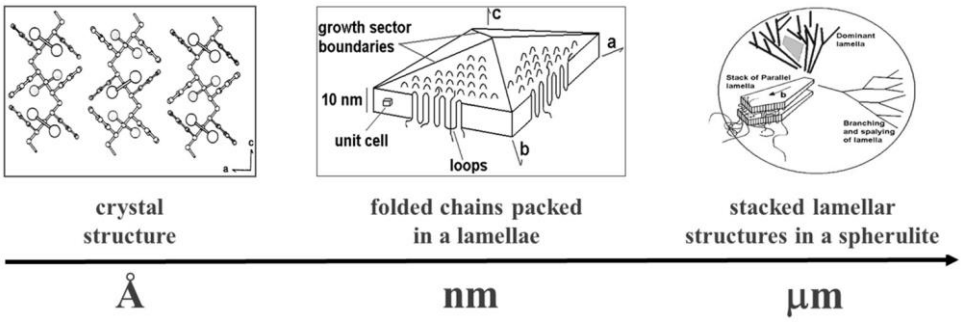

Figure 2.9 Three basic scales of crystal morphology including unit cell, lamellae and spherulite.

(Li, Y., Wang, Z., and He, T. Morphological Control of Polymer Spherulites via Manipulating Radial Lamellar Organization upon Evaporative Crystallization: A Mini Review. Crystals 7(4) (2017): 115.) [49]

Unit cell is the smallest crystal structure of materials in angstrom-scale. In small molecule materials, atoms and molecule are smaller than size of unit cell unlike individual polymer chain which pass through many unit cells resulting from its macromolecule. Thus, unit cell likewise a very small part of polymer chain. In unit cell, the chain must be arranged in the appropriate conformation and closed pack to each other by intermolecular interaction with similar pattern to form crystal structure such as zig-zag conformation of polyethylene [47].

The crystallization from solution at very dilute condition generates the lamellar single crystal with the thickness in a range of 5 to 50 nm [23] which composes of a number of unit cells. When semi-crystalline polymer is crystallization from molten state, polymer chain backbones are folding back in the direction that is perpendicular to lamellar surface. A large number of lamellae, which have many packed folded chains, is stacked and growth in the perpendicular direction of chain arrangement from the center of spherulite and extent in the same direction of spherulite radius. The

amorphous part of semi-crystalline polymer is the disorder chain such as the fold surface of lamellar and tie molecule between stacked lamellae layer in spherulite.

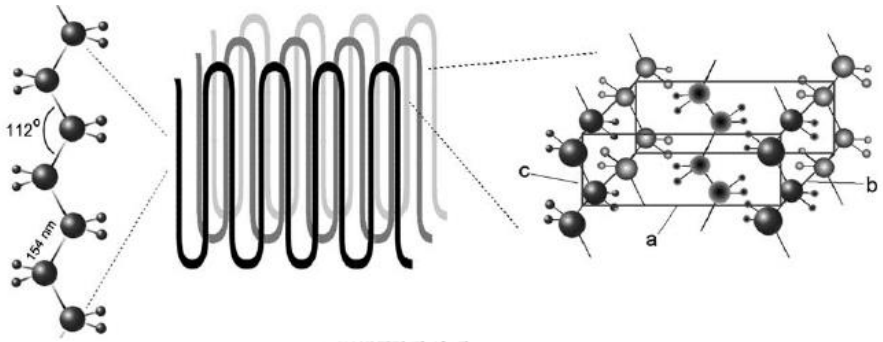

Figure 2.10 Molecular structure and unit cell of polyethylene.

(Raabe, D. Mesoscale simulation of spherulite growth during polymer crystallization by use of a cellular automaton. Acta Materialia 52(9) (2004): 2653-2664.) [47]

2.2.2. Polymer crystallization mechanism

Basically, crystallization mechanism is divided into two steps which are nucleation and crystals growth processes. Nucleation is the initial induction period of primary nucleation which takes the longest time to form a primary stable nucleus. Small molecules can rapidly crystallize at temperature nearly to their melting point. On the other hand, the crystallization of polymer molecule does not occur at its melting temperature, but it forms crystalline at lower temperature. Polymer never crystallizes at temperature closer to T_m by the reason of low supercooling, where T_c is approximately closed to T_m, gives rise to high thermodynamic Gibbs free energy barrier and chain mobility that requires large minimum fold period (l_{min}, lamellar thickness). So, it is difficult to build up the fully extended chain. Crystallization at high supercooling, the free energy is lower, and require shorter stable crystal thickness (minimum fold period). As previously state, it is very difficult to form stable nucleus in polymer. Thereby, crystallization rate of polymer is relatively slow [23, 48, 50, 51].

When polymer pass the energy barrier to form first folded chain or a primary nucleus at the critical temperature, it induces the other to grow and the secondary nucleation begins with fast lateral spreading in consequence of the energy barrier

reduction. The lamellae are radially grown and oriented from a center of nucleus to form spherulitic structure. This step is defined as primary crystallization that is a period of spherulite growth fastest. After that, secondary crystallization take place when the spherulites have impinged to one another and the crystallization rate is slowed down. Nevertheless, the crystallinity still slowly increases because thermodynamic drives to form more perfect crystalline in amorphous region between lamellae [23, 48, 50-52]. The crystallization mechanism is illustrated in Figure 2.11

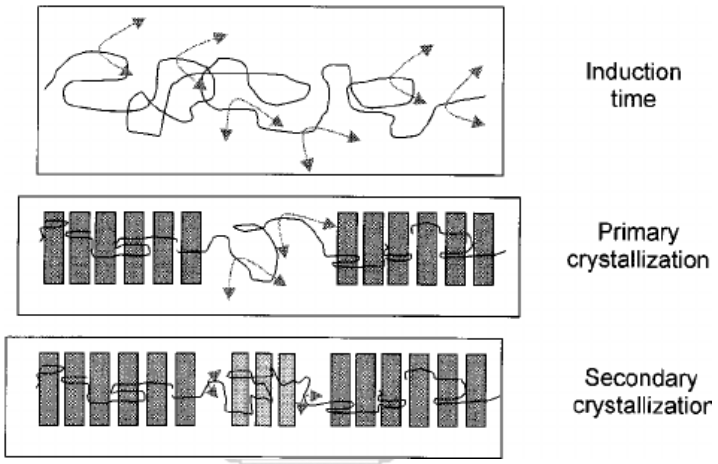

Figure 2.11 Illustration of crystallization mechanism involving induction time, primary crystallization and secondary crystallization.

(Nogales, A., Ezquerra, T., Denchev, Z., Sics, I., Baltá-Calleja, F., and Hsiao, B. Molecular dynamics and microstructure development during crystallization in poly(ether-ether-ketone) as revealed by real-time dielectric and X-ray methods. Journal of Chemical Physics 115 (2001): 3804-3813.) [52]

2.2.3. Polymer crystallization with the introduction of nucleating agents

There are two types of nucleation comprise homogeneous nucleation and heterogeneous nucleation. The first case is the process that parent crystalline phase of pure polymer occurs from melt stage at super-cooled condition. Heterogeneous nucleation is the process that crystalline take place on/near surfaces between polymer and foreign component such as nucleating agent, some impurity, additives and mold surface [51, 53-56].

As mention in the polymer crystallization kinetics section, the primary nucleation of pure polymer spontaneously formed as homogeneous nucleation at extreme degree of supercooling since it requires overcoming a large free energy barrier. However, most of nucleation from the melt is heterogeneous because the system is not truly pure. Figure 2.12 reveals that even if copolymer without nucleating agents can crystallize through both of homogeneous nucleation at high supercooling and heterogeneous nucleation at lower supercooling [23, 51, 56].

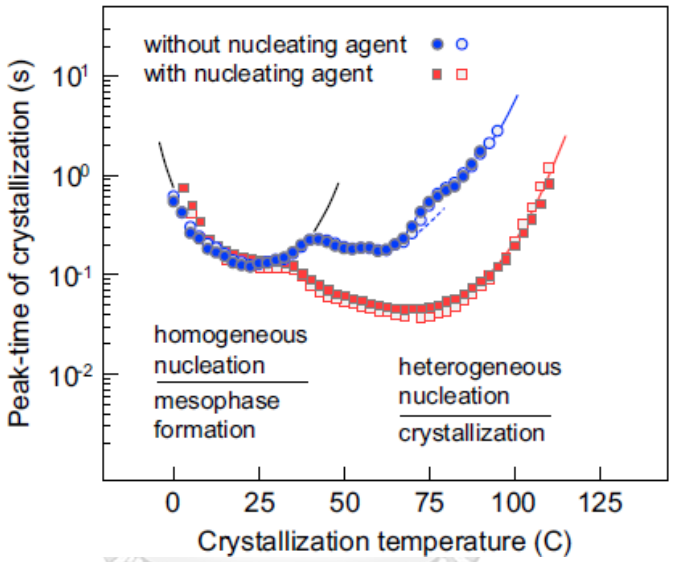

Figure 2.12 Peak-time of crystallization as a function of crystallization temperature. (Androsch, R., Monami, A., and Kucera, J. Effect of an alpha-phase nucleating agent on the crystallization kinetics of a propylene/ethylene random copolymer at largely different supercooling. Journal of Crystal Growth 408 (2014): 91-96.) [56]

The heterogeneous nucleation is generally take place at lower supercooling due to the foreign nucleating agent decrease the thermodynamic energy barrier to form new phase. Thus, nucleating agents are play an important role in polymer industry for a long time because they are the specific materials that have potential to accelerate the nucleation process of polymer. The addition of nucleating agents increases a number of crystalline center accordingly improve the phase transformation or crystallization rate. The uttermost size of final spherulites depend on the number of primary nuclei as show in Figure 2.13 that copolymer containing nucleating agent

have smaller crystal size compared to copolymer without nucleating agents. The two factors of spherulite size and the internal spherulite order determine the mechanical and physical properties of polymer. Consequently, the outstanding advantage of nucleating agents for the manufacturing is the reduction of processing time and cost together with the improvement of material performances and appearances.

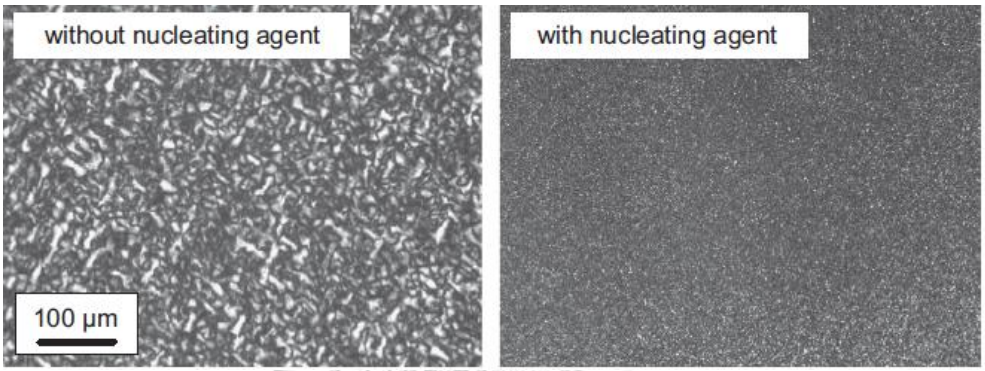

Figure 2.13 Spherulitic superstructure of a random polypropylene/ethylene copolymer with an ethylene content of 3.9 mol%, without (left) and with nucleating agent (right), respectively.

(Androsch, R., Monami, A., and Kucera, J. Effect of an alpha-phase nucleating agent on the crystallization kinetics of a propylene/ethylene random copolymer at largely different supercooling. Journal of Crystal Growth 408 (2014): 91-96.) [56]

2.2.4. Classification of nucleating agents and epitaxy crystallization

Nowadays, additives such as fillers, reinforcing agents, nucleating agents is generally used in polymer industry to reduce production cost and enhance polymer properties. The addition of these additive making the heterogeneity, which can induce the interfacial crystallization due to heterogeneous nucleation between surface of polymer and foreign substances and have a tendency to generate the hybrid crystalline supramolecular structure that different from conventional supramolecular crystalline structures which contain only polymer species [51, 57]. The hybrid crystals that occurred from various type of filler are presented in Figure 2.14.

Nucleating agents for heterogeneous crystallization of polymer can be classified as organic and inorganic materials [51, 57]. The classification diagram of nucleating agents is shown in Figure 2.15.

Organic nucleating agents can be soluble or insoluble substance. Soluble organic nucleating agent is partially or completely melted or dissolved in polymer matrix. Once the saturation of nucleating agent concentration is achieved, the nucleated crystals, which different from native crystals, are precipitated from the solution or the melt [51].

According to insoluble organic and Inorganic nucleating agents (such as calcium carbonate, talc, carbon nanotubes, graphene nanosheets). Nucleating seed which is existed before nucleation process of polymer is taken place induces the polymer lamellae grow on the filler surface. This mechanism defined as epitaxial crystallization involving 4 stepwise; absorption, orientation, nucleation and crystal growth which illustrated in Figure 2.16.

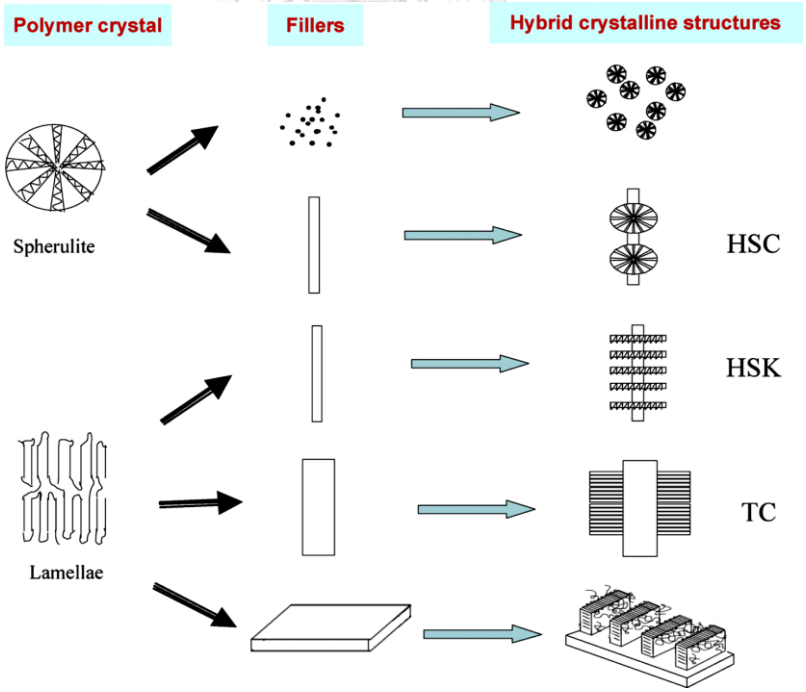

Figure 2.14 Schematic representation of various hybrid crystalline structures.

(Ning, N., et al. Realizing the enhancement of interfacial interaction in semicrystalline polymer/filler composites via interfacial crystallization. Progress in Polymer Science 37(10) (2012): 1425-1455.) [57]

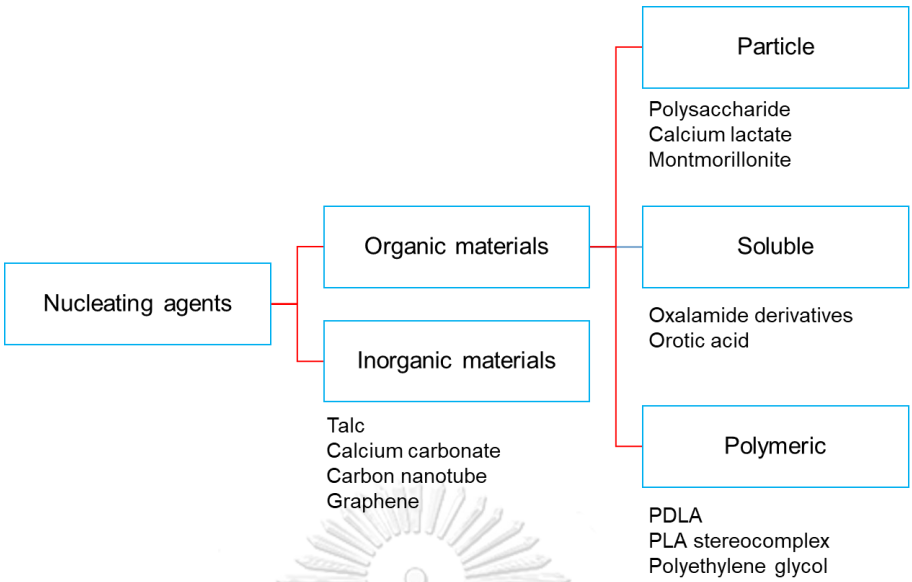

Figure 2.15 Classification diagram for nucleating agents.

The absorption of polymer chains onto nucleating agents surface are driven by physical or chemical forces such as hydrogen bonding. The absorption feasibility of this step depends on physical properties of surface including wettability and epitaxial match between host crystal and guest crystal. This epitaxial match stand for the similarity of crystal structure between polymer matrix and filler. Once the lamellae are deposited on the nucleation site, the orientation on the nucleating agent (host crystal) is occurrence followed by nucleation and growth of polymer, respectively. In case of polymer which has the radius of gyration (R_g) similar to the diameter of filler, it follows the soft epitaxy (geometric confinement) mechanism such as carbon nanotubes (CNTs) which has very small diameter [51, 56, 57].

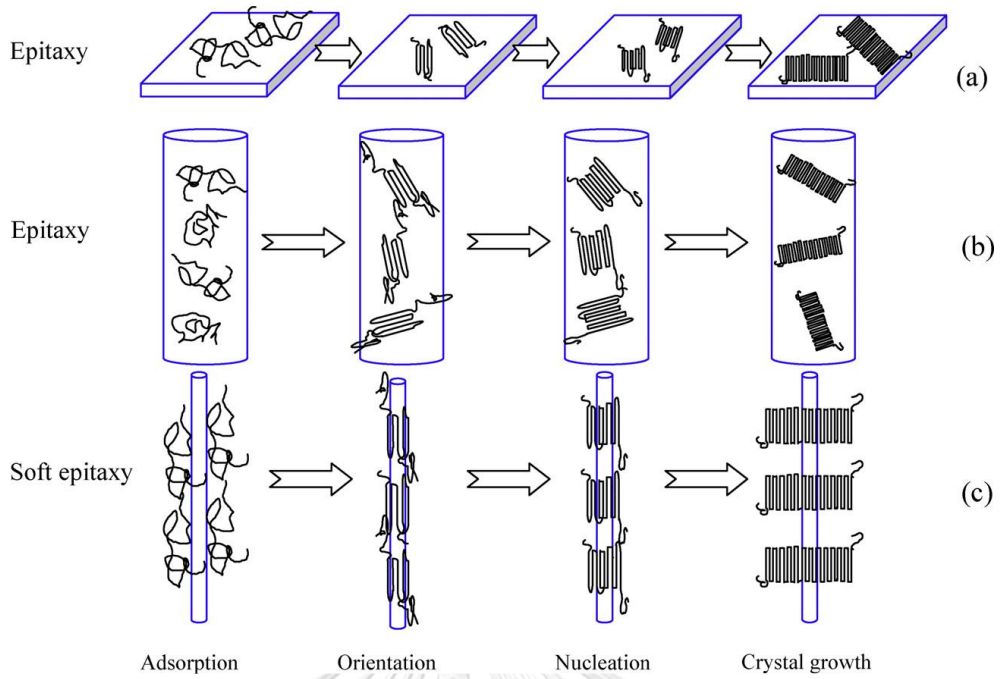

Figure 2.16 Schematic representation of epitaxy and soft epitaxy: the interfacial crystallization process of two dimensional lamellar fillers obeying epitaxy mechanism (a); fibers with a diameter much larger than the radius of gyration (R_g) of the polymer obeying epitaxy mechanism (b); and fillers with a diameter similar to the radius of gyration (R_g) of the polymer obeying soft epitaxy mechanism (c).

(Ning, N., et al. Realizing the enhancement of interfacial interaction in semicrystalline polymer/filler composites via interfacial crystallization. Progress in Polymer Science 37(10) (2012): 1425-1455.) [57]

2.3 Chitin

2.3.1. Background of chitin

Chitin, the second most abundant long-chain polysaccharide biopolymer, generally found in nature next to cellulose which is the structural function in plant, but chitin is the structural function in animal. It is fundamental component in exoskeleton structure of many invertebrate animals which are in the phylum Arthropoda including crustacea such as lobster, crab, prawn and insecta, such as cockroaches. It also presents in cell walls of fungi, green algae and yeast [16, 24-28, 31-33, 58-76].

The molecular structure of chitin is analogous to cellulose, which the monomer unit linked by β-(1,4)-glycosidic linkage. Unlike the pyranose unit of cellulose, chitin compose of *N*-acetylglucosamine and glucosamine unit. Hence, it is amino-polysaccharide copolymer of 2-acetamido-2-deoxy-D-glucopyranose linked by β-1,4-linkage. In general, the molar fraction of *N*-acetylglucosamine in copolymer defined as degree of acetylation (DA). Since chitin consists of *N*-acetylglucosamine as a major component, it has more than 50% of DA. In copolymer with lower than 50% of DA represented as chitosan. The chemical structure of cellulose and chitin/chitosan are illustrated in Figure 2.17.

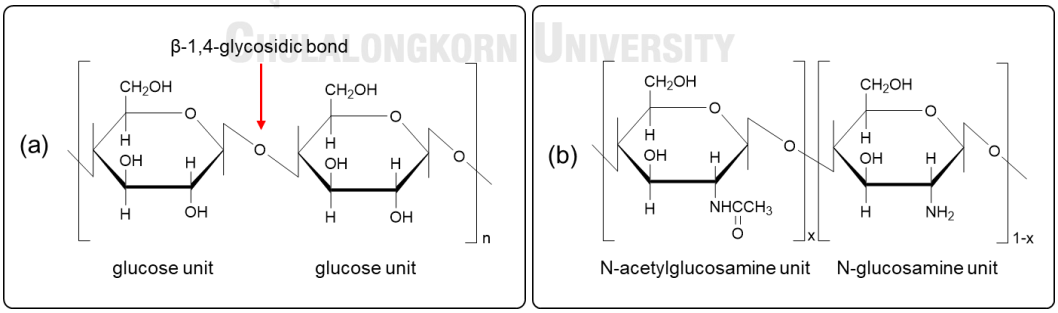

Figure 2.17 Chemical structure of cellulose and chitin/chitosan.

With its bioactivity, cytocompatibility, nontoxicity, biodegradability, low antigenicity, bio-absorbability and antimicrobial activity [58, 59, 64], it is not only widely known as a biocompatible substance which generally used as a raw material for the

production of chitosan but it is also often employed in biomedical, tissue engineering and pharmaceutical fields, for instance, scaffold, regenerative medicine, wound dressing, biosensor, enzyme immobilization, drug delivery system and cosmetics [58-60, 64].

2.3.2. Chitin in nature and the isolation of source material

Chitin exists in overall part of exoskeleton structure to protect living organism. The main raw material resources for chitin extracting is crustacean shell, especially cuticle of shrimps, lobsters and crabs. At molecular level, chitin chains form into highly crystalline nanofibrils linked with disorder region. These fibrils wrapped with protein layer and a number of chitin-protein fibers build up into bundle of fibers in microscale [24-28]. These bundle form network and embed in calcium carbonate-protein matrix to create the boligand structure (twisted plywood structure) and then repeats to form the multilayer of cuticle in structure of American lobster. The hierarchical structure of chitin is shown in Figure 2.18.

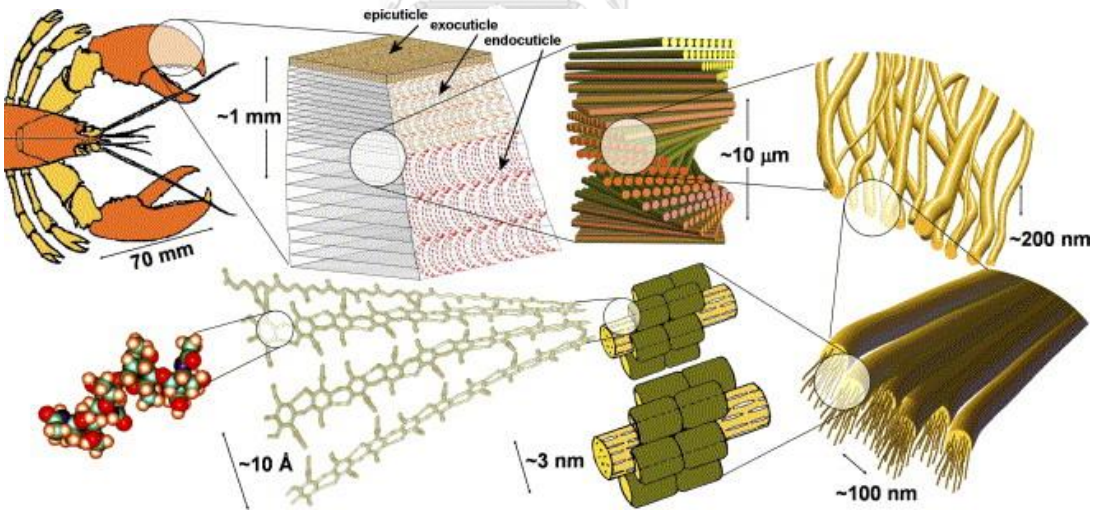

Figure 2.18 Scheme of the hierarchical structure of chitin in arthropod exoskeleton of American lobster.

(Raabe, D., Sachs, C., and Romano, P. The crustacean exoskeleton as an example of a structurally and mechanically graded biological nanocomposite material. Acta Materialia 53(15) (2005): 4281-4292.) [24]

The steps of isolation consist of the purification of source materials, deproteinization, demineralization (also called decalcification), decolorization and the purification of chitin. First, the source materials which usually from shellfish are purified and grinded. As mention above, chitin is wrapped by protein and mixed with mineral. Therefore, the next step, extracting chitin needs to get rid of protein and mineral impurity. [27, 28] There are two conditions to remove protein residue including conventional chemical method using NaOH and the enzymatic hydrolysis (mild condition). Acid treatment is used to remove the mineral salts followed by bleaching treatment for decolorization. Finally, chitin is washed and dried into small flake or powder or kept in suspension. The procedure for chitin extraction is explicated in Figure 2.19.

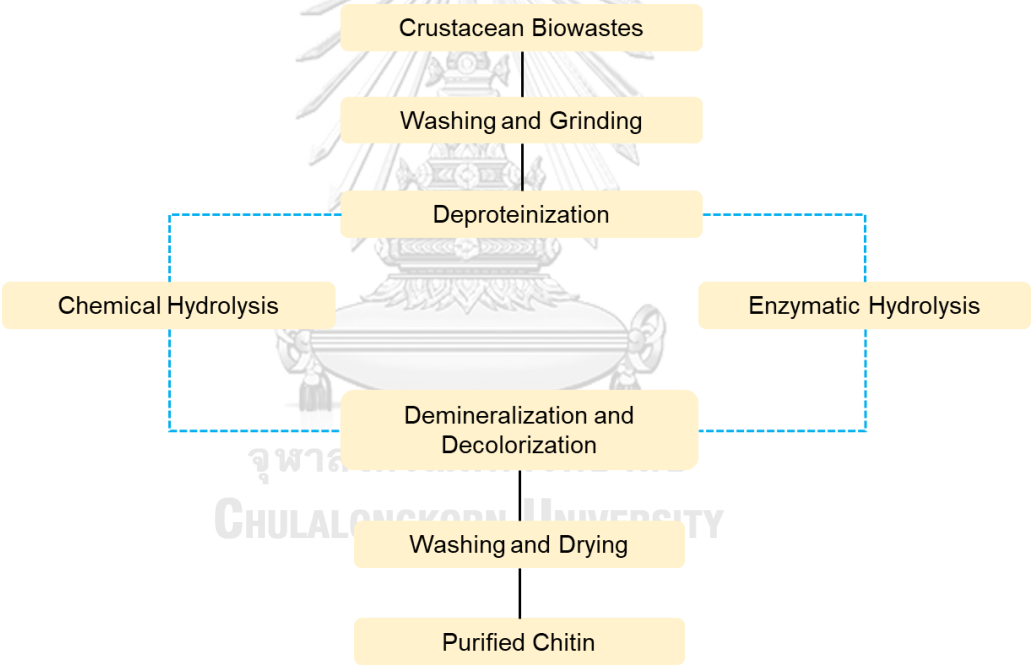

Figure 2.19 Scheme of the chitin isolation.

2.3.3. Crystalline polymorphs of chitin

Chitin presents in three crystalline polymorphic forms including α-, β-, and γ-chitin depending on its isolated resources. In nature, the α-chitin is the most abundant form that usually derived from fungal cell walls, lobster, crab, shrimp and insect cuticle. This form favors to arrange in the most stable antiparallel formation with very strong hydrogen bonding between sheet [16, 63, 70, 71]. The β-chitin exists in squid pens and tubeworms. Each chain arranges in parallel fashion without intersheet hydrogen bonding. In the γ-chitin, two chains arrange in the direction of antiparallel to another one chain. It exists in cocoon fibers of the *Ptinus* beetle and the stomach of *Loligo* squid [71]. The molecular chains arrangement of chitin in three forms are illustrated in Figure 2.20.

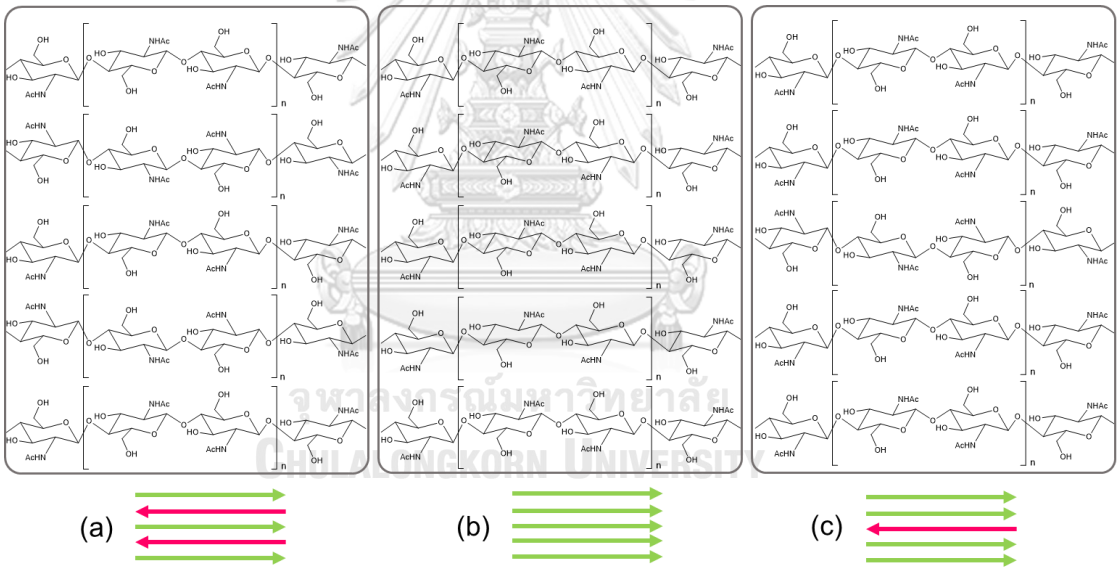

Figure 2.20 Arrangement of (a) α-chitin, (b) β-chitin and (c) γ-chitin.

2.3.4. Chitin whisker

Chitin whisker (also called chitin nanocrystal, chitin nanowhisker, chitin nanoparticle) is not similar to chitin fibers which are thin chitin fibrils, but it is rod-liked shape nanoscale material obtained from the further treatment by getting rid of amorphous parts and give rise to highly crystalline chitin. There are many methods used to prepare chitin whiskers including acid hydrolysis, 2,2,6,6-tetramethyl-piperidinyl-1-oxyl-mediated oxidation (TEMPO-mediated oxidation), partially deacetylation and ionic liquid [27, 33, 61-63, 65-70, 72-76].

1) Hydrolysis with strong acid

Chitins from shrimp, crab and lobster were usually hydrolyzed with strong acid (normally 3 N hydrochloric acid) under vigorous stirring at boiling temperature for 1.5 to 6 h depending on the sources of chitin. The disorder (amorphous) domain was removed whereas high crystalline region was entire remaining. The suspension was diluted with deionized water to stop reaction and the nanocrystal was separated from the solution by filtration and/or centrifugation and washing several times. For some studies, dialysis membrane was used to dialyzed against deionized water to ensure the purification of chitin nanocrystals [27, 61, 65, 67]. Several authors used further ultrasonication or homogenization to facilitate the chitin whiskers dispersion [33].

2) TEMPO-mediated oxidation

Similar to cellulose nanowhiskers [68, 72, 74], highly crystalline chitin whiskers from crab, tube worm and squid pen are successfully prepared through 2,2,6,6-tetramethyl-piperidinyl-1-oxyl-mediated oxidation (TEMPO-mediated oxidation) [27, 72, 75]. In brief, this case comprises two steps of oxidation and ultrasonication, chitin was suspended in water which contain TEMPO and sodium bromide with the addition of sodium hydroxide to control pH as 10. Next, sodium hypochlorite was added in order to start the oxidation reaction at room temperature. Afterward, the suspension was treated by ultrasonication and then bring about the individual chitin whiskers. The individualization of chitin whiskers was driven by the charge-induced electrostatic

repulsion on the surface cause by the anionic charges of carboxyl groups which converted from hydroxyl groups of C6 during oxidation [27, 62, 63, 72].

3) Partially deacetylation

As reported by Fan Y. et al. [69], the individual chitin whiskers had been obtained from **α**-chitin by surface cationization of partially deacetylated chitin. The process was carried out in three main steps, the first one was partially deacetylation, chitin was suspended in concentrated NaOH solution with the concentration of 33% (w/w) of concentration and the addition of $NaBH_4$ in order to inhibit the alkaline depolymerization under stirring at 90 ºC for 1-4 h. This treatment increased the amino groups of C2 at chitin surface. Afterward, the suspension was neutralized by deionized water. Second, the mechanical disintegration under acidic condition (pH 3-4) by adding acetic acid was performed for 5 days. The last step, the suspension was ultrasonicated to yield individual chitin whisker with average width and length approximately 6.2 and 520 nm, respectively. Along with the TEMPO-mediated oxidation, the electrostatic repulsion was the major driving force that generate the individualization but for this method gives the cationic charge on the surface of whiskers after adding acetic acid. An acid protonated whisker surface and induced the positive charges which lead to the separation of individual chitin from each other [27, 63, 69].

4) Ionic liquids

Salts which melted below a boiling point of water are termed ionic liquids [27, 66]. The ionic liquids have been used as alternative method to dissolve or swell biomaterials which ineffectively dissolved by organic and aqueous solvents [27, 66, 70, 73, 76]. In 2002, R. Swatloski et al. [66] used an ionic liquid (1- butyl- 3-methylimidazolium chloride) so as to dissolved cellulose at high concentration. Similar to cellulose, chitin formed weak ion-gels by 1-allyl-3-methylimidazolium bromide (AMIMBr) which first reported by K. Prasad et al. [76]. In short, chitin powder was soaked with AMIMBr at ambient temperature for 24 h followed by heating at 100 ºC. The formation of chitin gels was taken place during heating. Their work demonstrated that the gels viscosity was subjected to concentration of mixture. Later, K. Jun-ichi et al.

[73] developed the additional regeneration stage. After heating, chitin/AMIMBr gels were cooled down, then methanol was added dropwise followed by ultrasonication. The regeneration started when the methanol was added, and the chitin whisker suspension was obtained.

2.4 Literature reviews of nucleating agents used with PLA

Since, there are lots of researches with respect to enhance the crystallization behavior of PLA, several production conditions were studied. Moreover, the various type of nucleating agents (e.g. talc, calcium carbonate, carbon nanotubes, clay, polysaccharide, etc.) were used to accelerate crystallization rate and improve physical, thermal and mechanical properties of polymer [17-22, 77-80].

Battegazzore, D. et al. [18] melted blended talc and PLA by twin screw extruder to prepare composite with 1 wt%, 2.5 wt%, 5 wt%, 10 wt%, 15 wt% of talc (named as PLA1T, PLA2.5T, PLA5T, PLA10T and PLA15T, respectively). They reported that PLA did not crystallize during cooling whereas composite samples appeared the exothermic peak indicating the nucleating effect of talc. Moreover, the crystallization temperature and peak area increased when the content of talc filler was increased. At second heating, the cold crystallization temperature of composite decreases from 130 ºC to about 100-107 ºC compared with pure PLA. The PLA1T composite shows the optimal results of T_{cc} which lower than PLA approximately 23 ºC and the highest crystallinity values compared with all samples. The DSC thermogram during cooling and second heating of PLA and talc composites presented in Figure 2.21.

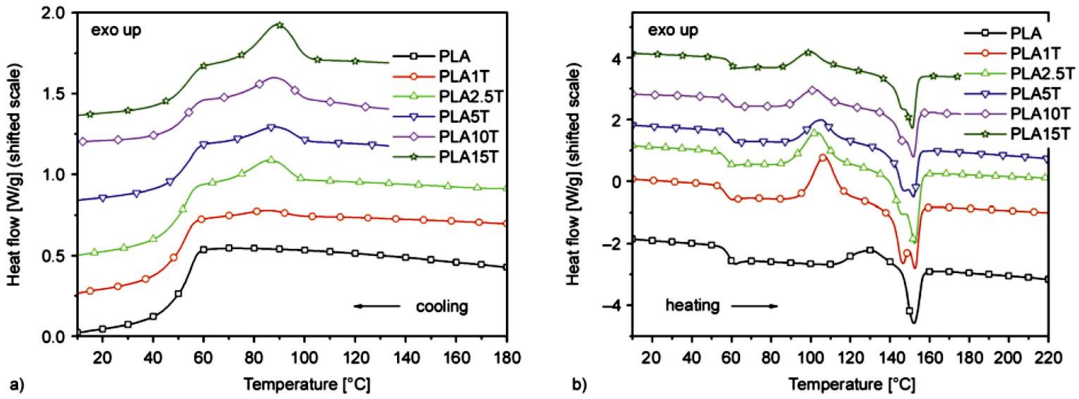

Figure 2.21 DSC analyses of samples at cooling (10°C/min 230–0°C) (a) second heating (10°C/min 0–230°C) (b).

(Battegazzore, D., Bocchini, S., and Frache, A. Crystallization kinetics of poly(lactic acid)-talc composites. Express Polymer Letters 5 (2011): 849-858.) [18]

Phetwarotai W. and Aht-Ong D. [21] investigated the nucleating effect of talc and nanoprecipitate calcium carbonate (NPCC) on PLA composite film. Non-isothermal and isothermal crystallization behavior were observed using DSC. Non-isothermal crystallization which performed at various cooling rate from 1 - 10 °C/min showed that it was not easy to crystallize neat PLA under fast cooling rate (10 °C/min) due to there was no exothermic peak during cooling step. So, the cold crystallization was appeared during heating in order to recrystallize the disordered parts. Alternatively, the crystallization peak was presented at slower cooling rate (1-5 °C/min), implied that the crystallization of PLA easily took place under slow cooling rate.

According to PLA composite with the incorporation of talc and NPCC, the effect of cooling rate showed the similar results to neat PLA. Comparing with neat PLA, the crystallization peak of nucleated PLA blend films with NPCC and talc was shift to higher temperature. Additionally, the crystallization temperature increased when the content of these nucleating agents was increased, indicating the proficient nucleating effect of both nucleating agents.

In case of isothermal crystallization condition, the declining of crystallization haft-time ($t_{1/2}$) revealed that the depression of crystallization temperature and the presence of nucleating agents accelerate the crystallization rate of neat PLA. POM

images from the isothermal crystallization at 115 °C also observed in order to confirm the nucleating behavior of talc and NPCC. The spherulite of PLA was growth after isothermal crystallization for 5 min whereas the spherulitic growth of nucleated PLA films with talc and NPCC clearly arise within 3 min. Both materials increased the density of nuclei, resulting in small and great number of spherulite. The POM images at isothermal crystallization were shown in Figure 2.22.

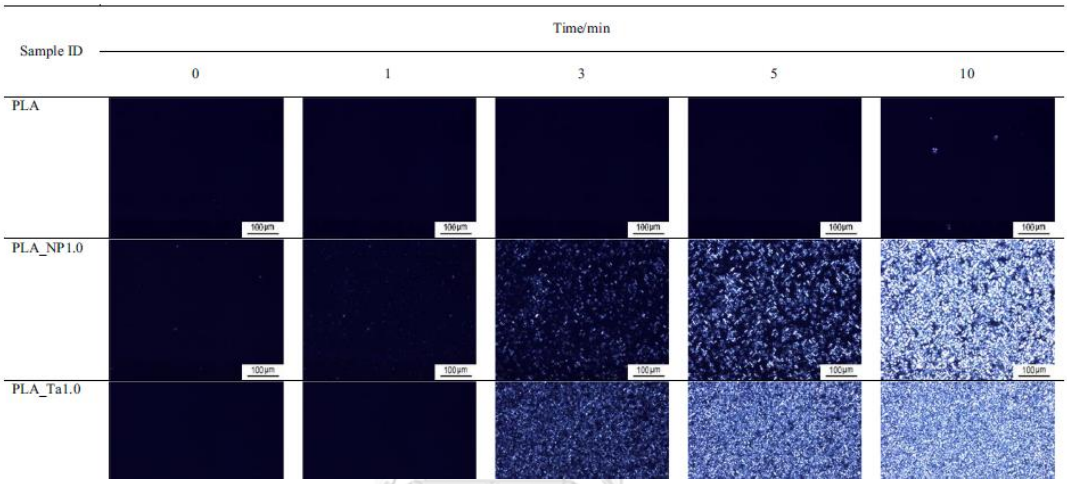

Figure 2.22 Polarized light micrographs of neat PLA and nucleated PLA blend films with 1 % of NPCC and talc during isothermal crystallization at 115 °C.

(Phetwarotai, W. and Aht-Ong, D. Nucleated polylactide blend films with nanoprecipitated calcium carbonate and talc. Journal of Thermal Analysis & Calorimetry 127(3) (2017): 2367-2381.) [21]

Modified montmorillonite layer silicate (MMT) or organic clay has been utilized to enhance the thermal, physical and mechanical and barrier properties of polymers [15]. It also acts as nucleating agent by develop the crystallization rate of PLA. Nam, J.Y. and co-workers [17] described that the addition of 4 wt% of MMT (denoted as PLACN4) increased the rate of crystallization approximately 50% . They also investigated the spherulitic texture of neat PLA and the PLACN4 nanocomposite using POM under a range of isothermal crystallization temperature. These images which represented in Figure 2.23 indicated the crystallization at higher temperature results in the larger spherulite for all samples. The spherulite of nanocomposite was smaller

than neat PLA for all range of experimental temperature. Especially at the crystallization temperature at 120 ºC, the nanocomposite obviously displayed very tiny spherulite comparing to neat PLA.

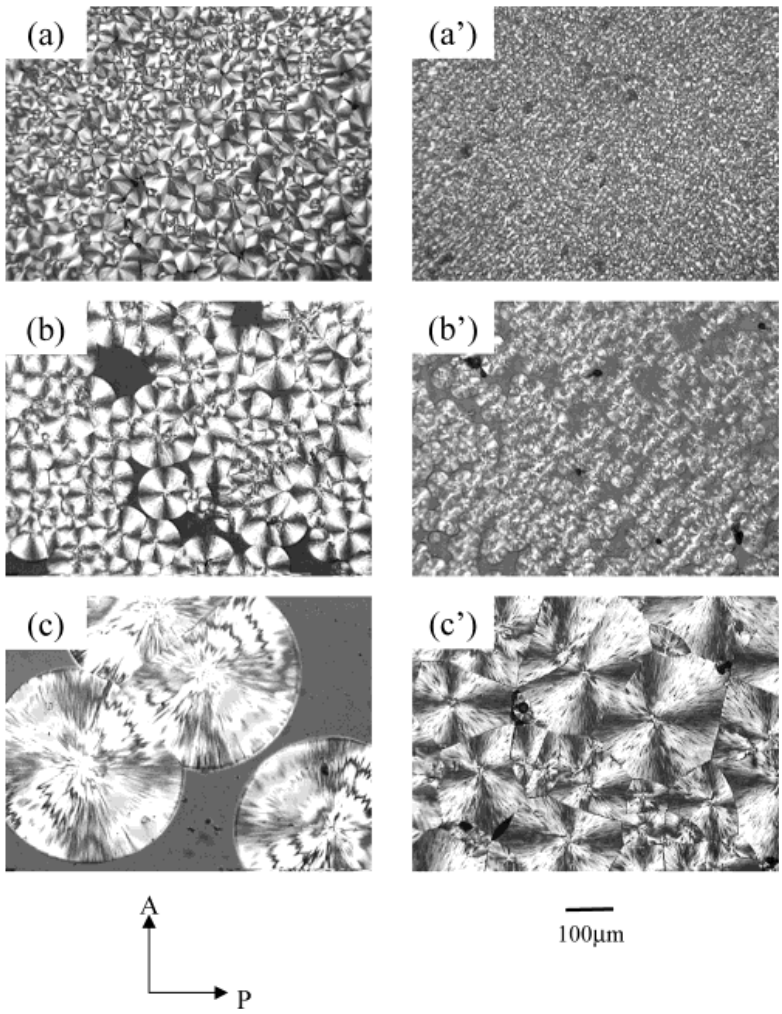

Figure 2.23 Optical micrograph of neat PLA (a-c) and PLACN4 (a'-c') at various crystallization temperature of 120 ºC (a, a') 130 ºC (b, b') and 140 ºC (c, c').

(Nam, J.Y., Sinha Ray, S., and Okamoto, M. Crystallization Behavior and Morphology of Biodegradable Polylactide/Layered Silicate Nanocomposite. Macromolecules 36(19) (2003): 7126-7131.) [17]

Zhang, R. et al. [79] successfully prepared PLA-IC which referred to inclusive complex (IC) between PLA and α-cyclodextrin (α-CD). Figure 2.24 is illustrated the inclusion complex of cyclodextrin and PLA. Neat PLA, PLA-IC and α-CD were separately

dispersed in PLA-chloroform solution and then casted into films. Three samples were investigated by DSC to study the crystallization behavior. α-CD show a little nucleation effect on PLA whereas PLA-IC can induce the crystallization of PLA/PLA-IC composite.

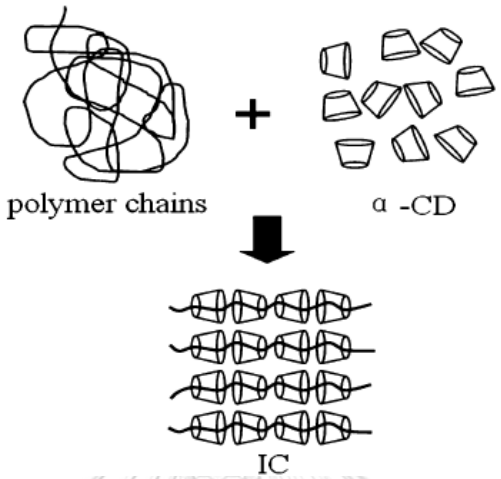

Figure 2.24 Schematic illustration of inclusive complex between polymer and cyclodextrin

(Li, H., et al. Crystallisation, mechanical properties and rheological behaviour of PLA composites reinforced by surface modified microcrystalline cellulose. Plastics, Rubber and Composites 45(4) (2016): 181-187.) [79]

Non-isothermal crystallization behavior of PLA/hydrazide compound (TMC) was studied by Xu, T. et al. [78]. They found that TMC is an effective nucleating agent for PLA due to the increasing of crystallization temperature (T_c) by a very loading of TMC.

Microcrystalline cellulose (MCC) was surface modified by 3-isocyanotopropyl triethoxysilane (K-MCC) before melt blending with PLA by extrusion and then injected to prepare the specimen. Li, H. et al. [77] reported that T_{cc} of PLA/5% MCC and PLA/5% K-MCC was significantly influenced. The PLA/5% K-MCC composite showed the maximum T_{cc} peak area, referring to the optimal content of this reinforcing fillers that positively influenced to crystallization of PLA. In addition, the Tcc value of PLA/5%MCC composite was lower than neat PLA approximately 2 ºC, indicating the effect of the addition of nucleating agent of K-MCC. The mechanical properties of PLA were enhanced by the addition of MCC and K-MCC, especially in PLA composite containing

K-MCC which showed significantly enhanced of mechanical properties compared with pure PLA and PLA/MCC composite due to the compatibility and the good dispersion between PLA and K-MCC after treatment with silane.

Herrera, N. et al. [32] successfully prepared the chitin nanocrystal (ChNC)/PLA nanocomposite using liquid feeding of ChNC together with triethyl citrate (TEC) which used as plasticizers into extrusion process and followed by compression molding. They found that the ChNC can act as nucleating agent in nanocomposite films. However, there is some agglomeration of ChNC due to the strong hydrogen bonding of ChNC and the hydrophobicity of PLA.

Li, C. et al. [31] prepared the grafted CHWs (g-CHWs) with l-lactide by ring-opening polymerization (ROP) and then the g-CHWs/PLLA nanocomposite films were prepared by solution-casting. The solid state ^{13}C NMR and IR results confirmed the successful modification of g-CHWs via ROP. The CHWs or g-CHWs can act as nucleating agent of PLLA nanocomposites. Hence, the addition of the whiskers affected the crystallization properties of PLLA matrix. As a result of the excellent interfacial adhesion between g-CHWs and PLLA matrix, uniform dispersion of g-CHWs/PLLA nanocomposites was improved.

CHAPTER 3
RESEARCH METHODOLOGY

3.1 Materials

1. Polylactide (PLA) is in a pellet form with the trademark of Ingeo™ biopolymer 2003D was supplied by NatureWorks® LLC, Minnesota, United States to be used as polymeric matrix.
2. Commercial chitin flake (CF) which made from shrimp shell was supported by A.N Lab, Samutsakorn, Thailand. The crystalline structure of CF is alpha polymorphic form confirmed by X-ray diffraction (XRD). In this experiment, CF was used as raw material of chitin whisker (CW) production.

3.2 Chemicals

1. Hydrochloric acid fuming 37% (HCl), ACS reagent grade was purchased from Merck KGaA, Darmstadt, Germany and used as hydrolyzed reagent to prepare CW.
2. *N, N*-dimethylformamide (DMF), UNIVAR® was supplied from Ajax Finechem, Auckland, New Zealand for using as solvent.
3. Acetone was supplied from RCI Labscan, Bangkok, Thailand.
4. Acid terminated poly (D, L-lactide) (PDLLA) with average MW of 15,000 was purchased from Sigma Aldrich, St. Louis, United State for using in the surface grafting reaction with CW. The chemical structure of PDLLA was shown in Figure 3.1

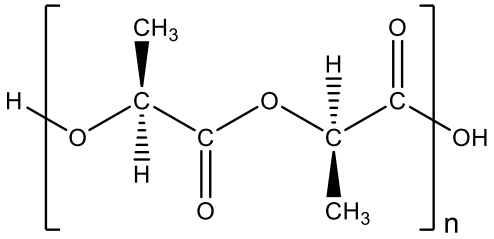

Figure 3.1 Chemical structure of acid terminated PDLLA.

5. *N*-(3-dimethylaminopropyl)-*N'*-ethyl carbodiimide hydrochloride (EDC.HCl) purum, ≥98.0% was purchased from Sigma Aldrich, St. Louis, United State for using as coupling agent in the grafting reaction. The chemical structure of EDC.HCl was shown in Figure 3.2

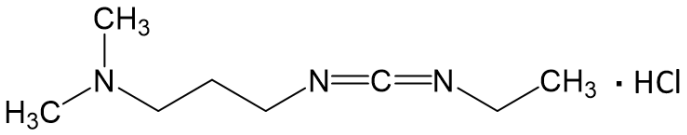

Figure 3.2 Chemical structure of EDC.HCl.

6. *N*-hydroxysuccinimide (NHS) 98+%, Alfa Aesar was purchased from Thermo Fisher Scientific, Heysham, Lancashire LA3 2XY, United Kingdom to use as proton donor in the grafting reaction. The chemical structure of NHS was shown in Figure 3.3

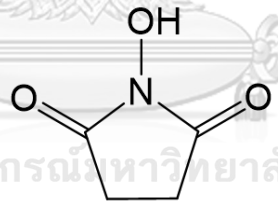

Figure 3.3 Chemical structure of NHS.

3.3 Equipment and Analytical Instruments

1. Flat Film and Sheet Chill Roll Lines, Model LE25-30/C, Labtech Engineering Company Ltd., Thailand
2. Fourier Transform Infrared Spectrometer (FT-IR), Nicolet 6700, Thermo scientific, Germany
3. Fourier Transform Nuclear Magnetic Resonance Spectrometer 400 MHz. (Solid) (NMR 400 MHz.), Bruker Avance III HD, Germany
4. X-ray diffractometer (XRD), Bruker AXS D8 Advance, England

5. Transmission Electron Microscope (TEM), Hitachi H-7650, Japan
6. Scanning Electron Microscope (SEM), JEOL JSM-6480LV, Japan
7. Differential Scanning Calorimeter (DSC), Mettler Toledo, Model DSC1, United State
8. Polarized light optical microscope (POM), ECLIPSE LV100NDA, Nikon, China
9. Hot stage, LPN95, LINKAM scientific instrument LTD., United Kingdom
10. Vortex mixer GENIE 2, G-560E, Scientific Industries INC., Bohemia, New York, United State
11. Derui Ultrasonic Cleaner, DR-MH60, Shenzhen Derui Ultrasonic Equipment Co., Ltd, Shenzhen, China

3.4 Experiment

3.4.1. Preparation of chitin whisker

Chitin flake was hydrolyzed by 3N HCl at boiling temperature (approximately 102 °C) under reflux with vigorous stirring for 6 h. The ratio of chitin to HCl was 1 g/30mL. Afterward, the chitin suspension was immediately diluted with deionized water to inhibit the reaction and then washed and centrifuged several times until its neutral. The suspension was subsequently freeze-dried to obtain CW.

3.4.2. Preparation of grafted chitin whisker

This step, two solutions was prepared under stirring using 30 mL of DMF as solvent. The first one was the solution of 0.75 g (0.05 mmol) of PDLLA, 19.08 mg (0.10 mmol) of coupling agent and 11.46 mg (0.10 mmol) of proton donor. The other was 0.5 g (4.98 equivalent mmol) of CW suspended in 30 mL of DMF. The first solution was added to CW suspension under ice bath (approximately 0°C) for 30 min. Then the reaction was performed at room temperature for 24 h. Next, the mixture was poured into 30 mL of acetone in order to stop the reaction. The solution was centrifuged to separate grafted chitin whisker (PLA-g-CW) and rinsed several times with DMF to remove unreacted PDLLA followed by washed with acetone to get rid of DMF solvent before leave PLA-g-CW dried under vacuum at room temperature. Then, the white

powder of PLA-g-CW was obtained. The synthetic scheme of PLA-g-CW was illustrated in Figure 3.4

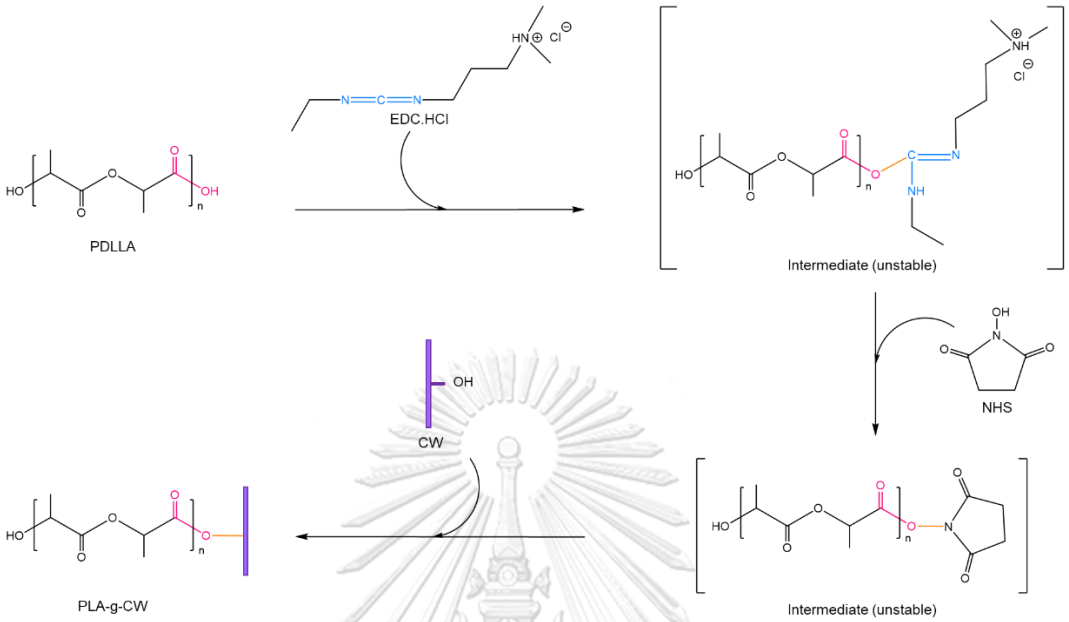

Figure 3.4 Scheme of surface chemical grafting reaction of PLA-g-CW

3.4.3. Preparation of nanocomposite film

The PLA nanocomposite films with the addition of 0.1-0.3 phr of CW and PLA-g-CW were fabricated by melt casting process using single screw extruder. The compounds were dried at 90 ºC for 30 min to remove moisture before mixed together in the zip-lock bag followed by feed into the hopper. The temperature profile from feed zone to slit die was increasing from 180 ºC to 205 ºC with the screw speed of 12 rpm. The extruded films were cooled on chill roll to room temperature after out of die. The neat PLA film was also produced at the same condition to use as reference. The process condition and the formulation of film was given in Figure 3.5 and Table 3.1, respectively.

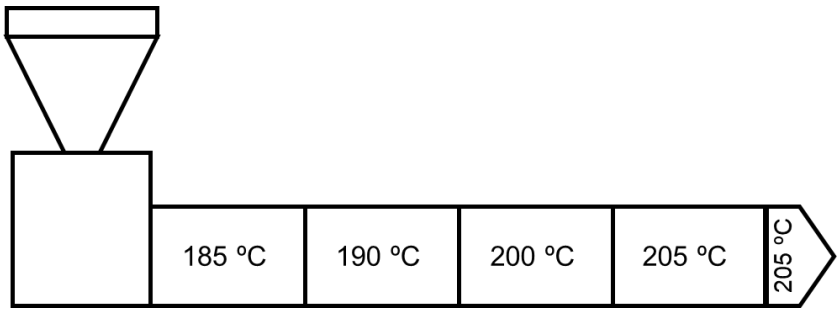

Figure 3.5 Process condition from feed zone to die zone.

Table 3.1 Composition of film materials (g)

Film materials	PLA	CW	PLA-g-CW
Neat PLA	100	-	-
PLA/CW0.1	100	0.1	-
PLA/CW0.2	100	0.2	-
PLA/CW0.3	100	0.3	-
PLA/PLA-g-CW0.1	100	-	0.1
PLA/PLA-g-CW0.2	100	-	0.2
PLA/PLA-g-CW0.3	100	-	0.3

3.5 Characterization

3.5.1. Characterization of whisker

Morphological properties and the dispersion of CW compared with PLA-g-CW were observed using TEM. The CW and PLA-g-CW samples were diluted about 0.01 %(w/v) with deionized water and stirred for 24 h to prepare the suspension. Then, the vibration using vortex mixer was applied to the suspension which subsequently dropped onto the carbon coated copper grid and left until dry in the desiccator before characterized. For the PLA-g-CW suspension, the ultrasonication was also applied for preparing individual whiskers for 5 min. TEM was performed with 100 kV acceleration voltage. The micrograph images were reported at the magnification of 2,000× and

calculated the diameter, length and aspect ratio of individual whiskers using ImageJ software (National Institutes of Health, NIH).

XRD was conducted to investigate the characteristic diffraction pattern of CF, CW and PLA-g-CW with Cu $K\alpha_1$ radiation in the scattering range (2θ) of 5°-60° and steps of 0.02°. The crystallinity indexes (CrI_{hkl}) were calculated according to Zhang, Y et al. as follow in equation (1) [81].

$$\%CrI_{hkl} = \frac{I_{hkl}-I_{am}}{I_{hkl}} \times 100 \quad (1)$$

Where I_{hkl} represents the intensity of peak at 2θ which corresponded to (hkl) plane and I_{am} stand for the intensity of amorphous diffraction at about 16 °

The functional groups before and after surface grafting were determined by FT-IR. The dried samples including CW and PLA-g-CW were compressed into KBr pellets and tested in the range of 500–4000 cm^{-1} with resolution of 16 and the number of scans at 64.

The structure of the CW and PLA-g-CW were also characterized by solid state cross-polarization/magic angle spinning (CP/MAS) ^{13}C-NMR (400 MHz) using an ASCEND 400WB Bruker spectrometer (Bremen, Germany). ^{13}C-NMR spectrometer resonates at frequency of 100 MHz, 3600 scans. The contact and delay times were set at 2 ms and 3 s, respectively.

3.5.2. Characterization of nanocomposite films

Surface morphology of nanocomposite films was inspected by SEM with 10 kV of beam accelerating voltage and the magnification of 10,000×. The film samples were mounted to carbon tape which attached to specimen holders and coated with gold before observation.

The thermal properties and non-isothermal crystallization were investigated using DSC under nitrogen atmosphere with heating and cooling rate at 5 °C/min. 5-10 mg of samples were heated from 25 °C to 200 °C and held for 5 min to remove thermal history. Samples were subsequently cooled to 25 °C followed by heated to 200 °C

and held at the same temperature for 5 min. The degree of crystallinity ($\%\chi_c$) was calculated according to Li, C. et al. [31] as follow in equation (2)

$$\%\chi_c = \frac{\Delta H_m}{\Delta H_f} \times \frac{1}{w} \times 100 \quad (2)$$

Where ΔH_m and ΔH_f were defined as the enthalpy of melting and the theoretical enthalpy of 100% crystalline polymer, respectively. w stands for weight fraction of polymer. ΔH_f was considered at 93 J/g for PLA [31].

The isothermal crystallization behavior was observed by POM using the magnification of 200×. The dried samples were melted and compressed between glass cover slips before moving to the hot stage. Then samples were heated to 200 ºC with the rate of 40 ºC/min and held for 2 min to remove the thermal history before cooled to 110 ºC and 120 ºC for 30 min and 60 min, respectively with the rate of 5 ºC/min. The optical micrographs were immediately captured when crystallization temperature was reached every 60 s.

3.6 Experimental flowcharts

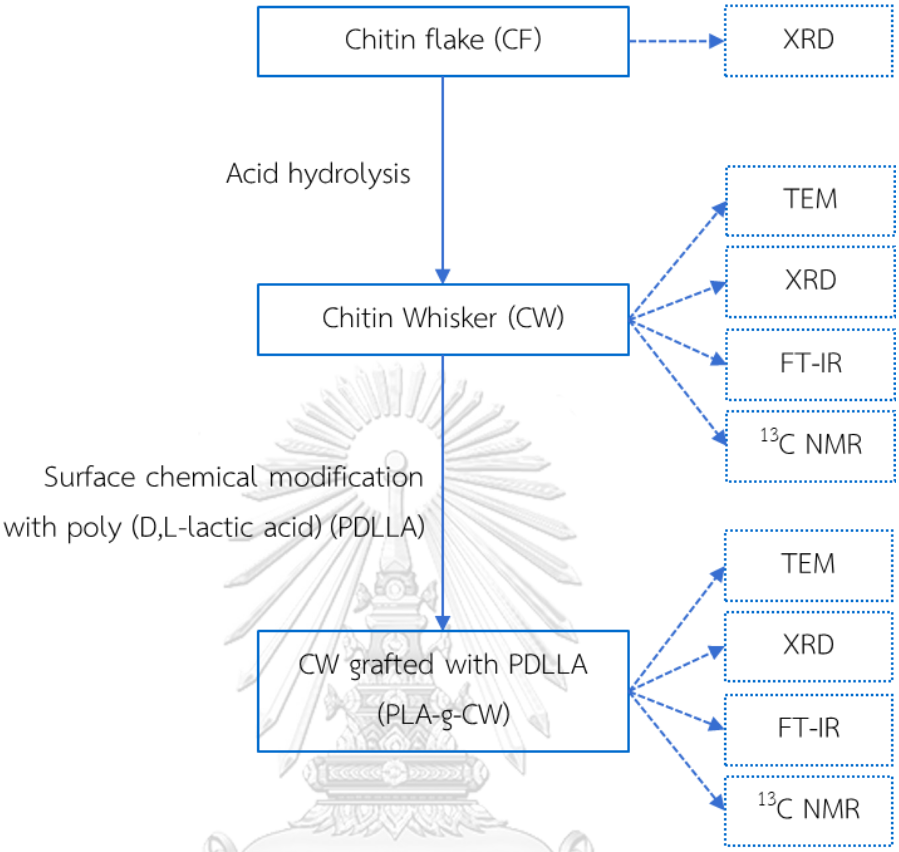

Figure 3.6 Scheme of preparation and characterization of CW and PLA-g-CW.

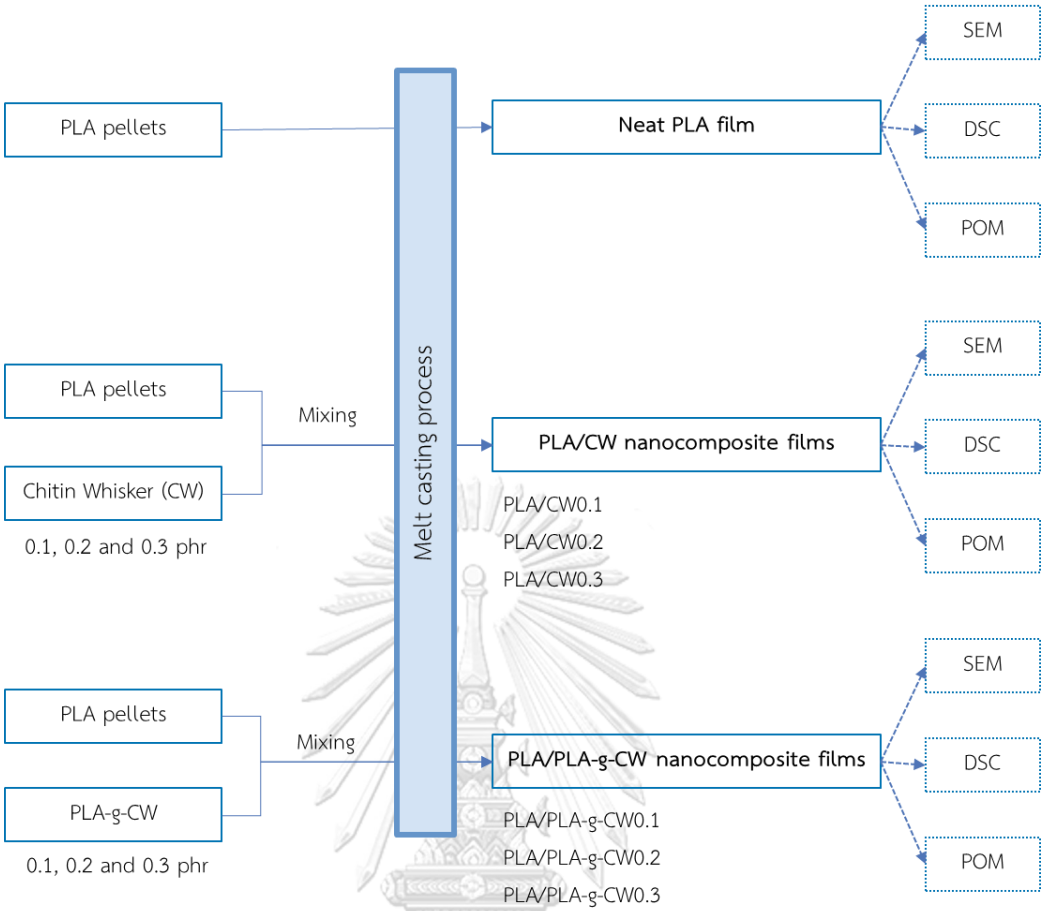

Figure 3.7 Scheme of preparation and characterization of PLA nanocomposite films.

CHAPTER 4
RESULTS AND DISCUSSIONS

The aim of this work was to improve the crystallization behavior of PLA. The CW was selected to be nucleating agent because of its high crystallinity with high surface area to volume [31, 32]. However, the CW tend to agglomerate in the matrix of PLA due to the hydrophobicity of PLA. Because of CW agglomeration, this work was starting from the surface chemical modification of CW with acid terminated PDLLA through coupling reaction using EDC.HCl as coupling agent and NHS as proton donor. The XRD also performed to investigate the crystallinity of CF, CW and PLA-g-CW. In addition, to confirm that grafting reaction was success, CW and PLA-g-CW were characterized by FT-IR and ^{13}C NMR. The dispersion of CW and PLA-g-CW in water was investigated by TEM.

4.1 Extraction and surface chemical modification of chitin whisker

4.1.1. Identification of PLA-g-CW using FT-IR

Figure 4.1 shows the characteristic set of FT-IR spectra of CW comparing with PLA-g-CW. The original CW shows the IR absorption range which assigned to the specific vibration of O-H stretching, N-H stretching, C=O stretching of acetyl group of amide I band (overlapped with N-H bending) and amide II at wavenumber of 3400, 3260, 1660 and 1560 cm^{-1}, respectively. These vibration signal corresponded to the characteristic molecules on the **α**-chitin structure which reported by several articles [31, 32, 81-83]. The double peaks of amide I at around 1660 cm^{-1} and 1630 cm^{-1} appeared only for **α**-chitin whereas this vibration signal of **β**-chitin appeared as single peak [83]. For the PLA-g-CW, the absorption spectra were similar to CW except for the appearing of absorption peak at wavenumber of 1750 cm^{-1} which related to the vibration of ester carbonyl group on PDLLA. The occurrence of this vibrational peak also caused by the reaction between the hydroxyl groups of CW and the carboxyl groups of PDLLA though esterification making the ester carbonyl linked between two molecules, indicated the PDLLA that grafted onto surface of CW.

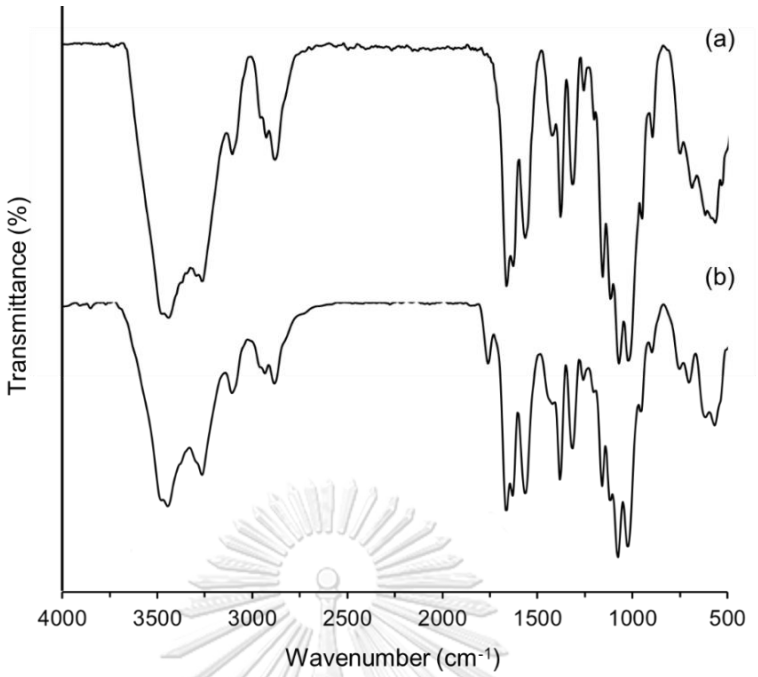

Figure 4.1 FT-IR spectra of CW (a) and PLA-g-CW (b).

4.1.2. Identification of PLA-g-CW using solid state ^{13}C NMR

In order to reassure that PDLLA was successfully grafted onto surface of CW, solid state ^{13}C NMR was used. Figure 4.2 (a) shows the resonance peak C1-C6 on the units of CW at 103, 55, 73, 83, 76, 60 ppm, respectively. The signal at 173 and 23 ppm attributed to the carbonyl and methyl on acetamido group (C7-C8) according to Li, C. et al. [31]. For the PLA-g-CW in Figure 4.2 (b), the resonance peak at about 15 ppm was appeared which corresponed to the CH_3 at chain end of PDLLA [31]. In addition, nearly C6 and C7 existed the hidden peaks of carbonyl (α') and carbon (β') on PDLLA chain end. These results point out to the success of surface grafting with PDLLA.

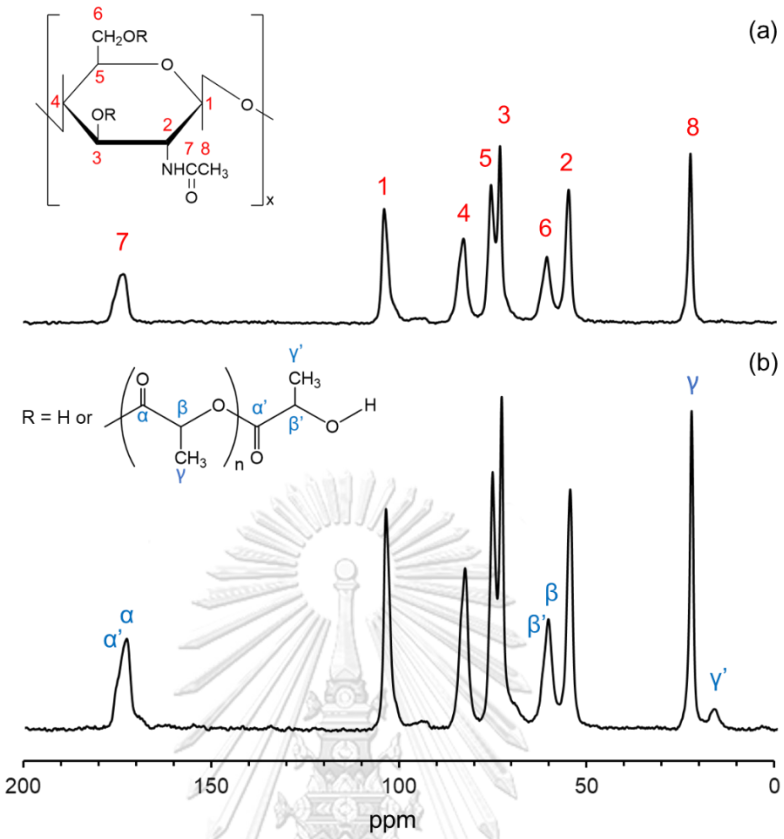

Figure 4.2 Solid state ^{13}C NMR spectra of the CW (a) and the PLA-g-CW (b).

4.1.3. Crystallinity indexes (CrI_{hkl}) from XRD

The XRD was performed to inspect the crystallinity indexes of chitin samples including CF, CW and PLA-g-CW. The diffractogram in the 2**θ** range of 5-50° which was presented in Figure 4.3 shows no different in the characteristic diffraction peak of **α**-chitin located at approximate to 2**θ** of 9.5 ° and 19.5° which related to (020) and (110) plane, respectively, as described by Zhang, Y. et al. [81]. However, the peak intensity of CW was significantly higher than CF caused by the acid hydrolysis eliminated amorphous parts in the CF structure. Thereby, the remaining crystalline domains affected the obvious appearing of peak located at 21°, 23° and 26° corresponded to (120), (101) and (130) plane, respectively [81]. The crystallinity indexes at 2**θ** of 9.5 °and 19.5° (CrI_{020} and CrI_{110}) were listed in Table 4.1. In case of PLA-g-CW, the angle of diffraction peak was similar to CW indicated that the distance of interlayer in CW crystalline was not changed due to the grafting reaction only took place on the surface

of whiskers [31]. As comparing with CW, the CrI_{020} and CrI_{110} of PLA-g-CW were slightly declined which might be described that surface of crystalline CW was destroyed during grafting with PDLLA.

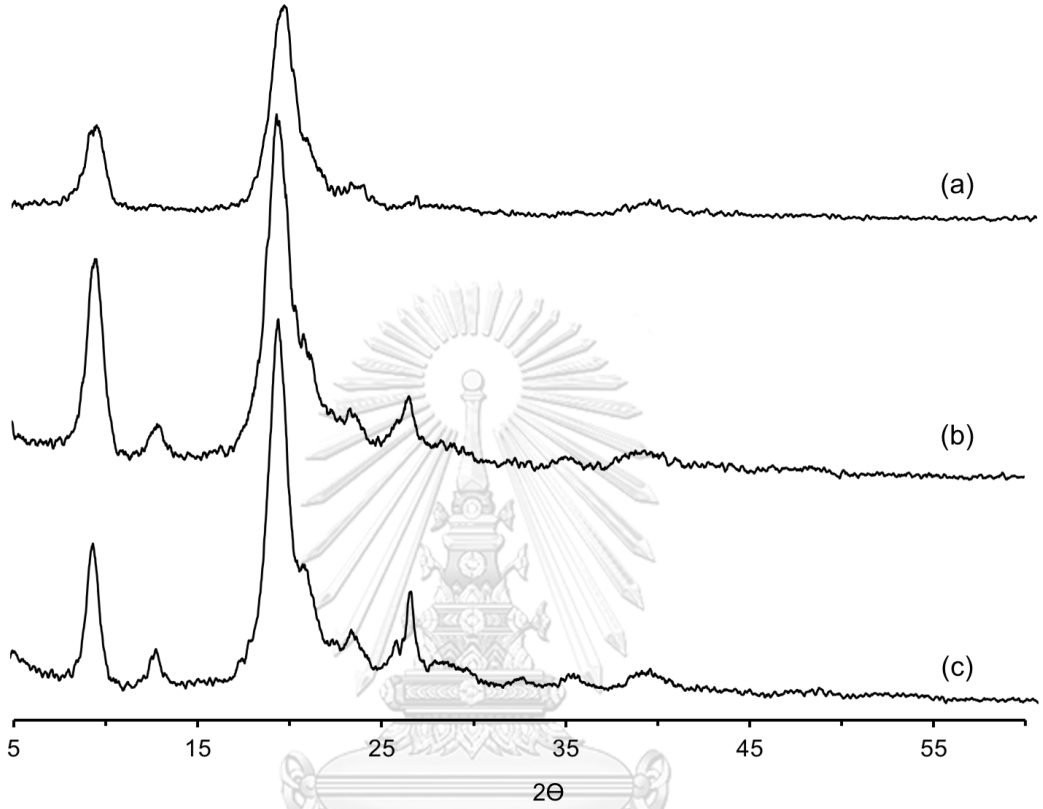

Figure 4.3 X-ray diffraction pattern of CF (a) CW (b) and PLA-g-CW (c).

Table 4.1 Crystallinity indexes (CrI_{hkl}) calculated from XRD

Samples	CrI_{020} (%)	CrI_{110} (%)
CF	80.98	90.06
CW	87.06	97.91
PLA-g-CW	83.76	94.31

4.1.4. Morphological properties of chitin whisker

Figure 4.4 (a-b) displays TEM images of CW and PLA-g-CW which dispersed in water using vortex mixer. The CW showed good dispersion in water and exhibited the rod-like shape in nano-scale. The length, diameter and aspect ratio of individual CW, which measured using ImageJ software, was approximate to 337 nm, 26 nm and 14 nm, respectively. On the other hand, PLA-g-CW showed the different behavior. It appeared a tendency to agglomerate into larger dimension which difficult to measure the dimension of individual whisker. This might hypothesize that each of individual whiskers was aggregated and rearranged into the bundle-liked due to the increasing of hydrophobicity after grafting with PDLLA. Figure 4.5 represents a hypothesis of PLA-g-CW which dispersed in water. In order to measure its dimension, the ultrasonication was applied to individualization of PLA-g-CW for 5 min. The dimension of individual CW and PLA-g-CW in water was listed in Table 4.2 and the dispersion of PLA-g-CW in water after ultrasonication was shown in Figure 4.4 (c). The PLA-g-CW exhibited the average length similar to CW whereas the average diameter was smaller. So, the aspect ratio of PLA-g-CW was higher than CW. The decreasing of diameter might be caused by the grafting with PDLLA on the whiskers surface. However, the sonicated PLA-g-CW showed some agglomeration comparing with CW.

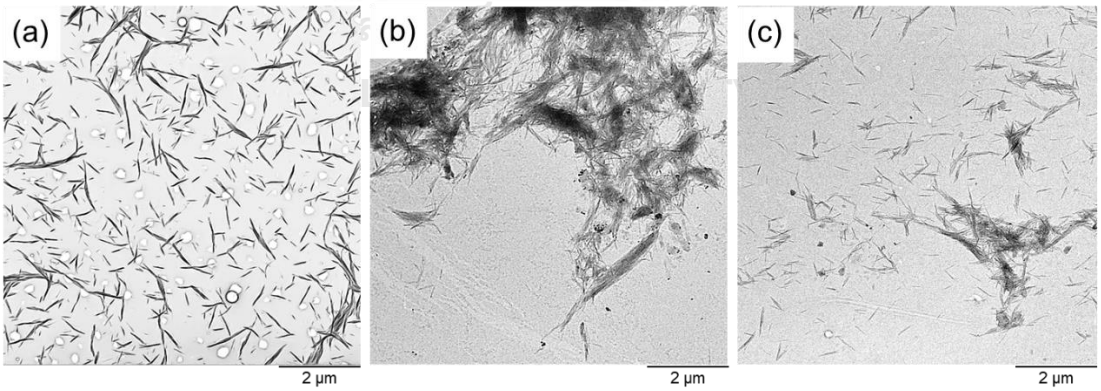

Figure 4.4 TEM micrograph images for CW (a) and PLA-g-CW (b) in water with applied vortex mixing and PLA-g-CW (c) in water with applied ultrasonication at the magnification of 2,000×.

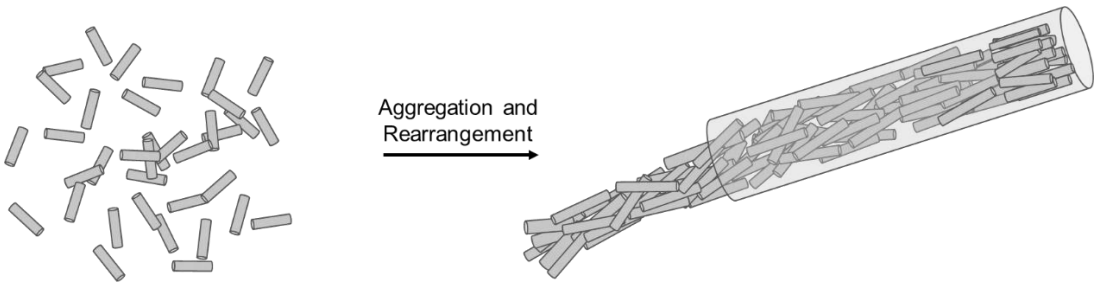

Figure 4.5 Assumption of PLA-g-CW rearrangement in water.

Table 4.2 Average dimension of individual CW and PLA-g-CW in water

Sample	Length (nm)	Diameter (nm)	Aspect ratio (nm)
CW	337.39±140.88	26.29±7.43	13.60±6.64
PLA-g-CW	337.85±141.51	16.63±9.30	24.06±12.45

4.2 Characterization of nanocomposite films

This step, the neat PLA and nanocomposite containing CW and PLA-g-CW were fabricated into film by melt casting process with the average thickness of 0.1 mm in order to investigate the effect of whisker on thermal and crystallization properties of PLA. The film thickness was listed on Table 4.3.

Table 4.3 Average thickness of film samples (mm)

Film samples	Average thickness
Neat PLA	0.091±0.012
PLA/CW0.1	0.109±0.029
PLA/CW0.2	0.113±0.026
PLA/CW0.3	0.098±0.020
PLA/PLA-g-CW0.1	0.092±0.012
PLA/PLA-g-CW0.2	0.101±0.028
PLA/PLA-g-CW0.3	0.104±0.033

4.2.1. Morphological properties of nanocomposite films

The morphological properties of nanocomposites comparing with neat PLA film were observed by SEM at the magnification of 10,000× which shown in Figure 4.6. The area of particles, which calculated using ImageJ software, were listed on Table 4.4. These images showed a surface of nanocomposite which was rougher than neat PLA due to the introduction of CW and PLA-g-CW. However, there was no phase separation between PLA matrix and the whiskers. Comparing in the group of PLA/CW nanocomposite films, the whiskers tended to agglomerate with the increasing of whisker content from 0.1-0.3 phr. The PLA/CW0.1 nanocomposite showed the smallest size of particle on the surface at around 108 nm. According to a group of PLA/PLA-g-CW nanocomposites, the particle size of PLA-g-CW was decreased comparing to CW by the reason of the surface grafting with PDLLA leading to more compatibility between chitin nanoparticles and PLA matrix. Hence, the film surface showed better dispersion and less agglomeration of whiskers especially at 0.1 phr. Despite the particle size of PLA-g-CW was larger when the amount of it was increased similar to a group of PLA/CW, it remains smaller than CW group at the same composition. However, the dispersion of whisker in PLA matrix contrasted with its dispersion in water, which observed by TEM in previous results. The nanoparticles aggregation in water caused by the increasing of hydrophobicity of CW after grafted with PDLLA. Therefore, PLA-g-CW showed more dispersion in the hydrophobic PLA matrix.

Table 4.4 Average particle size of whisker in PLA matrix

Film sample	Average size (nm^2)	Film sample	Average size (nm^2)
PLA/CW0.1	107.66±51.23	PLA/PLA-g-CW0.1	58.08±32.68
PLA/CW0.2	513.35±417.58	PLA/PLA-g-CW0.2	236.26±153.96
PLA/CW0.3	672.23±607.36	PLA/PLA-g-CW0.3	323.58±279.80

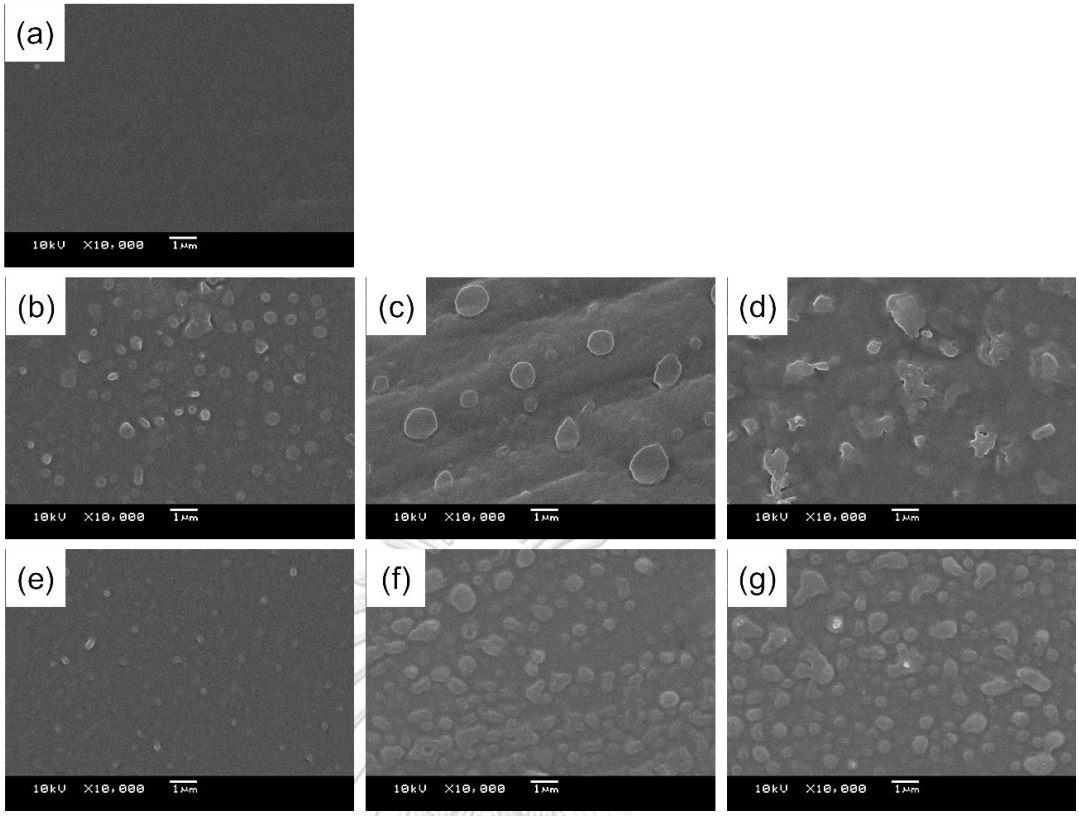

Figure 4.6 Micrograph images of film samples at the magnification of 10,000× for neat PLA (a) PLA/CW0.1 (b) PLA/CW0.2 (c) PLA/CW0.3 (d) PLA/PLA-g-CW0.1 (e) PLA/PLA-g-CW0.2 and (f) PLA/PLA-g-CW0.3 (g).

4.2.2. Thermal and crystallization properties of nanocomposite films

The effect of CW and PLA-g-CW on the non-isothermal crystallization of PLA were investigated by DSC. Figure 4.7 represents the crystallization behavior during cooling from 200 °C to 25 °C after removing thermal history with rate of 5 °C/min. As listed in Table 4.5 and shown in Figure 4.7 (a), neat PLA exhibited the exothermic curve of crystallization at about 110 °C and the peak area which refer to the enthalpy of crystallization (ΔHc) of 0.04 J/g. The PLA/CW nanocomposites in Figure 4.7 (b-d) showed dissimilar results at content of CW from 0.1 phr to 0.3 phr.

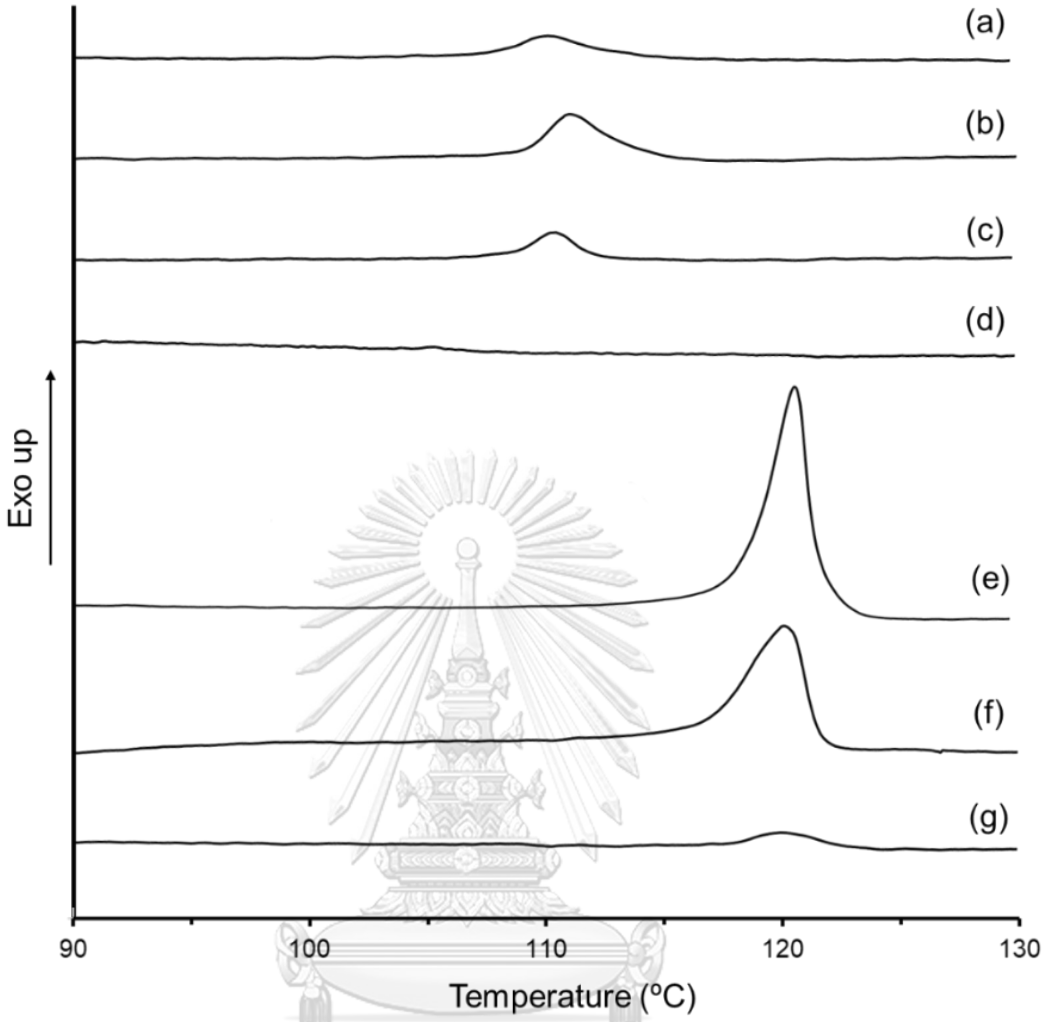

Figure 4.7 DSC thermograms at cooling scan of neat PLA (a) PLA/CW0.1 (b) PLA/CW0.2 (c) PLA/CW0.3 (d) PLA/PLA-g-CW0.1 (e) PLA/PLA-g-CW0.2 (f) and PLA/PLA-g-CW0.3 (g).

Table 4.5 Data of thermal transition temperature, enthalpy and degree of crystallinity (χ_c) which inspected and calculated from DSC for the film samples.

Samples	T_g (°C)	T_c (°C)	ΔH_c (J/g)	T_{cc} (°C)	ΔH_{cc} (J/g)	T_{m1} (°C)	T_{m2} (°C)	$-\Delta H_m$ (J/g)	χ_c (%)
Neat PLA	61.9	110.2	0.07	121.2	17.99	150.8	-	18.59	19.99
PLA/CW0.1	61.8	111.2	0.17	118.2	23.11	150.0	-	28.04	30.18
PLA/CW0.2	61.9	110.9	0.08	120.5	22.22	151.1	-	22.76	24.52
PLA/CW0.3	61.7	-	-	120.2	22.28	150.7	-	24.71	26.65
PLA/PLA-g-CW0.1	61.1	120.4	0.73	111.2	39.54	148.4	155.6	41.77	44.96
PLA/PLA-g-CW0.2	61.9	119.7	0.47	117.2	27.36	149.9	-	28.45	30.65
PLA/PLA-g-CW0.3	61.7	120.1	0.05	116.6	27.71	149.9	-	27.73	29.91

For the first one, the crystallization peak of PLA/CW0.1 nanocomposite slightly shifted to higher temperature at about 1 °C with the increasing of ΔH_c approximate to 0.10 J/g. PLA/CW0.2 showed similar T_c and ΔH_c comparing with neat PLA. At the composition of 0.3 phr of CW, ΔH_c was disappeared from the DSC thermograms. These results displayed the heterogeneous nucleation effect of CW, especially at 0.1 phr of CW. However, this effect was decreased at higher CW contents from 0.2-0.3 phr.

These trends also happened in the case of PLA/PLA-g-CW nanocomposites, which represented in Figure 4.7 (e-g), indicated that the ΔH_c was diminished with the rising of PLA-g-CW contents. These behaviors might be caused by more agglomerate at the higher number of whiskers restricted the crystallization of PLA. However, the ΔH_c of PLA-g-CW was significantly higher than PLA/CW at the same composition and clearly shown in the case of 0.3 phr of whiskers that appeared the crystallization peak after grafted with PDLLA.

In addition, there was not only the increasing in ΔH_c, but the crystallization temperature (T_c) also considerably raised to about 120 °C which ascribed by the better dispersion of PLA-g-CW improved the heterogeneous nucleation effect of CW [31, 32]. The nucleating effect was observed as an increase in crystallization temperature at a constant cooling rate. It was considerably influenced by the degree of dispersion of the nucleating agent [84]. These indicated that PLA-g-CW accelerated the

crystallization of PLA which was subjected to less agglomeration of whiskers observed by SEM. Although, the T_c of PLA/PLA-g-CW nanocomposite films were approximate to each other, the PLA-g-CW0.1 nanocomposite is the most effective nucleating agent comparing to the other due to T_c and the highest ΔH_c.

Table 4.5 and Figure 4.8 shows non-isothermal behavior at second heating scan. All samples exhibited the glass-transition temperature (T_g), exothermic peak of cold-crystallization and endothermic peak of melting. The addition of CW and PLA-g-CW did not influence to T_g of PLA which was approximately 62 ºC due to the small number of whiskers. The cold-crystallization temperature (T_{cc}) and melting temperature (T_m) of neat PLA were 121 ºC and 151 ºC, respectively. In case of PLA/CW nanocomposites, the T_m for this sample group was similar to a reference. The T_{cc} of PLA/CW0.1 was slightly decreased about 3 ºC whereas the other shown no different from neat PLA. Nevertheless, the enthalpy of cold-crystallization (ΔH_{cc}) of PLA/CW nanocomposites was higher than neat PLA.

The addition of CW at 0.1-0.3 phr exhibited the ΔH_{cc} at approximate to 23 J/g, 22 J/g and 22 J/g, respectively. These results reflected that the increasing of CW caused the decreasing of ΔH_{cc} which related to the previous investigation. Considering the degree of crystallinity which denoted as χ_c, the PLA/CW nanocomposites showed the χ_c values higher than neat PLA around 10.19%, 4.53% and 6.66% for PLA/CW0.1, PLA/CW0.2 and PLA/CW0.3, respectively. The amount of CW from 0.2-0.3 phr brought about the decrement of crystallinity of composite owing to their agglomeration confined the chain mobility during crystallization, associated with results of ΔH_c and ΔH_{cc}. Moreover, the dispersion of CW at 0.2 phr in PLA matrix, which observed from SEM, was not uniform leading to the lowest χ_c value. However, the crystallization rate of PLA was enhanced with the addition of CW.

For a group of PLA/PLA-g-CW in Figure 4.8 (e-f), the T_{cc} of all samples was obviously declined to lower temperature. The PLA/PLA-g-CW0.1 particularly showed the lowest T_{cc} at about 111.2 ºC which far from neat PLA for 10 ºC. The T_{cc} of PLA/PLA-g-CW0.2 was approximate to PLA/PLA-g-CW0.3, which lower than neat PLA around 4 ºC. In case of ΔH_{cc}, the addition of PLA-g-CW led to the higher values of ΔH_{cc} compared

with neat PLA. The PLA-g-CW0.1 exhibited the highest ΔH_{cc} close to 40 J/g whereas after 0.1 phr, the nanocomposites showed a tendency to decreased in ΔH_{cc}. The ΔH_{cc} of the PLA/PLA-g-CW0.2 was as high as PLA/PLA-g-CW0.3 at around 27 J/g. The cold-crystallization generally appeared when polymer cannot completely self-crystallize under previous too fast cooling. At the critical temperature which higher than T_g but lower than T_m, the amorphous chains have more mobility to crystallize and generate the more perfect crystal. Hence, the decreasing of T_{cc} and the increasing of ΔH_{cc} corresponded to the improvement of crystallization behavior of polymer [14, 77]. The incorporation of PLA-g-CW, showed more efficiency comparing to CW, indicating that grafting with PDLLA improved the potential of CW in a role of nucleating agent. Furthermore, the results confirmed that PLA/PLA-g-CW0.1 revealed the most effective nucleating agent for PLA because of the lowest T_{cc} and highest ΔH_{cc}.

In case of the endothermic peak of melting, Samples in a group of PLA/PLA-g-CW showed T_m approximately the same as that of neat PLA at around 150 ºC. Only PLA/PLA-g-CW0.1 evidently appeared double melting peaks at about 148 ºC and 156 ºC. The multi-melting peaks at lower and higher temperature denoted as T_{m1} and T_{m2}, respectively. The double melting behavior might be attributed to the existence of two crystal populations with different from each other in term of size or levels of perfection that has been reported in many literatures [11, 14, 80, 85-90]. These crystals involve the **α**'-crystal (the disordered crystal) and **α**-crystal (the ordered crystal) which transformed from **α**'-crystal into more perfect **α**-crystal [11, 85]. The low endothermic peak (T_{m1}) corresponded to the melting of secondary crystals or imperfect **α**'-crystal, which formed during the initial phase of cold-crystallization. The high endothermic peak (T_{m2}) associated with the melting of more perfect crystals or the larger lamellae thickness, which were the primary crystals, or the crystals formed during the latest phase of cold-crystallization [14]. Therefore, the presence of melting peak at higher temperature displayed the improvement of crystalline structure of PLA by the addition of PLA-g-CW at 0.1 phr. In fact, the nanocomposites of PLA/PLA-g-CW at 0.2 phr and 0.3 phr also appeared the double melting behavior but they did not obviously separate from each other. These might be associated to the other results and the dispersion of

whiskers in PLA matrix which restricted the chain mobility and limited space for crystallization. The χ_c of nanocomposites with 0.1-0.3 phr of PLA-g-CW showed a tendency to decrease with the increasing of PLA-g-CW contents. However, the nanocomposites exhibited the higher χ_c comparing to the neat PLA.

All of DSC results demonstrated that PLA-g-CW played a crucial role as nucleating agent of PLA due to it reduced the energy barrier of crystallization and increased the nuclei density of PLA. Hence, the crystallization rate of PLA was accelerated. Especially, PLA-g-CW0.1 at 0.1 phr generated the highest χ_c and showed a great efficient nucleating agent than the others based on the results of T_c, T_{cc} ΔH_c, ΔH_{cc} and well-dispersion in PLA matrix observed by SEM.

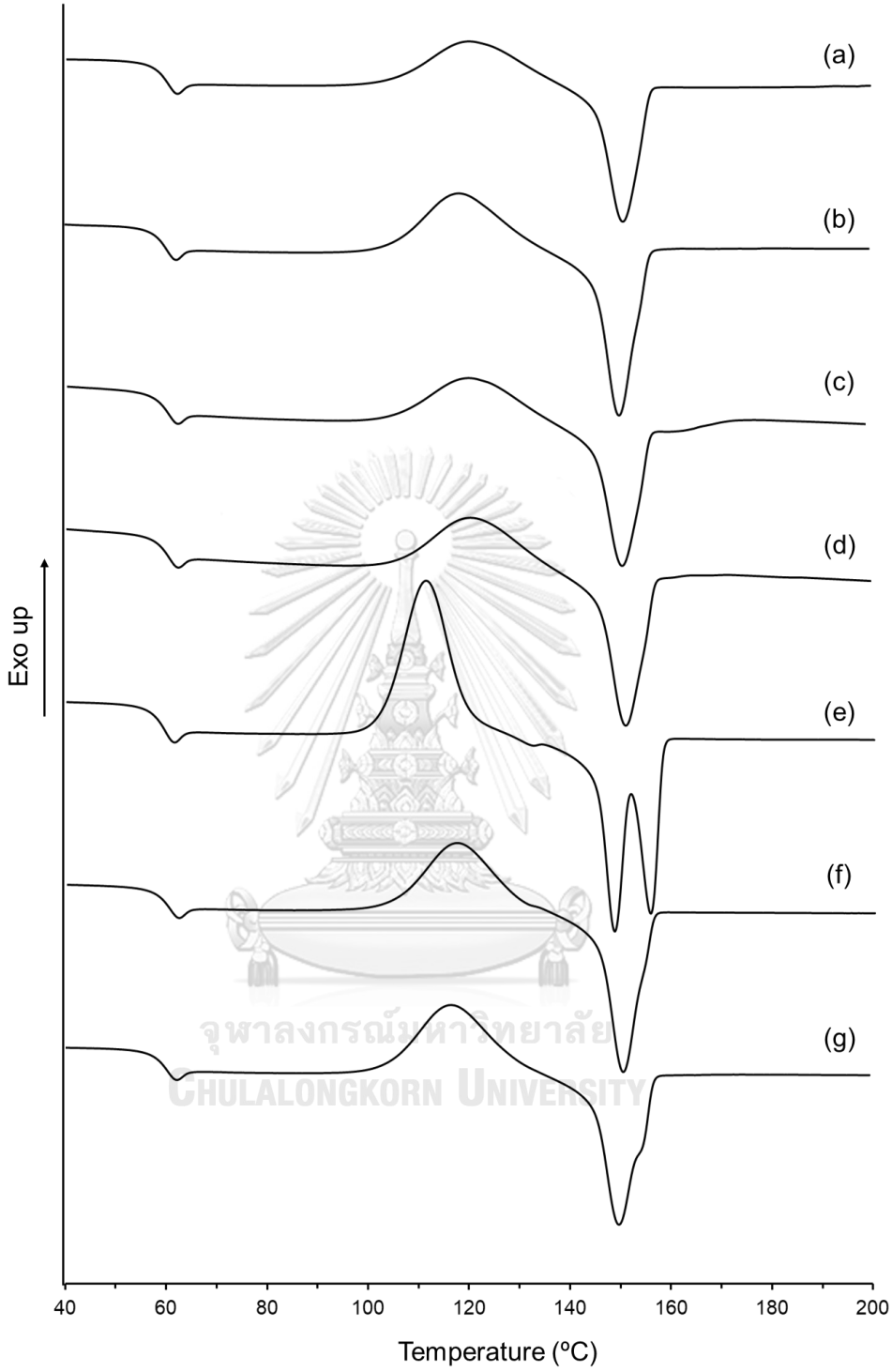

Figure 4.8 DSC thermograms at second heating of neat PLA (a) PLA/CW0.1 (b) PLA/CW0.2 (c) PLA/CW0.3 (d) PLA/PLA-g-CW0.1 (e) PLA/PLA-g-CW0.2 (f) and PLA/PLA-g-CW0.3 (g).

4.2.3. Isothermal crystallization behavior of nanocomposite films

The isothermal crystallization behavior of neat PLA and the nanocomposites was observed under polarized light optical microscope (POM). The samples were melted and compressed between glass cover slip and then heated on hot stage to eliminate heat history. The sample subsequently cooled down to 110 °C and 120 °C with the rate of 5 °C/min and maintained at that temperature for 30 min and 60 min, respectively. The POM images which were captured every 60s until the temperature reached to 110 °C and 120 °C were presented in Figure 4.9 and Figure 4.10, respectively.

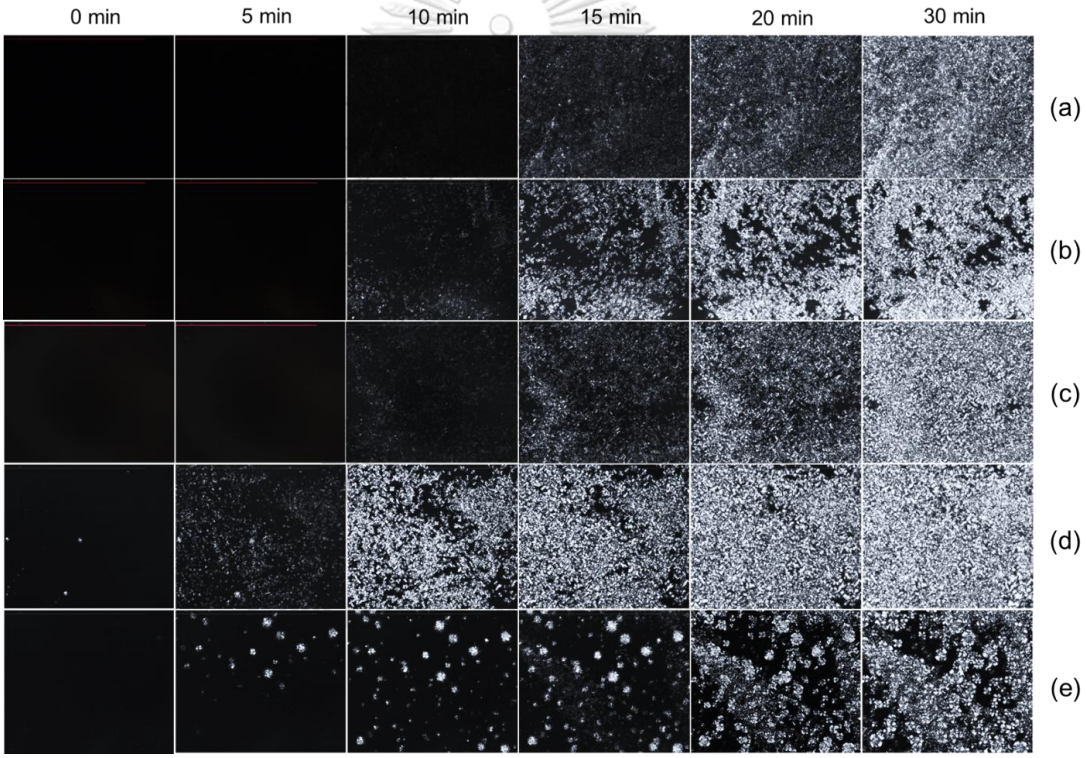

Figure 4.9 POM micrographs of isothermal crystallization for neat PLA (a) PLA/CW0.1 (b) PLA/CW0.3 (c) PLA/PLA-g-CW0.1 (d) PLA/PLA-g-CW0.3 (e) which the melt was cooled to 110 °C.

According to the crystallization at 110 °C, the neat PLA lightly appeared the spherulite at about 15 min left and the nuclei density quite low whereas the nanocomposites presented the spherulite at 10 min for a group of PLA/CW and at the beginning of captured time (0 min) for a group of PLA/PLA-g-CW. These confirmed that

the crystallization rate of PLA was accelerated by CW and PLA-g-CW. The PLA/PLA-g-CW0.1 specially showed the most intense of spherulite at only 10 min at 110 °C. However, it was difficult to identify the growth rate of spherulite at this temperature. The investigation at 120 °C was done in order to compare the rate of spherulite growth.

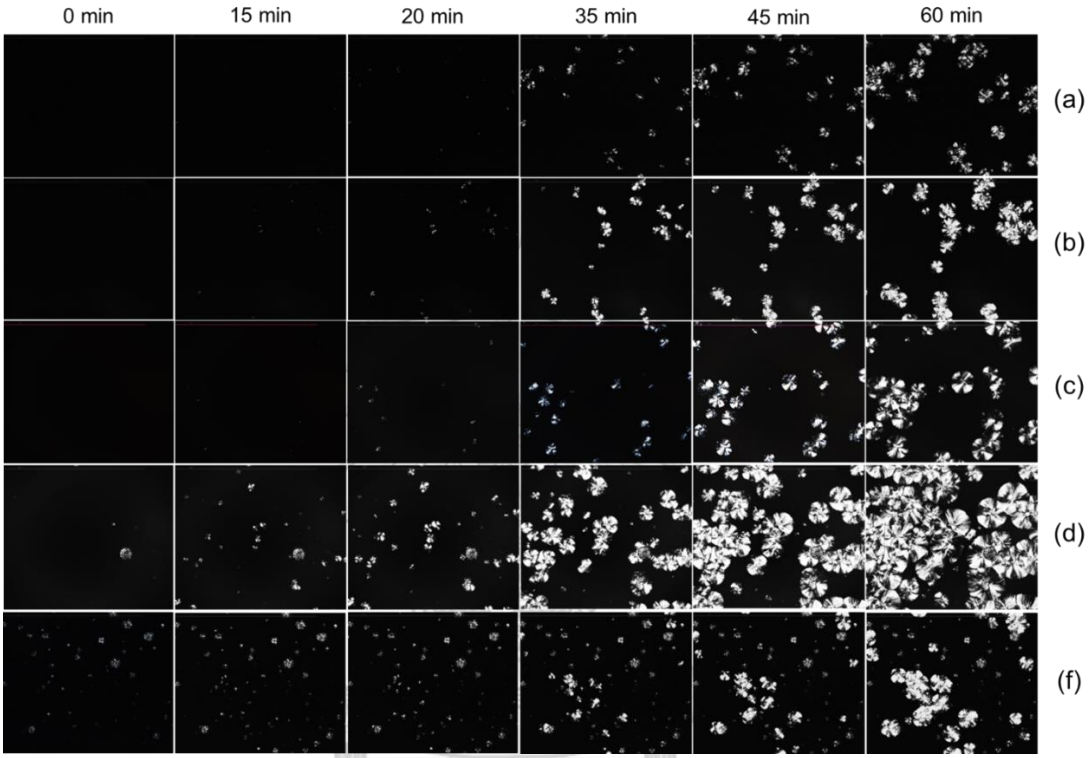

Figure 4.10 POM micrographs of isothermal crystallization for Neat PLA (a) PLA/CW0.1 (b) PLA/CW0.3 (c) PLA/PLA-g-CW0.1 (d) PLA/PLA-g-CW0.3 (e) which melted and cooled to 120 °C.

For the crystallization at 120 °C, the spherulite size was larger and the nuclei density was decreased comparing with those of at 110 °C for all samples due to polymer requited larger lamellar thickness with corresponding to higher thermodynamic energy barrier at higher crystallization temperature. Thereby, the crystallization at high temperature or low supercooling was more difficult than at lower temperature [23, 48, 51, 53-56]. At this condition, the spherulite of neat PLA appeared at 35 min of observation time. The nanocomposite of PLA/CW and PLA/PLA-g-CW showed the presence of spherulitic structure at 20 min and 0 min, respectively.

These related to the results at 110 ºC that CW and PLA-g-CW increased the rate of crystallization. The spherulite size of nanocomposite rather larger than neat PLA at 35 min cause by the existence of foreign particles which decreased the energy barrier and generated more nuclei density then the induction period of nucleation was decreased with corresponded to the higher crystallization rate. After primary nucleation was taken place, the spherulite grew rapidly until impinged to one another.

Therefore, the samples containing CW and PLA-g-CW early generated first stem of nuclei and underwent to step of spherulite growth, resulting in the larger spherulite at the same time. All above results confirmed that CW and PLA-g-CW can act as nucleating agent of PLA, especially at the composition of 0.1 phr of PLA-g-CW.

CHAPTER 5
CONCLUSIONS

The chitin whisker (CW) was prepared from the chitin flake (CF) by means of acid hydrolysis. Then CW was successfully grafted with low MW acid terminated poly(D, L-lactic acid)(PDLLA) by surface chemical modification though coupling reaction with EDC-HCl/NHS confirmed by XRD, FT-IR, and ^{13}C NMR. For the XRD which performed for CF, CW and PLA-g-CW indicated the peak intensity at 9.5° and 19.5° of CF was obviously increased after turned to CW because a number of amorphous chain was dissolved. There was not only the increasing of crystallinity indexes, but some peak located at 21°, 23° and 26° was also evidently appeared. According to FT-IR, the PLA-g-CW exhibited the molecular vibration signal of ester carbonyl group at 1750 cm^{-1} which existed in PDLLA structure and ester linkage indicating that esterification reaction took place between the hydroxyl groups of CW and the carboxyl groups of PDLLA. The ^{13}C NMR also conducted in order to reassure that grafting reaction was success. This result showed the presence of resonance peak at 15 ppm corresponded to methyl group on the chain end of PDLLA and the hidden peak at closed to C6 and C7 peaks corresponded to carbonyl in **α**' position and methylene carbon in **β**'position, respectively. The dispersion of CW in water observed under TEM was different from PLA-g-CW. The PLA-g-CW showed the larger dimension than CW caused by the hydrophobicity of PDLLA chain which grafted on the CW surface brought about the aggregation of individual PLA-g-CW in water.

The prepared CW and PLA-g-CW were mixed with polylactide (PLA) pellets and fabricated into film by melt casting process. The morphological properties of nanocomposite film showed a rough surface without phase separation comparing with neat PLA film, observed by SEM. Moreover, the agglomeration was increased with the increasing of CW or PLA-g-CW contents at all formulations. In spite of the PLA/CW nanocomposite displayed good dispersion in PLA matrix, the PLA/PLA-g-CW showed better dispersion at all composition due to the grafted PDLLA increased the compatibility between CW and PLA. The film with 0.1 phr of CW or PLA-g-CW exhibited less agglomeration comparing with that of 0.2 or 0.3 phr. However, The PLA/PLA-g-

CW0.1 was the best formulation due to the best dispersion and the smallest agglomerated particle size.

In accordance with DSC, the addition of CW and PLA-g-CW did not influence the T_g of PLA because small number of nanoparticles. In contrast to the other thermal transition involving T_c, T_{cc} and T_m, the CW and PLA-g-CW were played an important role in the crystallization and melting behavior during cooling and heating of PLA. The T_c of sample in a group of PLA/PLA-g-CW nanocomposite was higher than neat PLA approximate to 10 °C. There was not only T_c but ΔH_c also higher than neat PLA and samples in PLA/CW group. In case of cold crystallization, only the PLA/CW0.1 and a group of PLA/PLA-g-CW nanocomposites showed the decreasing of T_{cc} and the increasing of ΔH_{cc}. The melting behavior of PLA/PLA-g-CW obviously different from the other due to the existence of multi-melting peak which associated to two different crystal of PLA. Especially, the nanocomposite sample containing 0.1 phr of PLA-g-CW which significantly appeared the separation of meting peak up to higher temperature. The degree of crystallinity (χ_c) of the nanocomposites was higher than neat PLA for all formulations and the PLA/PLA-g-CW0.1 showed the highest of χ_c values. These results related to the well-dispersion of whisker in PLA matrix which increased the proficiency of nucleating agent. The POM images at 110 °C and 120 °C indicated that the crystallization rate of nanocomposites with the introduction of PLA-g-CW at 0.1 and 0.3 phr was higher than the other. For all investigation, the PLA-g-CW0.1 nanocomposite was the most effective formulation which accelerated the crystallization rate and increased the degree of crystallinity of PLA due to the heterogeneous nucleation effect of well-dispersed nanoparticles.

REFERENCES

[1] The future of plastic. Nature Communications 9(1) (2018): 2157.

[2] Imre, B. and Pukánszky, B. Compatibilization in bio-based and biodegradable polymer blends. European Polymer Journal 49(6) (2013): 1215-1233.

[3] North, E.J. and Halden, R.U. Plastics and Environmental Health: The Road Ahead. Reviews on environmental health 28(1) (2013): 1-8.

[4] Thompson, R.C., Moore, C.J., vom Saal, F.S., and Swan, S.H. Plastics, the environment and human health: current consensus and future trends. Philosophical Transactions of the Royal Society B: Biological Sciences 364(1526) (2009): 2153-2166.

[5] Song, J.H., Murphy, R.J., Narayan, R., and Davies, G.B.H. Biodegradable and compostable alternatives to conventional plastics. Philosophical Transactions of the Royal Society B: Biological Sciences 364(1526) (2009): 2127-2139.

[6] Farah, S., Anderson, D.G., and Langer, R. Physical and mechanical properties of PLA, and their functions in widespread applications — A comprehensive review. Advanced Drug Delivery Reviews 107 (2016): 367-392.

[7] Auras, R., Harte, B., and Selke, S. An Overview of Polylactides as Packaging Materials. Macromolecular Bioscience 4(9) (2004): 835-864.

[8] Avérous, L. Polylactic Acid: Synthesis, Properties and Applications in Mohamed Naceur Belgacem, A.G. (ed.)Monomers, Polymers and Composites from Renewable Resources, pp. 433-450. Amsterdam: Elsevier, 2008.

[9] Hideto, T. Poly(lactide) Stereocomplexes: Formation, Structure, Properties, Degradation, and Applications. Macromolecular Bioscience 5(7) (2005): 569-597.

[10] Di Lorenzo, M.L. Crystallization behavior of poly(l-lactic acid). European Polymer Journal 41(3) (2005): 569-575.

[11] Pan, P. and Inoue, Y. Polymorphism and isomorphism in biodegradable polyesters. Progress in Polymer Science 34(7) (2009): 605-640.

[12] Nanthananon, P., Seadan, M., Pivsa-Art, S., and Suttiruengwong, S. Enhanced crystallization of poly (lactic acid) through reactive aliphatic bisamide. IOP Conference Series: Materials Science and Engineering 87(1) (2015): 012067.

[13] Hideto, T., Hiroki, T., Norio, F., and Hirofumi, T. Non-Isothermal Crystallization Behavior of Poly(L-lactic acid) in the Presence of Various Additives. Macromolecular Materials and Engineering 291(4) (2006): 325-335.

[14] Valapa, R., Hussain, S., Krishnan Iyer, P., Pugazhenthi, G., and Katiyar, V. Non-isothermal crystallization kinetics of sucrose palmitate reinforced poly(lactic acid) bionanocomposites. Polymer Bulletin 73(1) (2016): 21-38.

[15] Saeidlou, S., Huneault, M.A., Li, H., and Park, C.B. Poly(lactic acid) crystallization. Progress in Polymer Science 37(12) (2012): 1657-1677.

[16] Scaffaro, R., Botta, L., Lopresti, F., Maio, A., and Sutera, F. Polysaccharide nanocrystals as fillers for PLA based nanocomposites. Cellulose 24(2) (2017): 447-478.

[17] Nam, J.Y., Sinha Ray, S., and Okamoto, M. Crystallization Behavior and Morphology of Biodegradable Polylactide/Layered Silicate Nanocomposite. Macromolecules 36(19) (2003): 7126-7131.

[18] Battegazzore, D., Bocchini, S., and Frache, A. Crystallization kinetics of poly(lactic acid)-talc composites. Express Polymer Letters 5 (2011): 849-858.

[19] Yeong-Tarng, S., Yawo-Kuo, T., Chean-Cheng, S., Rong-Hsien, L., and Gin-Lung, L. Crystallization kinetics study of poly(L-lactic acid)/carbon nanotubes nanocomposites. Journal of Polymer Science Part B: Polymer Physics 48(9) (2010): 983-989.

[20] Sung-Il, M., Fengzhe, J., Cheol-jin, L., Sadami, T., and Suong-Hyu, H. Novel Carbon Nanotube/Poly(L-lactic acid) Nanocomposites; Their Modulus, Thermal Stability, and Electrical Conductivity. Macromolecular Symposia 224(1) (2005): 287-296.

[21] Phetwarotai, W. and Aht-Ong, D. Nucleated polylactide blend films with nanoprecipitated calcium carbonate and talc. Journal of Thermal Analysis & Calorimetry 127(3) (2017): 2367-2381.

[22] Zhang, D., Kandadai, M.A., Cech, J., Roth, S., and Curran, S.A. Poly(l-lactide) (PLLA)/Multiwalled Carbon Nanotube (MWCNT) Composite: Characterization and Biocompatibility Evaluation. The Journal of Physical Chemistry B 110(26) (2006): 12910-12915.

[23] Wypych, G. Polymer crystallization with and without nucleating agents. in Wypych, G. (ed.)Handbook of Nucleating Agents, pp. 33-51: ChemTec Publishing, 2016.

[24] Raabe, D., Sachs, C., and Romano, P. The crustacean exoskeleton as an example of a structurally and mechanically graded biological nanocomposite material. Acta Materialia 53(15) (2005): 4281-4292.

[25] Nikolov, S., et al. Robustness and optimal use of design principles of arthropod exoskeletons studied by ab initio-based multiscale simulations. Journal of the Mechanical Behavior of Biomedical Materials 4(2) (2011): 129-145.

[26] Anyarat, W., Pitt, S., Hiroshi, T., Seiichi, T., and Ratana, R. Fabrication, structure, and properties of chitin whisker-reinforced alginate nanocomposite fibers. Journal of Applied Polymer Science 110(2) (2008): 890-899.

[27] Salaberria, A.M., Labidi, J., and Fernandes, S.C.M. Different routes to turn chitin into stunning nano-objects. European Polymer Journal 68 (2015): 503-515.

[28] Hudson, S.M. and Smith, C. Polysaccharides: Chitin and Chitosan: Chemistry and Technology of Their Use As Structural Materials. in Kaplan, D.L. (ed.)Biopolymers from Renewable Resources, pp. 96-118. Berlin, Heidelberg: Springer Berlin Heidelberg, 1998.

[29] Kulapa, S.K., P.J., D., and John, L. The export competitiveness of the tuna industry in Thailand. British Food Journal 115(3) (2013): 328-341.

[30] Clarke, S. Inside Thailand: The Fish and Seafood Trade. 2015: Agriculture and AgriFood Canada.

[31] Li, C., et al. Nanocomposites of poly(L-lactide) and surface-modified chitin whiskers with improved mechanical properties and cytocompatibility. Vol. 81, 2016.

[32] Herrera, N., et al. Functionalized blown films of plasticized polylactic acid/chitin nanocomposite: Preparation and characterization. Materials & Design 92 (2016): 846-852.

[33] Paillet, M. and Dufresne, A. Chitin Whisker Reinforced Thermoplastic Nanocomposites. Macromolecules 34(19) (2001): 6527-6530.

[34] Garlotta, D. A Literature Review of Poly(Lactic Acid). Journal of Polymers and the Environment 9(2) (2001): 63-84.

[35] Wee, Y.-J., Kim, J.-N., and Ryu, H.-W. Biotechnological Production of Lactic Acid and Its Recent Applications. Food Technology and Biotechnology 44(2) (2006): 163-172.

[36] Lunt, J. Large-scale production, properties and commercial applications of polylactic acid polymers. Polymer Degradation and Stability 59(1) (1998): 145-152.

[37] Groot, W., Krieken, J.v., Sliekersl, O., and Vos, S.d. Production and Purification of Lactic Acid and Lactide. in Auras, R., Lim, L.T., Selke, S.E.M., and Tsuji, H. (eds.),Poly(Lactic Acid): Synthesis, Structures, Properties, Processing, and Applications, pp. 1-18. Hoboken, New Jersey: John Wiley & Sons, Inc., 2010.

[38] Hartmann, M.H. High Molecular Weight Polylactic Acid Polymers. in Kaplan, D.L. (ed.)Biopolymers from Renewable Resources, pp. 367-411. Berlin, Heidelberg: Springer Berlin Heidelberg, 1998.

[39] Xiao, L., Wang, B., Yang, G., and Gauthier, M. Poly(Lactic Acid)-Based Biomaterials: Synthesis, Modification and Applications. in Ghista, D.N. (ed.)Biomedical Science, Engineering and Technology: Intech, 2012.

[40] Stanford, M.J. and Dove, A.P. Stereocontrolled ring-opening polymerisation of lactide. Chemical Society Reviews 39(2) (2010): 486-494.

[41] Pan, P., Liang, Z., Zhu, B., Dong, T., and Inoue, Y. Blending Effects on Polymorphic Crystallization of Poly(l-lactide). Macromolecules 42(9) (2009): 3374-3380.

[42] Hoogsteen, W., Postema, A.R., Pennings, A.J., Brinke, G.T., and Zugenmaier, P. Crystal structure, conformation and morphology of solution-spun poly(L-lactide) fibers. Macromolecules 23(2) (1990): 634-642.

[43] Eling, B., Gogolewski, S., and Pennings, A.J. Biodegradable materials of poly(l-lactic acid): 1. Melt-spun and solution-spun fibres. Polymer 23(11) (1982): 1587-1593.

[44] Cartier, L., Okihara, T., Ikada, Y., Tsuji, H., Puiggali, J., and Lotz, B. Epitaxial crystallization and crystalline polymorphism of polylactides. Polymer 41(25) (2000): 8909-8919.

[45] Van de Velde, K. and Kiekens, P. Biopolymers: overview of several properties and consequences on their applications. Polymer Testing 21(4) (2002): 433-442.

[46] Strobl, G.R. Metastable Partially Crystalline States. in The Physics of Polymers: Concepts for Understanding Their Structures and Behavior, pp. 143-190. Berlin, Heidelberg: Springer Berlin Heidelberg, 1997.

[47] Raabe, D. Mesoscale simulation of spherulite growth during polymer crystallization by use of a cellular automaton. Acta Materialia 52(9) (2004): 2653-2664.

[48] Sperling, L.H. The Crystalline State. in Introduction to Physical Polymer Science, pp. 239-323: John Wiley & Sons, Inc., 2005.

[49] Li, Y., Wang, Z., and He, T. Morphological Control of Polymer Spherulites via Manipulating Radial Lamellar Organization upon Evaporative Crystallization: A Mini Review. Crystals 7(4) (2017): 115.

[50] Hu, W. and Zha, L. Theoretical aspects of polymer crystallization. in Mitchell, G.R. and Tojeira, A. (eds.),Controlling the Morphology of Polymers: Multiple Scales of Structure and Processing, pp. 101-143. Cham: Springer International Publishing, 2016.

[51] Wypych, G. Mechanisms of crystallization. in Wypych, G. (ed.)Handbook of Nucleating Agents, pp. 87-92: ChemTec Publishing, 2016.

[52] Nogales, A., Ezquerra, T., Denchev, Z., Sics, I., Baltá-Calleja, F., and Hsiao, B. Molecular dynamics and microstructure development during crystallization in poly(ether-ether-ketone) as revealed by real-time dielectric and X-ray methods. Journal of Chemical Physics 115 (2001): 3804-3813.

[53] Nikolov, S., Lebensohn, R.A., and Raabe, D. Self-consistent modeling of large plastic deformation, texture and morphology evolution in semi-crystalline

polymers. Journal of the Mechanics and Physics of Solids 54(7) (2006): 1350-1375.

[54] Okada, K., Watanabe, K., Urushihara, T., Toda, A., and Hikosaka, M. Role of epitaxy of nucleating agent (NA) in nucleation mechanism of polymers. Polymer 48(1) (2007): 401-408.

[55] Chatterjee, A.M., Price, F.P., and Newman, S. Heterogeneous nucleation of crystallization of high polymers from the melt. Doctor of Philosophy (PhD), Polymer Science and Engineering University of Massachusetts Amherst, 1974.

[56] Androsch, R., Monami, A., and Kucera, J. Effect of an alpha-phase nucleating agent on the crystallization kinetics of a propylene/ethylene random copolymer at largely different supercooling. Journal of Crystal Growth 408 (2014): 91-96.

[57] Ning, N., et al. Realizing the enhancement of interfacial interaction in semicrystalline polymer/filler composites via interfacial crystallization. Progress in Polymer Science 37(10) (2012): 1425-1455.

[58] Jayakumar, R., et al. Bioactive and osteoblast cell attachment studies of novel α- and β-chitin membranes for tissue-engineering applications. International Journal of Biological Macromolecules 45(3) (2009): 260-264.

[59] Anitha, A., et al. Chitin and chitosan in selected biomedical applications. Progress in Polymer Science 39(9) (2014): 1644-1667.

[60] Rita, S., Parashuram, C.M., and Kumar, M.A. Chitin membrane for wound dressing application – preparation, characterisation and toxicological evaluation. International Wound Journal 5(5) (2008): 665-673.

[61] Salaberria, A.M., Labidi, J., and Fernandes, S.C.M. Chitin nanocrystals and nanofibers as nano-sized fillers into thermoplastic starch-based biocomposites processed by melt-mixing. Chemical Engineering Journal 256 (2014): 356-364.

[62] Fan, Y., Saito, T., and Isogai, A. Chitin Nanocrystals Prepared by TEMPO-Mediated Oxidation of α-Chitin. Biomacromolecules 9(1) (2008): 192-198.

[63] Zeng, J.-B., He, Y.-S., Li, S.-L., and Wang, Y.-Z. Chitin Whiskers: An Overview. Biomacromolecules 13(1) (2012): 1-11.

[64] João, C.F.C., Silva, J.C., and Borges, J.P. Chitin-Based Nanocomposites: Biomedical Applications. in Thakur, V.K. and Thakur, M.K. (eds.),Eco-friendly Polymer Nanocomposites: Chemistry and Applications, pp. 439-457. New Delhi: Springer India, 2015.

[65] Gopalan Nair, K. and Dufresne, A. Crab Shell Chitin Whisker Reinforced Natural Rubber Nanocomposites. 1. Processing and Swelling Behavior. Biomacromolecules 4(3) (2003): 657-665.

[66] Swatloski, R.P., Spear, S.K., Holbrey, J.D., and Rogers, R.D. Dissolution of Cellose with Ionic Liquids. Journal of the American Chemical Society 124(18) (2002): 4974-4975.

[67] Ang-atikarnkul, P., Watthanaphanit, A., and Rujiravanit, R. Fabrication of cellulose nanofiber/chitin whisker/silk sericin bionanocomposite sponges and characterizations of their physical and biological properties. Composites Science and Technology 96 (2014): 88-96.

[68] Saito, T., Nishiyama, Y., Putaux, J.-L., Vignon, M., and Isogai, A. Homogeneous Suspensions of Individualized Microfibrils from TEMPO-Catalyzed Oxidation of Native Cellulose. Biomacromolecules 7(6) (2006): 1687-1691.

[69] Fan, Y., Saito, T., and Isogai, A. Individual chitin nano-whiskers prepared from partially deacetylated α-chitin by fibril surface cationization. Carbohydrate Polymers 79(4) (2010): 1046-1051.

[70] João, C.F.C., Baptista, A.C., Ferreira, I.M.M., Silva, J.C., and Borges, J.P. Natural Nanofibres for Composite Applications. in Rana, S. and Fangueiro, R. (eds.),Fibrous and Textile Materials for Composite Applications, pp. 261-299. Singapore: Springer Singapore, 2016.

[71] Mi-Kyeong, J., Byeong-Gi, K., Young-Il, J., Hyung, L.C., and Jae-Woon, N. Physicochemical characterization of α-chitin, β-chitin, and γ-chitin separated from natural resources. Journal of Polymer Science Part A: Polymer Chemistry 42(14) (2004): 3423-3432.

[72] Kadokawa, J.-i. Preparation and Applications of Chitin Nanofibers/Nanowhiskers. in Dufresne, A., Thomas, S., and Pothen, L.A. (eds.),Biopolymer Nanocomposites: Processing, Properties, and Applications: John Wiley & Sons, Inc., 2013.

[73] Kadokawa, J.-i., Takegawa, A., Mine, S., and Prasad, K. Preparation of chitin nanowhiskers using an ionic liquid and their composite materials with poly(vinyl alcohol). Carbohydrate Polymers 84(4) (2011): 1408-1412.

[74] Saito, T. and Isogai, A. TEMPO-Mediated Oxidation of Native Cellulose. The Effect of Oxidation Conditions on Chemical and Crystal Structures of the Water-Insoluble Fractions. Biomacromolecules 5(5) (2004): 1983-1989.

[75] Fan, Y., Saito, T., and Isogai, A. TEMPO-mediated oxidation of β-chitin to prepare individual nanofibrils. Carbohydrate Polymers 77(4) (2009): 832-838.

[76] Prasad, K., Murakami, M.-a., Kaneko, Y., Takada, A., Nakamura, Y., and Kadokawa, J.-i. Weak gel of chitin with ionic liquid, 1-allyl-3-methylimidazolium bromide. International Journal of Biological Macromolecules 45(3) (2009): 221-225.

[77] Li, H., et al. Crystallisation, mechanical properties and rheological behaviour of PLA composites reinforced by surface modified microcrystalline cellulose. Plastics, Rubber and Composites 45(4) (2016): 181-187.

[78] Xu, T., Zhang, A., Zhao, Y., Han, Z., and Xue, L. Crystallization kinetics and morphology of biodegradable poly(lactic acid) with a hydrazide nucleating agent. Polymer Testing 45 (2015): 101-106.

[79] Zhang, R., Wang, Y., Wang, K., Zheng, G., Li, Q., and Shen, C. Crystallization of poly(lactic acid) accelerated by cyclodextrin complex as nucleating agent. Polymer Bulletin 70(1) (2013): 195-206.

[80] Yeong-Tarng, S. and Gin-Lung, L. Effects of carbon nanotubes on crystallization and melting behavior of poly(L-lactide) via DSC and TMDSC studies. Journal of Polymer Science Part B: Polymer Physics 45(14) (2007): 1870-1881.

[81] Zhang, Y., Xue, C., Xue, Y., Gao, R., and Zhang, X. Determination of the degree of deacetylation of chitin and chitosan by X-ray powder diffraction. Carbohydrate Research 340(11) (2005): 1914-1917.

[82] Jalal, U.A., Jun, A., Masahiro, F., Shinichiro, S., and Yasuo, G. Interfacial interaction and mechanical properties of chitin whisker–poly(vinyl alcohol) gel-spun nanocomposite fibers. Polymer International 61(6) (2012): 1010-1015.

[83] Liu, H., et al. Electrospun composite nanofiber membrane of poly(l-lactide) and surface grafted chitin whiskers: Fabrication, mechanical properties and cytocompatibility. Carbohydrate polymers 147 (2016): 216-225.

[84] Binsbergen, F.L. Heterogeneous nucleation in the crystallization of polyolefins: Part 1. Chemical and physical nature of nucleating agents. Polymer 11(5) (1970): 253-267.

[85] Lai, W.-C. Thermal Behavior and Crystal Structure of Poly(l-lactic acid) with 1,3:2,4-Dibenzylidene-d-sorbitol. The Journal of Physical Chemistry B 115(38) (2011): 11029-11037.

[86] Defeng, W., Liang, W., Lanfeng, W., Bin, X., Yisheng, Z., and Ming, Z. Nonisothermal cold crystallization behavior and kinetics of polylactide/clay nanocomposites. Journal of Polymer Science Part B: Polymer Physics 45(9) (2007): 1100-1113.

[87] Yasuniwa, M., Sakamo, K., Ono, Y., and Kawahara, W. Melting behavior of poly(l-lactic acid): X-ray and DSC analyses of the melting process. Polymer 49(7) (2008): 1943-1951.

[88] Kong, Y. and Hay, J.N. Multiple melting behaviour of poly(ethylene terephthalate). Polymer 44(3) (2003): 623-633.

[89] Fukushima, K., Abbate, C., Tabuani, D., Gennari, M., and Camino, G. Biodegradation of poly(lactic acid) and its nanocomposites. Polymer Degradation and Stability 94(10) (2009): 1646-1655.

[90] Fortunati, E., et al. Microstructure and nonisothermal cold crystallization of PLA composites based on silver nanoparticles and nanocrystalline cellulose. Polymer Degradation and Stability 97(10) (2012): 2027-2036.

APPENDIX

A. The amount of substances used in the chemical grafting reaction

Calculate equivalent mole of chitin

In nature, chitin is copolymers composed of D-glucosamine (GlcN) and *N*-acetyl-D-glucosamine (GlcNAc) units. The equivalent molecular weight of chitin (M_{chitin}) can be calculated from equation (3)

$$M_{chitin} = (M_{GlcN} \times DD) + (M_{GlcNAc} \times DA) \quad (3)$$

Where, The degree of acetylation (DA) = Molar fraction of GlcNAc in the copolymers

The degree of deacetylation (DD) = Molar fraction of GlcN in the copolymers

M_{GlcN} = Formula weight of glucosamine unit

M_{GlcNAc} = Formula weight of glucosamine unit

In this experiment, DA of chitin was 0.95. Therefore, DD = 1 - 0.95 = 0.05

So, $M_{chitin} = (161 \times 0.05) + (203 \times 0.95)$

$M_{chitin} = 200.9$ g/mole

Calculate the mole of chitin when the grams of chitin are 0.5 g

$$N_{chitin} = \frac{0.5 \text{ g}}{200.9 \text{ g/mole}}$$

$N_{chitin} = 2.48$ equivalent mmole

Where 1 equivalent mole of chitin composed of 2 moles of hydroxyl group (OH)

Then, $N_{OH} = 2 \times N_{chitin}$

$N_{OH} = 2 \times 2.48$ mmole

$N_{OH} = 4.98$ mmole

Calculate grams of PDLLA

Assign a mole of OH react with 0.01 moles of carboxyl group.

$N_{COOH} = 0.01N_{OH}$

$N_{COOH} = 0.01 \times 4.98$

$N_{COOH} = 0.05$ mmole

Next, calculate grams of PDLLA from

$g_{COOH} = N_{COOH} \times M_{COOH}$

$g_{COOH} = 0.05 \times 15{,}000$ mg

$g_{COOH} = 746.64$ mg

$g_{COOH} = 0.75$ g

Thereby, the grams of PDLLA used in the reaction was 0.75 g

Calculate grams of EDC.HCl

Assign 2 moles of EDC.HCl reacted with a mole of COOH

$N_{EDC.HCl} = 2N_{COOH}$

$N_{EDC.HCl} = 2 \times 0.05$ mmole

$N_{EDC.HCl} = 0.10$ mmole

Then,

$g_{EDC.HCl} = N_{EDC.HCl} \times M_{EDC.HCl}$

$g_{EDC.HCl} = 0.01 \times 191.7$ mg

$g_{EDC.HCl} = 19.08$ mg

Calculate grams of NHS

Assign the mole ratio of NHS is equal to EDC.HCl.

$N_{EDC.HCl} = N_{NHS}$

$N_{NHS} = 0.10$ mmole

Then,

$g_{NHS} = N_{NHS} \times M_{NHS}$

$g_{NHS} = 0.01 \times 115.09$ mg

$g_{NHS} = 11.46$ mg

B. Fourier Transform Infrared Spectroscopy (FT-IR)

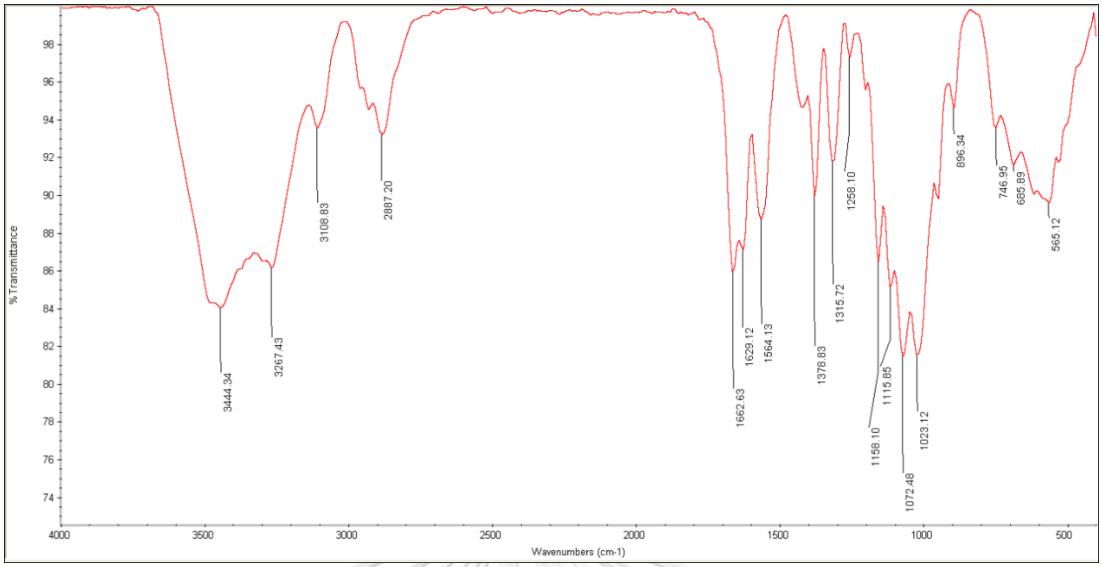

Figure B.1 FTIR Spectra of CW

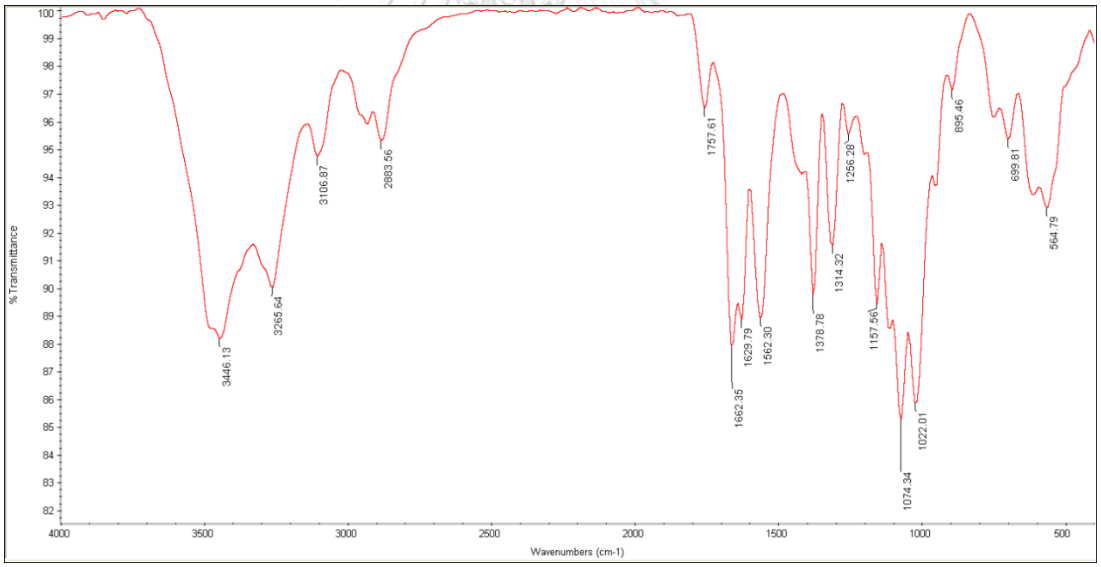

Figure B.2 FTIR Spectra of PLA-g-CW

C. Fourier Transform Nuclear Magnetic Resonance Spectroscopy (NMR)

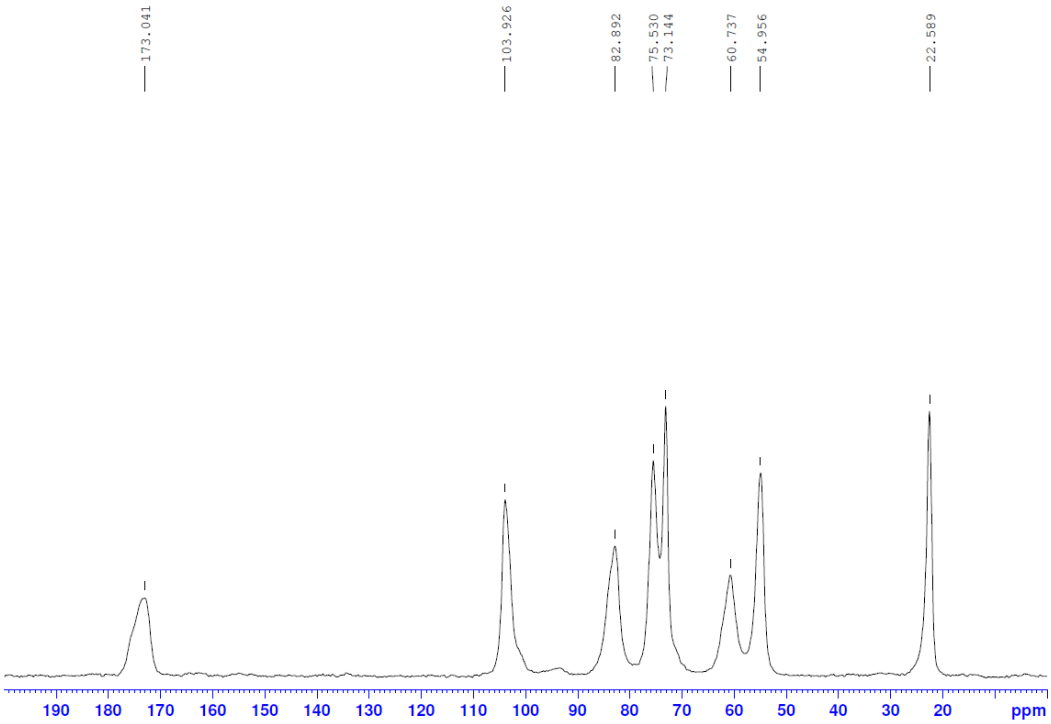

Figure C.1 ^{13}C NMR Spectra of CW

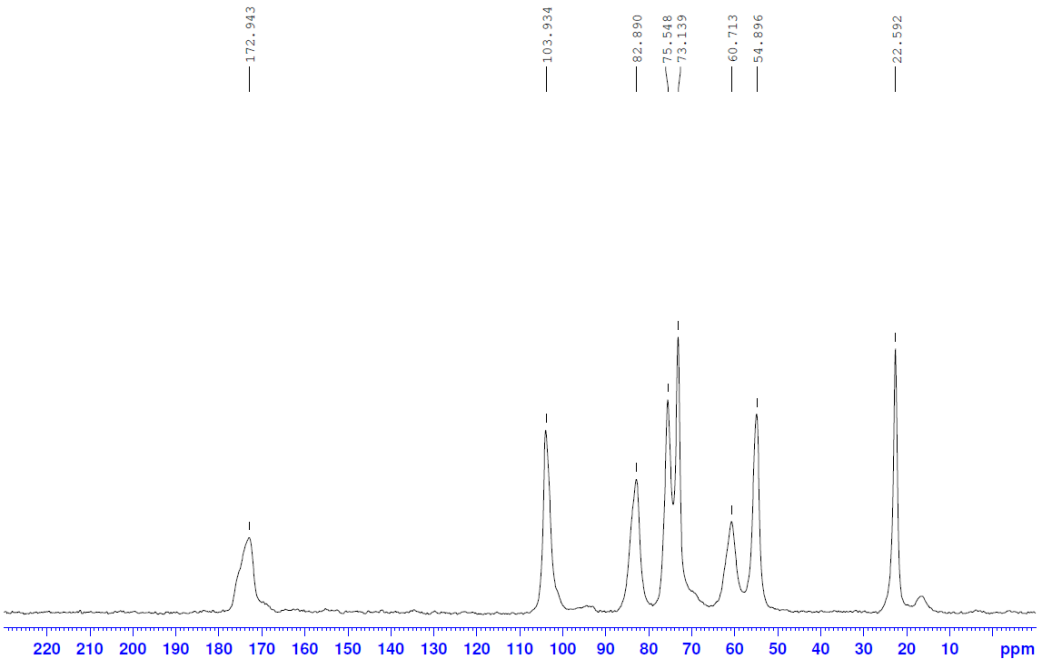

Figure C.2 ^{13}C NMR Spectra of PLA-g-CW

D. X-ray Diffractometry (XRD)

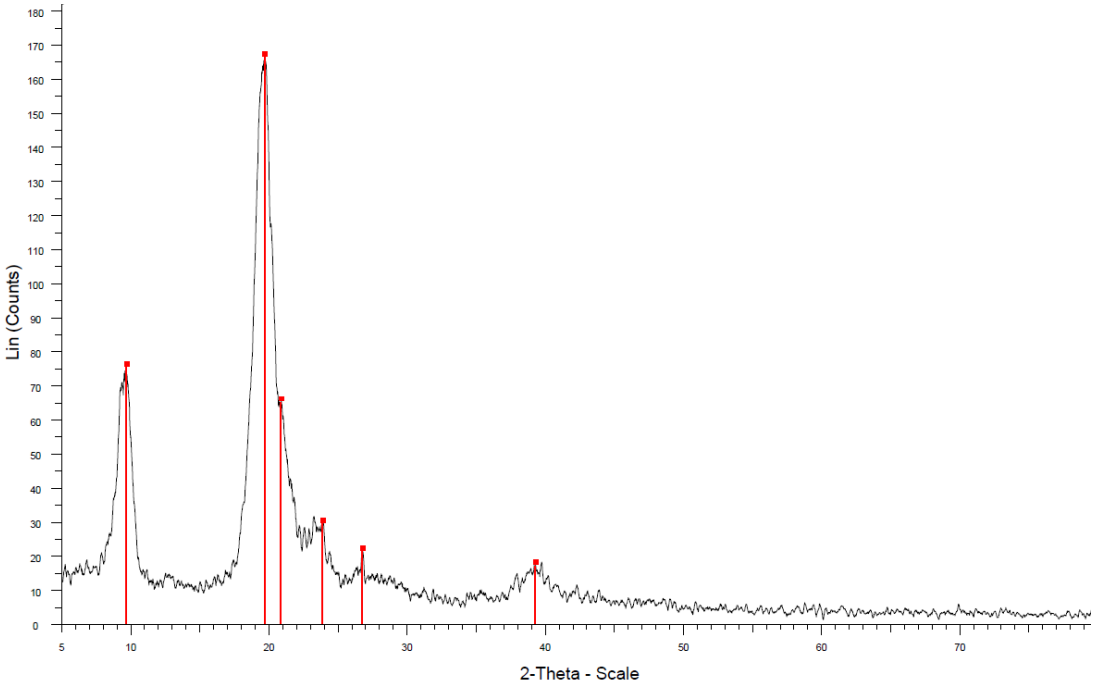

Figure D.1 Diffraction pattern of CF

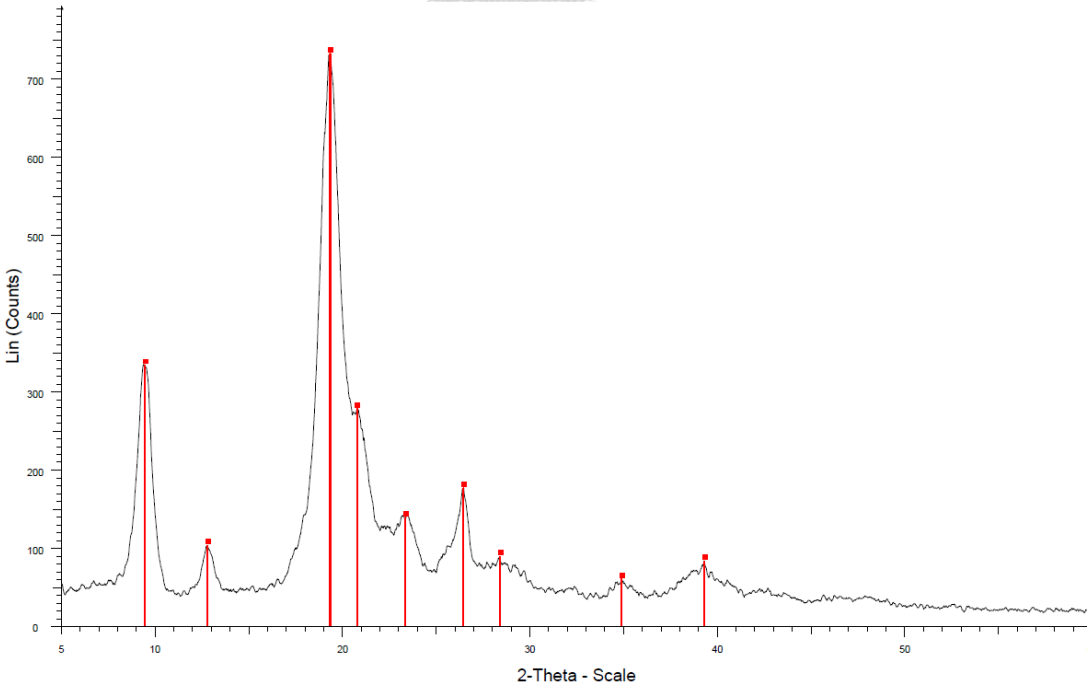

Figure D.2 Diffraction pattern of CW

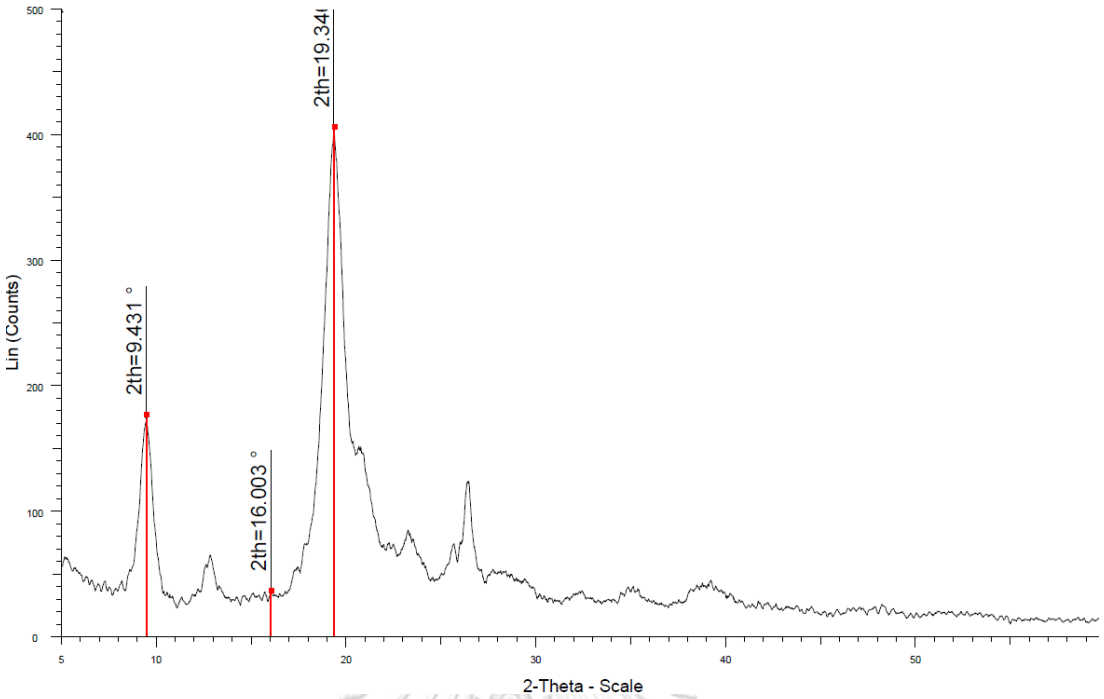

Figure D.3 Diffraction pattern of PLA-g-CW

Calculation of the crystallinity indexes (CrI)

The crystallinity indexes of chitin samples were determined by following equation

$$\%CrI_{hkl} = \frac{I_{hkl}-I_{am}}{I_{hkl}} \times 100 \quad (1)$$

Where, I_{hkl} = the maximum intensity of (hkl) planes

I_{am} = the intensity of amorphous diffraction

For instance, the maximum intensity of chitin flake at angle of 9° which corresponded to (020) plane was 42.9% and intensity of amorphous diffraction at 16° was 8.2%. Then,

$$\%CrI_{020} = \frac{I_{020}-I_{am}}{I_{020}} \times 100$$

$$\%CrI_{020} = \frac{42.9 - 8.2}{42.9} \times 100$$

$$\%CrI_{020} = 80.98$$

E. Transmission Electron Microscopy (TEM)

Table E.1 Length, diameter and aspect ratio of CW

Label	Length (nm)	Diameter (nm)	Aspect Ratio
1	570	29	19.66
2	283	18	15.72
3	288	20	14.40
4	423	31	13.65
5	260	23	11.30
6	180	23	7.83
7	517	30	17.23
8	473	31	15.26
9	404	31	13.03
10	253	30	8.43
11	406	45	9.02
12	360	29	12.41
13	274	27	10.15
14	556	15	37.07
15	473	10	47.30
16	188	13	14.46
17	239	20	11.95
18	216	17	12.71
19	320	27	11.85
20	384	18	21.33
21	552	22	25.09
22	264	18	14.67
23	403	25	16.12
24	421	29	14.52
25	585	30	19.50

Table E.1 Length, diameter and aspect ratio of CW (continued)

Label	Length (nm)	Diameter (nm)	Aspect Ratio
26	228	17	13.41
27	196	22	8.91
28	289	21	13.76
29	411	23	17.87
30	451	31	14.55
31	292	23	12.70
32	357	30	11.90
33	353	31	11.39
34	175	24	7.29
35	185	25	7.40
36	355	21	16.90
37	151	27	5.59
38	167	24	6.96
39	323	19	17.00
40	176	22	8.00
41	175	23	7.61
42	198	21	9.43
43	215	28	7.68
44	267	24	11.13
45	249	21	11.86
46	185	24	7.71
47	261	27	9.67
48	421	19	22.16
49	189	15	12.60
50	253	27	9.37

Table E.1 Length, diameter and aspect ratio of CW (continued)

Label	Length (nm)	Diameter (nm)	Aspect Ratio
51	320	24	13.33
52	298	40	7.45
53	293	31	9.45
54	238	30	7.93
55	302	42	7.19
56	243	49	4.96
57	344	27	12.74
58	286	39	7.33
59	320	20	16.00
60	469	26	18.04
61	508	27	18.81
62	315	29	10.86
63	188	29	6.48
64	394	23	17.13
65	207	29	7.14
66	315	24	13.13
67	173	29	5.97
68	286	27	10.59
69	446	23	19.39
70	312	16	19.50
71	503	20	25.15
72	378	31	12.19
73	499	35	14.26
74	824	41	20.10
75	328	16	20.50

Table E.1 Length, diameter and aspect ratio of CW (continued)

Label	Length (nm)	Diameter (nm)	Aspect Ratio
76	930	40	23.25
77	470	24	19.58
78	368	28	13.14
79	310	23	13.48
80	161	25	6.44
81	296	31	9.55
82	318	25	12.72
83	320	27	11.85
84	254	23	11.04
85	257	27	9.52
86	230	34	6.76
87	390	30	13.00
88	447	44	10.16
89	490	40	12.25
90	339	41	8.27
91	231	31	7.45
92	306	33	9.27
93	331	26	12.73
94	759	21	36.14
95	235	16	14.69
96	607	37	16.41
97	328	14	23.43
98	125	17	7.35
99	267	18	14.83
100	367	27	13.59
Average	337.39	26.29	13.60
SD	140.88	7.43	6.64

Table E.2 Length, diameter and aspect ratio of PLA-g-CW

Label	Length (nm)	Diameter (nm)	Aspect Ratio
1	424	28	15
2	309	41	8
3	276	13	21
4	254	17	15
5	568	8	71
6	387	26	15
7	183	27	7
8	522	26	20
9	566	38	15
10	482	18	27
11	703	25	28
12	545	35	16
13	362	10	36
14	199	9	22
15	474	23	21
16	711	21	34
17	250	23	11
18	391	17	23
19	580	29	20
20	313	16	20
21	373	22	17
22	486	17	29
23	505	16	32
24	279	25	11
25	267	14	19

Table E.2 Length, diameter and aspect ratio of PLA-g-CW (continued)

Label	Length (nm)	Diameter (nm)	Aspect Ratio
26	216	18	12
27	381	12	32
28	216	19	11
29	418	18	23
30	479	25	19
31	467	17	27
32	416	17	24
33	786	16	49
34	267	37	7
35	225	17	13
36	541	31	17
37	736	29	25
38	500	14	36
39	536	69	8
40	649	16	41
41	304	22	14
42	236	10	24
43	214	10	21
44	238	20	12
45	302	27	11
46	232	18	13
47	193	18	11
48	222	8	28
49	270	12	23
50	406	17	24

Table E.2 Length, diameter and aspect ratio of PLA-g-CW (continued)

Label	Length (nm)	Diameter (nm)	Aspect Ratio
51	284	12	24
52	570	16	36
53	493	29	17
54	212	17	12
55	422	6	70
56	274	22	12
57	302	14	22
58	237	14	17
59	222	17	13
60	302	9	34
61	334	19	18
62	249	22	11
63	220	10	22
64	444	14	32
65	301	19	16
66	352	16	22
67	200	13	15
68	211	15	14
69	268	14	19
70	187	9	21
71	224	12	19
72	308	8	39
73	266	12	22
74	281	12	23
75	253	12	21

Table E.2 Length, diameter and aspect ratio of PLA-g-CW (continued)

Label	Length (nm)	Diameter (nm)	Aspect Ratio
76	207	6	35
77	312	12	26
78	208	6	35
79	238	6	40
80	347	13	27
81	274	9	30
82	500	12	42
83	301	5	60
84	184	4	46
85	389	8	49
86	234	10	23
87	140	10	14
88	260	13	20
89	283	6	47
90	243	12	20
91	225	9	25
92	231	20	12
93	351	12	29
94	235	13	18
95	238	9	26
96	190	8	24
97	173	10	17
98	169	8	21
99	268	12	22
100	310	6	52
Average	337.85	16.63	24.06
SD	141.5108	9.302317	12.45

F. Scanning Electron Microscopy (SEM)

Table F.1 Particle size of CW in PLA matrix

Label	Area (nm)		
	PLA/CW0.1	PLA/CW0.2	PLA/CW0.3
1	222	1112	302
2	102	672	581
3	152	161	107
4	138	316	1487
5	153	736	221
6	146	887	215
7	102	644	712
8	102	1081	149
9	34	287	1291
10	49	434	2003
11	81	137	289
12	58	129	1273
13	91	193	109
14	112	1522	
15	79	112	
16	86	148	
17	102	156	
18	48		
19	166		
20	145		
21	146		
22	101		
23	165		
24	74		
25	201		

Table F.1 Particle size of CW in PLA matrix (continued)

Label	Area (nm)		
	PLA/CW0.1	PLA/CW0.2	PLA/CW0.3
26	298		
27	110		
28	86		
29	96		
30	137		
31	102		
32	125		
33	108		
34	146		
35	58		
36	90		
37	38		
38	120		
39	187		
40	108		
41	67		
42	80		
43	72		
44	20		
45	102		
46	83		
47	71		
48	23		
49	120		
50	81		
Average	107.66	513.35	672.23
SD	51.23	417.58	607.36

Table F.2 Particle size of PLA-g-CW in PLA matrix

Label	Area (nm)		
	PLA/PLA-g-CW0.1	PLA/PLA-g-CW0.2	PLA/PLA-g-CW0.3
1	54	159	142
2	68	126	170
3	47	94	189
4	174	83	217
5	82	86	222
6	48	201	105
7	40	102	146
8	31	75	142
9	52	178	120
10	86	166	263
11	42	364	102
12	35	322	237
13	38	325	73
14	60	364	190
15	43	153	159
16	58	116	129
17	21	274	166
18	40	781	171
19	45	673	450
20	35	580	441
21	32	344	422
22	189	224	636
23	32	147	371
24	30	156	315
25	63	179	458

Table F.2 Particle size of PLA-g-CW in PLA matrix (continued)

Label	Area (nm)		
	PLA/PLA-g-CW0.1	PLA/PLA-g-CW0.2	PLA/PLA-g-CW0.3
26	27	148	706
27	51	219	170
28	65	214	92
29	44	332	159
30	76	395	135
31	33	239	170
32	44	308	111
33	73	204	264
34	75	69	123
35	42	84	193
36	56	66	259
37	78	359	807
38	51	535	1109
39	123	237	809
40	90	331	171
41	91	66	1072
42	81	182	971
43	30	172	609
44	10	115	327
45	61	235	1035
46	49	276	74
47	48	353	122
48	61	103	310
49	42	148	110
50	58	151	235
Average	58.08	236.26	323.58
SD	32.68	153.96	279.80

G. Film thickness

Table G.1 Thickness of neat PLA and PLA/CW film

Label	Film thickness (mm)			
	Neat PLA	PLA/CW0.1	PLA/CW0.2	PLA/CW0.3
1	0.084	0.102	0.121	0.082
2	0.087	0.082	0.163	0.08
3	0.098	0.166	0.098	0.124
4	0.092	0.088	0.12	0.088
5	0.088	0.148	0.094	0.107
6	0.081	0.154	0.088	0.127
7	0.085	0.111	0.099	0.113
8	0.081	0.073	0.088	0.083
9	0.091	0.089	0.092	0.084
10	0.089	0.08	0.165	0.081
11	0.084	0.098	0.114	0.081
12	0.113	0.084	0.085	0.093
13	0.128	0.125	0.145	0.105
14	0.088	0.14	0.09	0.144
15	0.083	0.093	0.138	0.085
Average	0.091	0.109	0.113	0.098
SD	0.012	0.029	0.027	0.020

Table G.2 Thickness of PLA/PLA-g-CW film

Label	Film thickness (mm)		
	PLA/PLA-g-CW0.1	PLA/PLA-g-CW0.2	PLA/PLA-g-CW0.3
1	0.112	0.098	0.189
2	0.121	0.121	0.137
3	0.09	0.156	0.096
4	0.08	0.08	0.134
5	0.078	0.071	0.073
6	0.079	0.07	0.099
7	0.093	0.141	0.153
8	0.102	0.07	0.079
9	0.089	0.082	0.087
10	0.076	0.08	0.095
11	0.095	0.072	0.085
12	0.091	0.133	0.07
13	0.098	0.123	0.097
14	0.099	0.112	0.083
15	0.083	0.1	0.085
Average	0.092	0.101	0.104
SD	0.012	0.028	0.033

H. Differential Scanning Calorimetry (DSC)

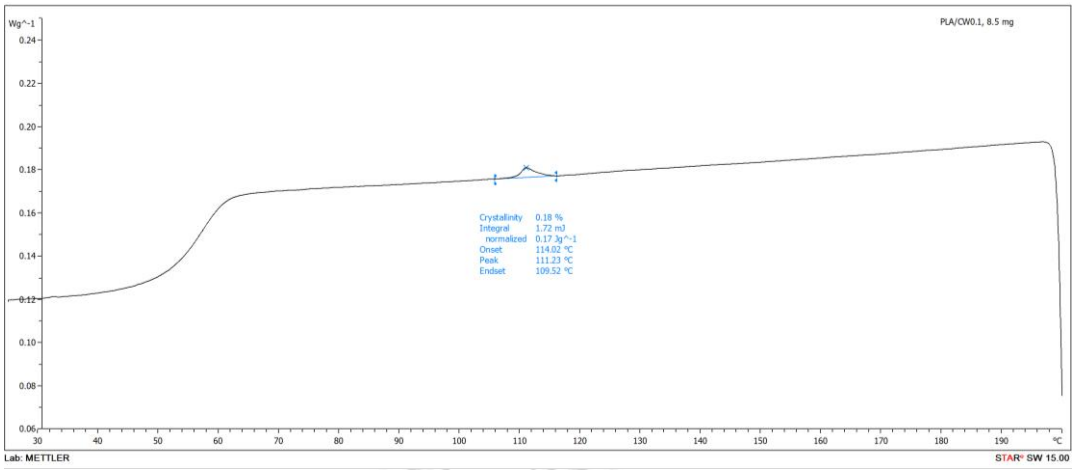

Figure H.1 DSC thermogram at cooling scan of PLA/CW0.1

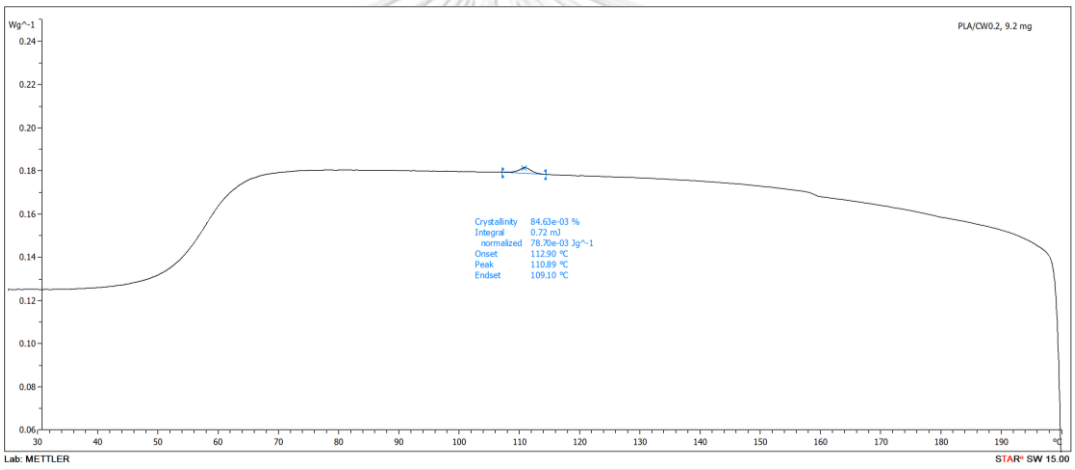

Figure H.2 DSC thermogram at cooling scan of PLA/CW0.2

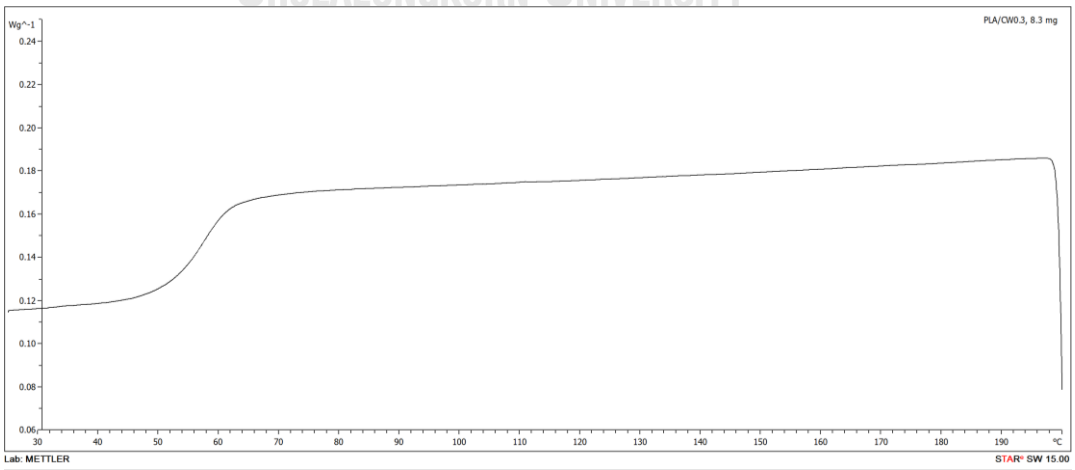

Figure H.3 DSC thermogram at cooling scan of PLA/CW0.3

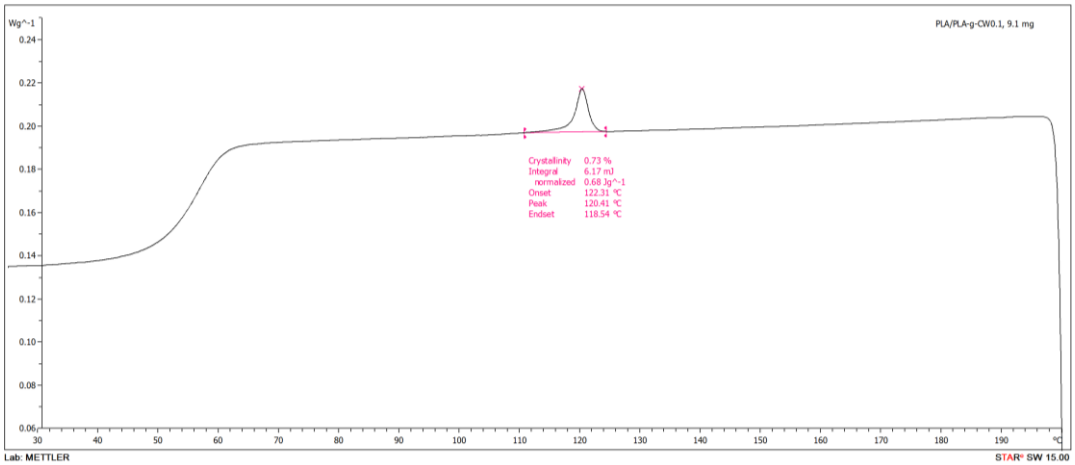

Figure H.4 DSC thermogram at cooling scan of PLA/PLA-g-CW0.1

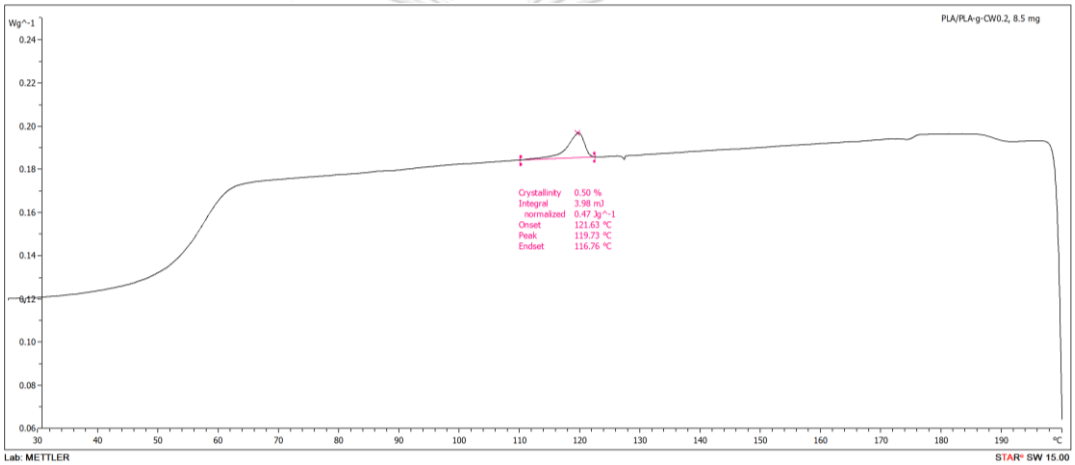

Figure H.5 DSC thermogram at cooling scan of PLA/PLA-g-CW0.2

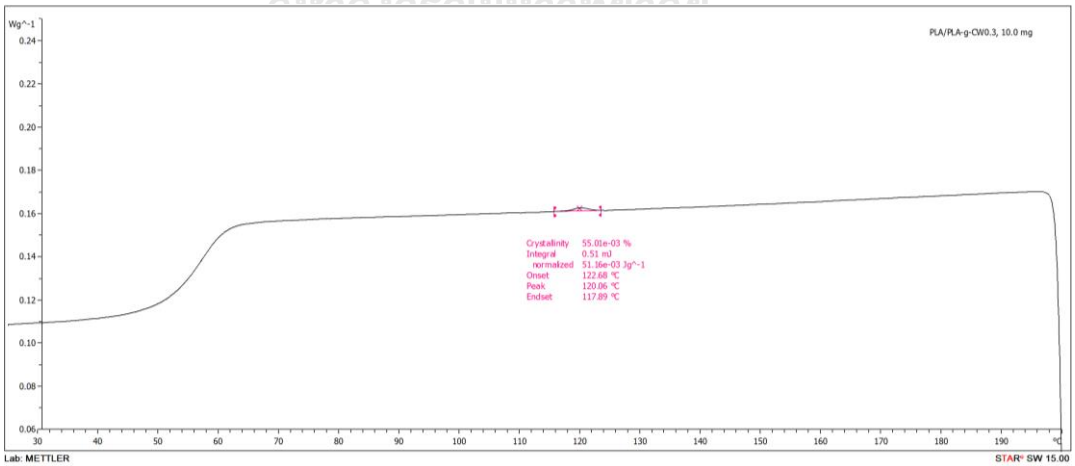

Figure H.6 DSC thermogram at cooling scan of PLA/PLA-g-CW0.3

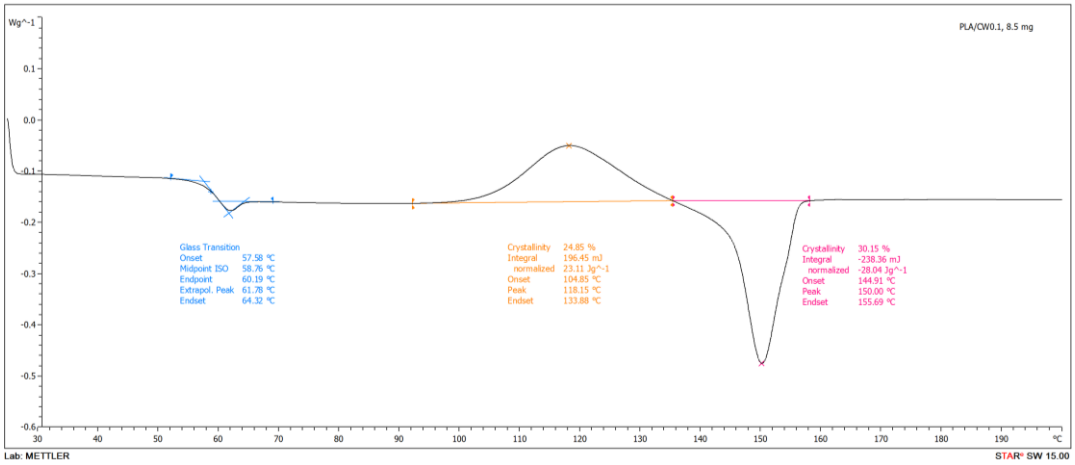

Figure H.7 DSC thermogram at second heating scan of PLA/CW0.1

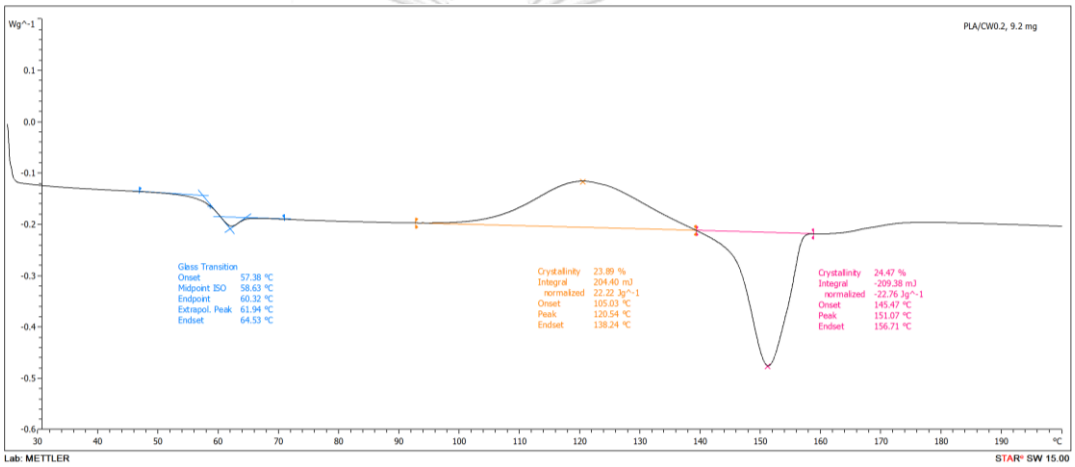

Figure H.8 DSC thermogram at second heating scan of PLA/CW0.2

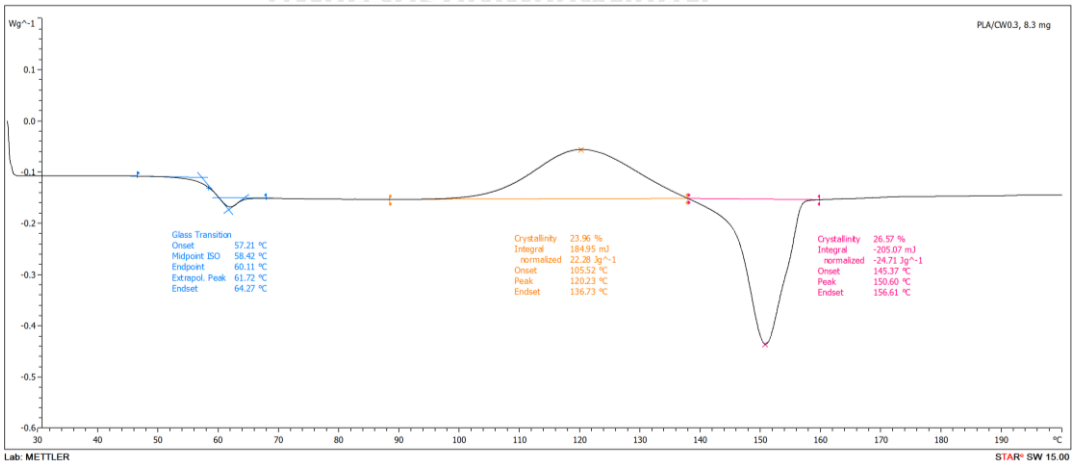

Figure H.9 DSC thermogram at second heating scan of PLA/CW0.3

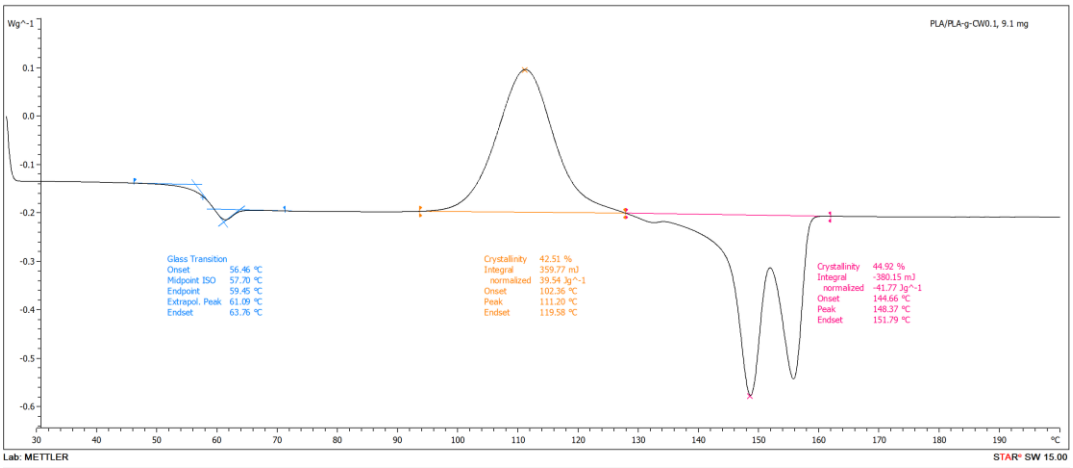

Figure H.10 DSC thermogram at second heating scan of PLA/PLA-g-CW0.1

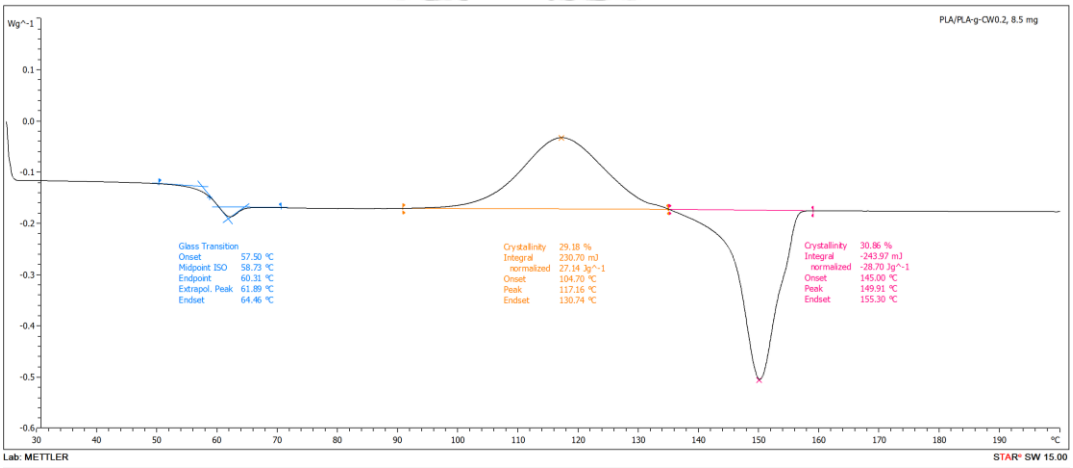

Figure H.11 DSC thermogram at second heating scan of PLA/PLA-g-CW0.2

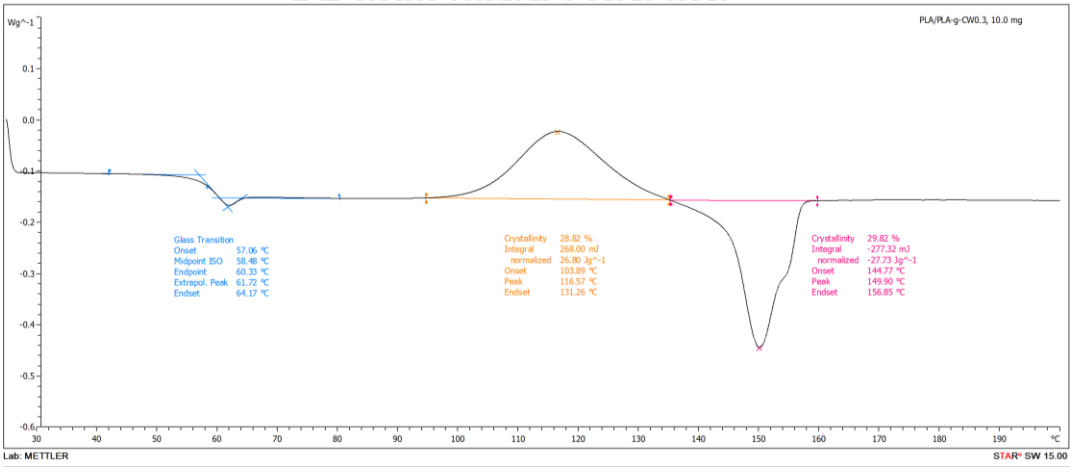

Figure H.12 DSC thermogram at second heating scan of PLA/PLA-g-CW0.3

Calculation of the degree of crystallinity (χ_c)

The crystallinity indexes of chitin samples were determined by following equation

$$\%\chi_c = \frac{\Delta H_m}{\Delta H_f} \times \frac{1}{w} \times 100 \quad (2)$$

Where, ΔH_m = the melting enthalpy of PLA based nanocomposites

ΔH_f = the theoretical enthalpy of 100% crystalline polymer

w = the weight fraction of PLA in nanocomposite

For instance, the PLA/CW0.1 nanocomposite film has ΔH_m of 27.86 J/g and ΔH_f of 93 J/g. The weight fraction of PLA was approximate to 0.999.

$$\%\chi_c = \frac{27.86}{93} \times \frac{1}{0.999} \times 100$$

$$\%\chi_c = 29.99$$

VITA

Miss Nichaphat Passornraprasit was born on April 26, 1994 in Chaiyaphum, Thailand. She achieved a bachelor's degree of engineering in Petrochemical and Polymeric Materials from Faculty of Engineering and Industrial technology, Silpakorn University in 2015, and then, she has studied a master's degree of Applied Polymer Science and Textile Technology at Department of Materials Science, Faculty of Science, Chulalongkorn University for 2 years. She completely graduated on August 2018.

International Presentation:

1. N. Passornraprasit and W. Tachaboonyakiat, "Preparation of Chitin Whisker and Effect to Crystallization of Polylactide", The Third International Conference on Applied Engineering, Materials and Mechanics, Okinawa Island, Japan, April 20-22, 2018.

Additional Academic Activities:

1. Participated in Japan-Asia Youth Exchange Program in Science (SAKURA Exchange Program in Science) at Nagaoka University of Technology, Nagaoka, Niigata, Japan.